ON THE USE OF FIBER REINFORCED POLYMER COMPOSITE ELEMENTS FOR ENHANCING STRUCTURAL STEEL MEMBER DUCTILITY

by

Noah Blaine Accord

BS, University of Pittsburgh, 2004

Submitted to the Graduate Faculty of

The School of Engineering in partial fulfillment

of the requirements for the degree of

Master of Science

University of Pittsburgh

2005

UNIVERSITY OF PITTSBURGH

SCHOOL OF ENGINEERING

This thesis was presented

by

Noah Blaine Accord

It was defended on

July 18, 2005

and approved by

Dr. J.S. Lin, Associate Professor, Civil and Environmental Engineering

Dr. K.A Harries, Assistant Professor, Civil and Environmental Engineering

Thesis Advisor: Dr. C.J. Earls, Associate Professor, Civil and Environmental Engineering

ON THE USE OF FIBER REINFORCED POLYMER COMPOSITE ELEMENTS FOR ENHANCING STRUCTURAL STEEL MEMBER DUCTILITY]

Noah Blaine Accord, M.S.

University of Pittsburgh, 2005

An innovative use of fiber reinforced polymer (FRP) composite materials, to control the manifestation of local buckling in a steel section during plastic hinging is discussed in the present work. Specifically, details related to how the high stiffness and linear behavior of FRP materials may be utilized to provide "bracing" against flange local buckling (FLB), in a way that strategically leverages the unique mechanical properties of each material in an efficient application domain, are discussed. The proposed method is not aimed at increasing the load carrying capacity of the steel section, *per se*; although this may certainly be accomplished if desired. Rather, the present paper reports on a novel technique that is aimed at providing stability (in the sense of bracing) to the steel section through the imposition FRP strips whose function is to enforce a nodal line along a plate element for the purposes of: increasing its critical load; and constraining plastic flow in the plate element. The member becomes, in affect, an *FRP stabilized steel section*. The research work discussed herein is primarily analytical in nature. Detailed nonlinear finite element models are created using the commercially available software system ADINA.

TABLE OF CONTENTS

ACKNOWLEDGEMENTS xii

1.0 INTRODUCTION 1

1.1 GLASS FIBER REINFORCED POLYMER (GFRP) BACKGROUND 3

1.2 LITERATURE REVIEW 4

1.3 SCOPE OF WORK 10

1.4 THESIS ORGANIZATION 11

2.0 BEAM GEOMETRY AND FINITE ELEMENT MODEL 12

2.1 BEAM GEOMETRY 12

2.2 FINITE ELEMENT ANALYSIS 19

2.2.1 Finite Element Modeling Approach and Assumptions 19

2.2.2 Verification Study 23

3.0 RESULTS 29

3.1 PRESENTATION OF RESULTS 29

4.0 DISCUSSION 49

4.1 PHYSICAL BEHAVIOR 49

4.2 LOAD-DEFLECTION PLOTS 52

4.3 MOMENT-ROTATION PLOTS 55

4.4 BEAM 30 57

5.0 CONCLUSIONS 58

APPENDIX A 59

DEFLECTION AND STRESS FIGURES 59

BIBLIOGRAPHY 127

LIST OF TABLES

Table 2.1 Geometric Properties of Modeled Beams. 14

Table 2.2 Logarithmic Strain and True Stress of A36 Steel Inputted Into ADINA Program..... 21

Table 2.3 Geometric Properties of Verification Beam. 25

Table 3.1 Rotations and Rotational Capacities for Modeled Beams 33

Table 4.1 Ultimate Load and Increase in Ultimate Load (%) Compared to Bare Steel. 53

LIST OF FIGURES

Figure 1.1 Small scale specimens tested by Mertz and Gillespie. 5

Figure 1.2 Schematic of Full Scale Specimens Tested by Mertz and Gillespie. 7

Figure 2.1 Schematic of Geometric Properties of Modeled Beams. 16

Figure 2.2 Elevation View Along Beam Length. 17

Figure 2.3 Depiction of Finite Element Modeled GFRP-Steel Composite Beam. 18

Figure 2.4 Finite Element Model Showing Loading and Boundary Conditions. (Check indicates a free condition) 22

Figure 2.5 Schematic of Geometric Properties of Verification Beam. 26

Figure 2.6 Finite Element Model of Verification Beam. 27

Figure 2.7 Plot Showing the Results of the Verification Study. 28

Figure 3.1 Load-Deflection Plot Showing Results as GFRP Strips are Moved Along the Width of the Compression Flange. (t_f = 10.16mm) 35

Figure 3.2 Load-Deflection Plot Showing Results as GFRP Strip Longitudinal Lengths Are Varied Along the Compression Flange. (t_f = 10.16 mm) 36

Figure 3.3 Load-Deflection Plot Showing Similarities Between A Beam With GFRP Strips and A Beam With An Increased Compression Flange Thickness. 37

Figure 3.4 Load-Deflection Plot Showing Results as GFRP Strips are Moved Along the Width of the Compression Flange. (t_f = 5.08 mm) 38

Figure 3.5 Load-Deflection Plot Showing Results as GFRP Strip Longitudinal Lengths Are Varied Along the Compression Flange. (t_f = 5.08 mm) 39

Figure 3.6 Moment-Rotation Plot Showing Results as GFRP Strips are Moved Along the Width of the Compression Flange. (t_f = 10.16 mm) 40

Figure 3.7 Moment-Rotation Plot Showing Results as GFRP Strip Longitudinal Lengths Are Varied Along the Compression Flange. (t_f = 10.16 mm) 41

Figure 3.8 Moment-Rotation Plot Showing Results as GFRP Strips are Moved Along the Width of the Compression Flange. (t_f = 5.08 mm) 42

Figure 3.9 Moment-Rotation Plot Showing Results as GFRP Strip Longitudinal Lengths Are Varied Along the Compression Flange. (t_f = 5.08 mm) 43

Figure 3.10 Depiction of Deflection and Twist of Beam 9. (Fixed End Forground) 45

Figure 3.11 Depiction of the Effective Stress on Beam 9 46

Figure 3.12 Depiction of the Effective Stress in the Plastic Hinge Region of Beam 9 47

Figure 3.13 Depiction of the Effective Stress in the Bottom of the Compression Flange and GFRP Strips of Beam 9 48

Figure 4.1 Plot of Normalized Theoretical Moment-Rotation Curve. 56

Figure A.1 Bare Steel 1 60

Figure A.2 Bare Steel 1 61

Figure A.3 Bare Steel 1 62

Figure A.4 Beam 9 63

Figure A.5 Beam 9 64

Figure A.6 Beam 9 65

Figure A.7 Beam 9 66

Figure A.8 Beam 11 67

Figure A.9 Beam 11 68

Figure A.10 Beam 11 69

Figure A.11 Beam 11 70

Figure A.12 Beam 12 71

Figure A.13 Beam 12 72

Figure A.14 Beam 12 73
Figure A.15 Beam 12 74
Figure A.16 Beam 13 75
Figure A.17 Beam 13 76
Figure A.18 Beam 13 77
Figure A.19 Beam 13 78
Figure A.20 Beam 14 79
Figure A.21 Beam 14 80
Figure A.22 Beam 14 81
Figure A.23 Beam 14 82
Figure A.24 Beam 15 83
Figure A.25 Beam 15 84
Figure A.26 Beam 15 85
Figure A.27 Beam 15 86
Figure A.28 Beam 16 87
Figure A.29 Beam 16 88
Figure A.30 Beam 16 89
Figure A.31 Beam 16 90
Figure A.32 Bare Steel 2 91
Figure A.33 Bare Steel 2 92
Figure A.34 Bare Steel 2 93
Figure A.35 Bare Steel 2 94
Figure A.36 Beam 10 95

Figure A.37 Beam 10 96
Figure A.38 Beam 10 97
Figure A.39 Beam 10 98
Figure A.40 Beam 17 99
Figure A.41 Beam 17 100
Figure A.42 Beam 17 101
Figure A.43 Beam 17 102
Figure A.44 Beam 18 103
Figure A.45 Beam 18 104
Figure A.46 Beam 18 105
Figure A.47 Beam 18 106
Figure A.48 Beam 19 107
Figure A.49 Beam 19 108
Figure A.50 Beam 19 109
Figure A.51 Beam 19 110
Figure A.52 Beam 20 111
Figure A.53 Beam 20 112
Figure A.54 Beam 20 113
Figure A.55 Beam 20 114
Figure A.56 Beam 21 115
Figure A.57 Beam 21 116
Figure A.58 Beam 21 117
Figure A.59 Beam 21 118

Figure A.60 Beam 22 119
Figure A.61 Beam 22 120
Figure A.62 Beam 22 121
Figure A.63 Beam 22 122
Figure A.64 Beam 30 123
Figure A.65 Beam 30 124
Figure A.66 Beam 30 125
Figure A.67 Beam 30 126

ACKNOWLEDGEMENTS

I would especially like to thank my advisor, Dr. C.J. Earls for his constant support and guidance throughout my undergraduate and graduate career. I would also like to give a special thanks to Dr. K.A. Harries for his assistance in my graduate work. Finally, I would like to thank my committee, Dr. Earls, Dr. Harries, and Dr. Lin.

1.0 INTRODUCTION

The past several years have seen increased use of Fiber Reinforced Polymers (FRP) to help strengthen and repair concrete structures through retrofit programs involving the application of FRP strips and thin plates (Yost et al. 2001). A wide variety of FRP-concrete systems have been researched and implemented over the past decades (Domingo et al. 2002, Duthinh et al. 2004). FRP has been used as sheets, plates and wraps to strengthen deficient concrete beams and columns. FRP has also been used as reinforcement within concrete structures, effectively replacing steel reinforcement (Sonobe, Fukuyama, et al. 1997, Cosenza et al. 1997).

In comparison to the use of FRP-concrete composite systems relatively little work has been done in the applications involving FRP-steel composites. As FRP is more widely used and its capabilities are more fully understood it has become clear that FRP-steel composites can be efficiently used in specific situations where the material properties of each material can be properly exploited to maximize advantage. One conspicuous application area involves enhancing the ductility in steel connection regions through the use of FRP reinforcing strategies.

One potential application area involves the consideration of steel moment connections in rigid frame lateral load resisting systems used in multi-storey structures. Within these connection regions very large ductility demands are not uncommon during extreme events such as earthquake and blast loading. Within this context, the mobilization of the inherent energy dissipation capacity of available steel structural elements can be compromised by the manifestation of inelastic instabilities such as flange or web local buckling. In general, such inelastic instabilities are not uncommon in I-section members that are proportioned and

optimized for economical performance under service loading conditions. Currently, design specifications promulgate an approach by which detailing rules and dimensional limits are used to ensure ductile structural behavior in the case of overloads during extreme events. In addition to such design considerations within the context of new construction, older structures, with substandard seismic details, are also particularly susceptible to instability-causing overloads. In instances of extreme loading associated with these and other conditions, structural ductility at the member level and connection level are at a premium since system-wide redundancy relies heavily on individual member ductility. In fact, local member ductility in individual plastic hinges is requisite for the manifestation of favorable system-wide response; characterized by the formation of a predictable global collapse mechanism. Finally, extreme loading of any kind may result in partial collapse of the structure; significantly overloading the remaining members and connections. In this case, the predicted collapse mechanism is not permitted to form, but the requirement for safety remains. To address this condition, it is required that structural ductility and energy dissipation characteristics of the remaining structure be preserved; a feat that requires inelastic instabilities to be mitigated.

In cases such as these the use of FRP-steel composite systems employed at the member level can utilize the unique properties of the FRP material, in conjunction with the properties of the underlying steel element, to efficiently stabilize the member cross-section (i.e. enforcing a nodal line within a critical plate component). Using FRP also provides several advantages over traditional methods of retrofit and stabilization, such as welding and bolting additional steel. FRP can quickly and easily be placed using epoxy, therefore avoiding the need for heavy steel plates and the fatigue problems that can come with welding or bolting of steel. Also, since no welding is required, no heat or flame is needed in the installation. In addition, FRP has a high

resistance to corrosion and therefore corrosion issues will not be as critical as they would be with steel retrofit and strengthening options.

What seems obvious as strategies for reinforcing steel with FRP are explored is that the unique and favorable behavioral qualities of each material ought to be leveraged to gain as much efficiency as possible in the new structural context.

1.1 GLASS FIBER REINFORCED POLYMER (GFRP) BACKGROUND

Fiber reinforced polymer (FRP) composite materials are created by a process wherein fiber strands and woven fabrics are wetted-out and cured within a polymeric resin matrix. The fibers used in the FRP are generally high strength, high modulus fibers; as compared with the mechanical properties of the matrix material. The fiber materials most commonly used in the Civil Engineering field are carbon (CFRP) and glass (GFRP) fibers. Both materials are high strength, high modulus materials however CFRP fibers frequently have a much higher modulus than GFRP. In addition to fiber type, the orientation of the fibers plays a large role in the strength and stiffness properties exhibited by the FRP material. Generally, the fibers are oriented so that the bulk of the fibers are oriented to contribute strength and stiffness within the principle stress direction associated with the dominant structural response of the element under consideration.

The polymeric resin matrix serves to confine, protect, and transfer force into and between the fibers. Epoxy and polyester resins are commonly used for GFRP applications.

While it is that GFRP material has reasonably large material stiffness properties in directions coinciding with the orientation direction of the majority of fibers, the modulus of elasticity is still approximately one order of magnitude less than that of steel. As a result of this modular mis-match, GFRP-steel retrofit strategies that rely on strength enhancement through reinforcement of

the steel section by direct shear transfer into the GFRP will invariably be inefficient and unattractive from a practical point of view. What is sought in the present research program is a reinforcement methodology that leverages the important strength characteristics of each material as a means for realizing significant performance enhancement rather than modest incremental strength gains. In the current research, GFRP was chosen over CFRP due to the lower cost and greater availability of the GFRP material. The specific properties of the GFRP material used in the research can be seen in Yulismana (2005).

1.2 LITERATURE REVIEW

The investigation and use of FRP-steel composite materials is a relatively new field with very little research and implementation completed up to the current point in time (July 2005). There are no standard codes or widely accepted guidelines for the use of FRP-steel systems. The vast majority of the work that has been completed focuses on the use of FRP for retrofitting existing steel structures.

The closest resource to a design guide for the use of FRP-steel systems is a British publication written by Cadei et al. (2004). The publication is a broad based resource dealing with many aspects of FRP reinforcement on a variety of metals. The publication gives suggestions for all steps of the process wherein FRP composite elements are applied to metal structural components: from surface preparation, to material selection, to expected results. However, the guide uses theoretical processes for its design procedures and therefore cautions that all implementation of the theory should be confirmed with appropriate testing.

A significant portion of the research concerning FRP-steel composites was done in a series of projects completed at the University of Delaware in the late 1990's, and a few related papers emanating from this work. Mertz and Gillespie completed a pair of NCHRP-IDEA projects,

IDEA-011 (Mertz and Gillespie 1996) and IDEA-051 (Mertz and Gillespie 2002), both of which dealt with the retrofit of steel bridge girders. The projects were based on the rehabilitation of simple flexural steel bridge girders using CFRP. The tests conducted focused exclusively on CFRP-steel composites where the CFRP strip material is bonded to the corroded tension flange of the girders.

The IDEA-011 study was a two part study where: first, a series of small scale girders were tested; and then a pair of full scale corroded girders was tested. The small scale tests were conducted using six (6) W8x10 members each 1.52 m (5') long. Five (5) of the beams were each fitted with a different variation of a FRP-steel composite system, while the sixth served as a bare steel control specimen. The different FRP-steel composite systems used can be seen in Figure 1.1. The fifth girder was similar to the girder in Figure 1.1a, but with CFRP strips replacing the solid CFRP plate.

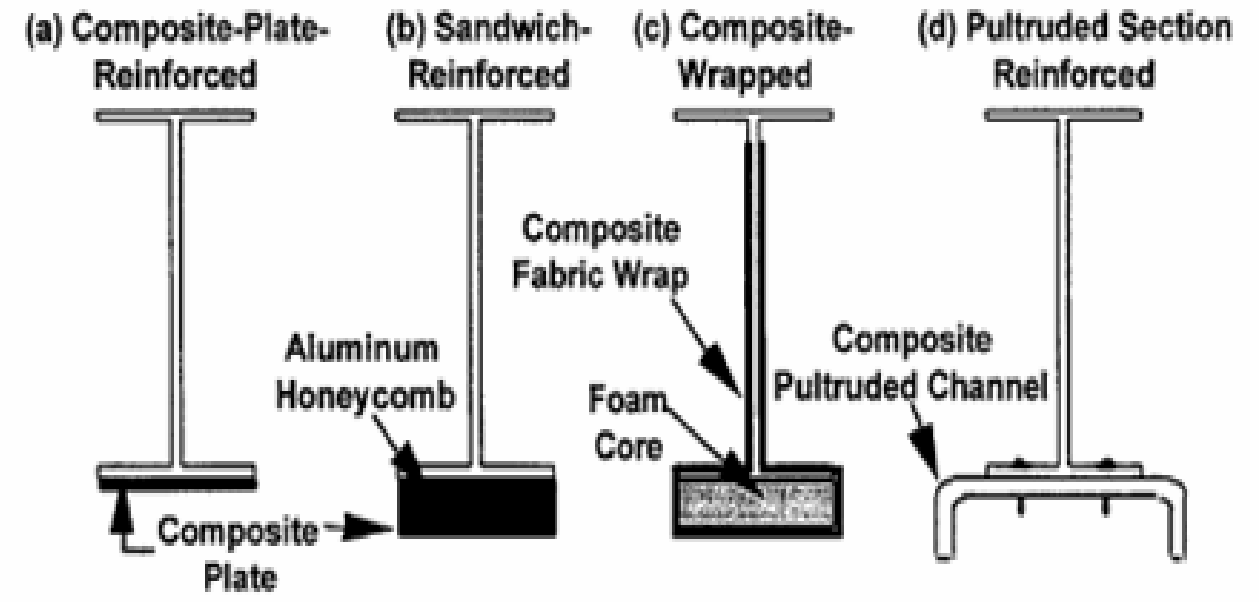

Figure 1.1 Small scale specimens tested by Mertz and Gillespie.

As the figures show, the first and fifth test specimens were reinforced by a CFRP plate (strips in specimen 5) bonded directly to the tension flange of the plate using an epoxy adhesive. The second specimen was reinforced using the exact same plate as the first specimen but with an aluminum honeycomb core added to maintain distance between the tension flange and the plate. The third specimen was reinforced using a composite fabric wrapped around the web of the beam and extending around a foam core placed on the tension flange of the beam. The fourth specimen used a GFRP pultruded channel screwed to the tension flange of the specimen.

The results of the tests involved in the research work at the University of Delaware showed that FRP reinforcement applied to the tension flange of steel members can greatly improve the strength and stiffness of the steel members. All of the specimens tested showed significant increases in strength and stiffness. The biggest increases in both strength and stiffness were found in the section using a CFRP plate separated from the flange by an aluminum honeycomb (specimen 2 – see figure 1.1b). This specimen showed a 30% increase in mid-span stiffness compared to the control beam and a 71% increase in elastic yield strength. The CFRP strip system (specimen 5 – similar to specimen 1.1a with CFRP strips instead of a plate) showed slightly less, but comparable, gains to specimen 2 (27% increase in stiffness, 65% increase in elastic strength).

A portion of IDEA-011 involved testing two full-scale highly corroded bridge girders retrofit with CFRP material. The bridge girders used in this portion of work at the University of Delaware came from an old bridge with corrosion severe enough to warrant demolition of the bridge. The girders were 9.75 m (32') long with dimensions similar to those of a W24x84, but with sloping flanges (see Figure 1.2). The girders were retrofit with CFRP strips on both the top and bottom of the tension flange.

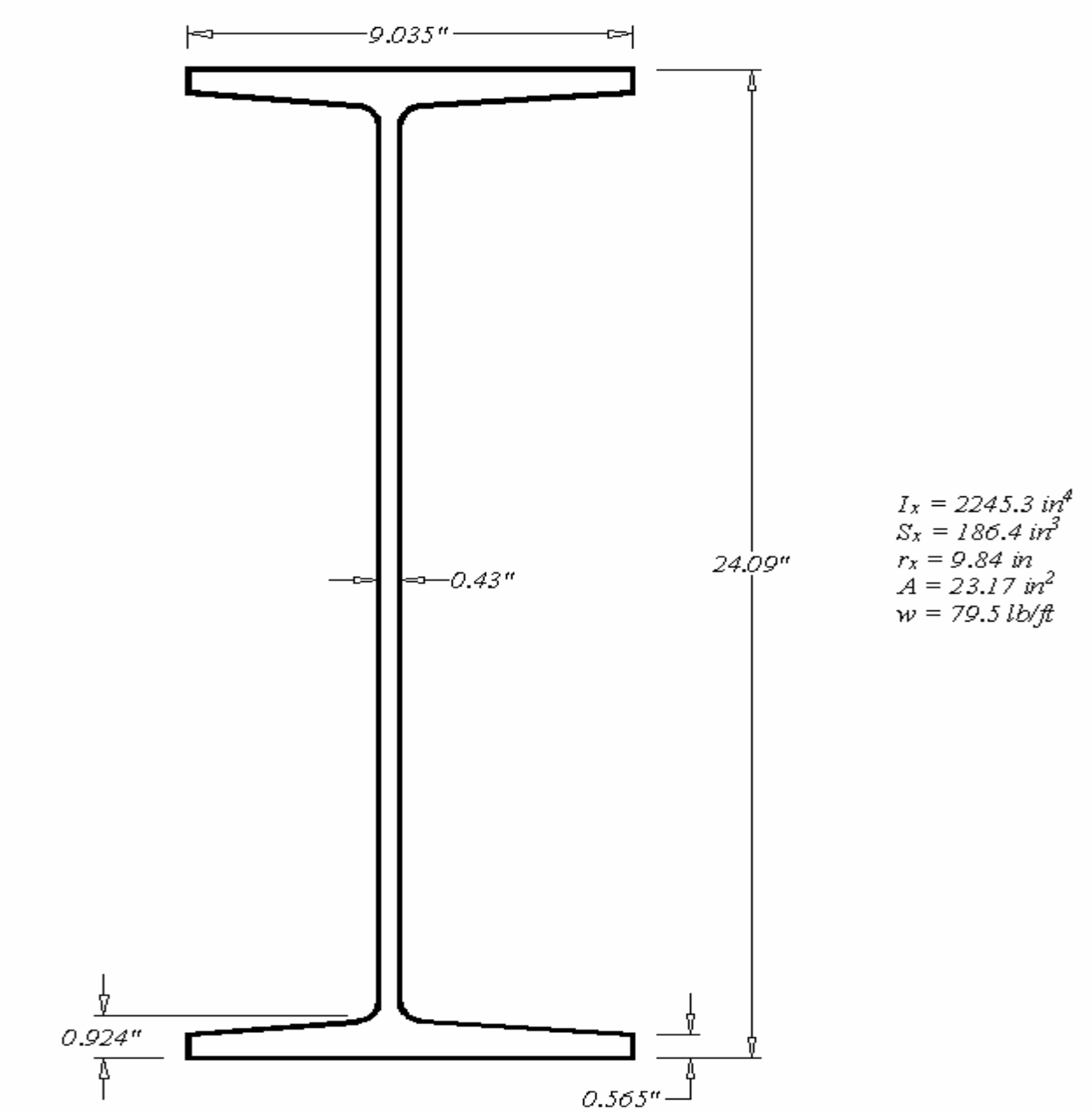

Figure 1.2 Schematic of Full Scale Specimens Tested by Mertz and Gillespie**.**

The results of the full-scale tests again showed the CFRP-steel composite systems improved both the strength and stiffness of the beams. In the less corroded of the two beams, stiffness was returned to 100% of the uncorroded value while at the same time strength levels that exceeded the uncorroded girder strength capacity, were achieved. It is, however, pointed out that in the more corroded beam, strength and stiffness both showed great increase but were unable to achieve 100% of the uncorroded values.

In an extension of this study both Mertz and Gillespie (2002) and Miller et al. (2001) took the laboratory techniques presented in IDEA-011 and applied them in the field to a full-scale bridge. The bridge, 1-704 on I-95 in Newark, Delaware, was chosen because it was of a common slab-on-girder bridge type subjected to heavy truck traffic volumes. A single W24x84 girder, 7.47 m (24.5') long, in the bridge was retrofit with CFRP on the bottom of the tension flange. The results of the test showed an 11.6% increase in global flexural stiffness with the use of CFRP reinforcement.

A similar project performed by Chacon et al. (2004) showed similar results on a different bridge. Two girders on the Ashland Bridge, carrying SR-82 in Delaware, were retrofitd with CFRP plates on the bottom of the tension flanges. The results showed an average live load strain reduction in the rehabilitated floor beam of 5.5% due to the CFRP plates. Sen et al. (2001) performed similar tests on lab models of girder tension flanges of bridges. The girders were loaded past the yield point then the CFRP strips were applied and the girders were re-loaded. Results showed significant gains in ultimate strength and moderate gains in elastic behavior.

Sayed-Ahmed (2004) performed a finite element based study dealing with the use of CFRP strips on the compression region of the web sections of I-beams. Four different I-sections with varying h_w/t_w values were investigated. The finite element analysis showed that through the use

of the CFRP strips, the local buckling of the beam's web was delayed resulting in increases in critical load and ultimate strength. The critical local buckling load was shown to increase 20%-60% and subsequently the ultimate strength was increased by 2%-9% for the varying depth to thickness ratios.

Patnaik and Bauer (2004) conducted tests to demonstrate the advantages of reinforcing steel I-sections with CFRP for both flexural strength and shear strength. Two beams, designed to fail in flexure, were fitted with CFRP strips attached to the tension flange of the beams. Two beams, designed to fail in shear, were fitted with CFRP strips along their webs. The test results showed both flexure-strengthened beams displayed a capacity increase of approximately 14% in strength. One of the shear-strengthened beams failed unexpectedly but the other showed a 26% increase in strength.

Ekiz et al. (2004) performed tests dealing with wrapping the plastic hinge region of a steel beam with CFRP. The lab tests were conducted using cantilever double-channel sections of different sizes. The beams were designed to represent specific members in a truss moment frame. The sections were wrapped using two different wrapping schemes: one which fully wrapped the beam; and one which wrapped only the flanges of the beam. The results showed that the wrapped specimens significantly improved the overall structural behavior of the beams by increasing the size of the zone of yielding within the plastic hinge region; thus inhibiting the occurrence of local buckling, and delaying lateral-torsional buckling.

A variety of studies (Mertz et al. 2002, Buyukozturk et al. 2003, Damatty et al. 2003, Wu et al.2002, Karbhari et al. 1995 and Momber et al. 2004) have investigated the behaviors that take place in the interactions between the steel, FRP, and adhesive. These behaviors include peel,

shear, de-bonding, transfer length, bond fatigue, fracture propagation, and surface preparation. These issues are key practical issues in the investigation of FRP-steel composite systems; however, these issues are not dealt with in the current research.

The literature surveyed in the foregoing covers a variety of issues in the field of FRP-steel composites. Despite the number of issues covered by previous research, there remains a large void in the area of research considered by the current project: GFRP stabilization of steel cross-sectional plate components in the inelastic range.

1.3 SCOPE OF WORK

The objective of the current study is to investigate the innovative use of Glass Fiber Reinforced Polymer (GFRP) composite materials, to control the manifestation of local buckling in a steel section during plastic hinging. In this study, the high stiffness and linear behavior of GFRP materials are simulated and utilized to provide "bracing" against flange local buckling (FLB) and web local buckling (WLB) in a way that strategically leverages the unique mechanical properties of each material in an efficient application domain. The proposed research work is aimed at providing stability (in the sense of bracing) to the steel section through the imposition GFRP strips whose properties are consistent with GFRP and whose function it is to enforce a nodal line along a plate element for the purposes of: increasing its critical load; and constraining plastic flow in the plate element. The member becomes, in affect, a GFRP stabilized steel section.

Parametric studies are conducted to maximize the efficiency of the GFRP-steel system. Parameters investigated in the study include: GFRP strip position along the flange width, GFRP strip length along the member longitudinal axis, and flange thickness (t_f) of the steel section under investigation. Results from the study are used to make recommendations about the use of GFRP-steel composite materials.

1.4 THESIS ORGANIZATION

Chapter 2 details the geometry of the beams used in the study and some relevant background information related to the commercial finite element software system used in the conduct of this research: ADINA. The geometry of the steel section, details regarding the GFRP material, and the properties of the interface material used in the steel-GFRP system is also detailed for each beam modeled in the study. The background, methods, inputs, outputs, and validity of ADINA are discussed. The results of the present study conducted are presented in Chapter 3; this includes graphs and figures depicting the behavior of the modeled beams. Chapter 4 provides a discussion on the results presented in Chapter 3. Conclusions based on these results and discussions are made in Chapter 5 of the presented work.

2.0 BEAM GEOMETRY AND FINITE ELEMENT MODEL

2.1 BEAM GEOMETRY

The beams modeled in this study employed bonded 25.4 mm (1") x 6.35 mm (.25") glass fiber reinforced plastic (GFRP) strips on the compression flange of cantilevered steel I-section beams. A flexible transition zone was employed at the interface between the steel and the GFRP in order to model an adhesive bond layer that might be used in a practical application of the proposed approach. The GFRP strips were oriented so that their length axis corresponds with the beam longitudinal axis. The GFRP strips were subsequently shifted to several different cross-sectional locations along both the top and the bottom of the compression flange of the I-section as a parameter of investigation within the scope of the current research. Fig. 2.1 through Fig 2.3 detail the layout of the GFRP-steel assembly. The longitudinal length of the GFRP strips varies as a parameter for study in the beams and information in this regard can be found in Table 2.1.

The steel I-sections themselves are of a depth of 381mm (15"), flange width of 152.4 mm (6"), and web thickness of 6.35 mm (.25"). Other beam geometrical properties varied as part of the current work and are detailed in Table 2.1. The general beam geometry is shown in Fig. 2.1. All of the beams included in the study were 3.81m (150") in length. The interfacial zone occurring between the GFRP material and the underlying steel was considered to be consistent with an

adhesive layer and thus modeled as a linear elastic, isotropic zone of material placed between the steel I-sections and the GFRP strips: for all tests the interface material had dimensions 25.4 mm (1”) x 1.27 mm (.05”).

Two bare steel models are included as part of the present study as a baseline case representing the unreinforced condition from which any improvements in performance can be gauged. These models have no GFRP strips and their geometric proportions and material properties are identical to the steel components used in the other beams. Beam 30 is also a bare steel model with a thicker compression flange section employed over a portion of the beam longitudinal axis beginning at the fixed end. These beams dimensions are shown in Table 2.1; along with the model naming convention adopted herein.

Table 2.1 Geometric Properties of Modeled Beams.

	d (mm)	b_f (mm)	t_f (mm)	t_w (mm)	L (m)	L_{FRP} (m)	b_{FRP} (mm)	d_{FRP} (mm)	x (mm)
Bare Steel$_1$	381	152.4	10.16	6.35	3.81	-	-	-	-
Beam 9	381	152.4	10.16	6.35	3.81	3.81	25.4	6.35	38.1
Beam 10	381	152.4	10.16	6.35	3.81	3.81	25.4	6.35	38.1
Beam 11	381	152.4	10.16	6.35	3.81	3.81	25.4	6.35	50.8
Beam 12	381	152.4	10.16	6.35	3.81	3.81	25.4	6.35	63.5
Beam 13	381	152.4	10.16	6.35	3.81	3.81	25.4	6.35	25.4
Beam 14	381	152.4	10.16	6.35	3.81	3.81	25.4	6.35	12.7
Beam 15	381	152.4	10.16	6.35	3.81	1.905	25.4	6.35	38.1

Table 2.1 (continued)

	d (mm)	b_f (mm)	t_f (mm)	t_w (mm)	L (m)	L_{FRP} (m)	b_{FRP} (mm)	d_{FRP} (mm)	x (mm)
Beam 16	381	152.4	10.16	6.35	3.81	.762	25.4	6.35	38.1
Beam 17	381	152.4	5.08	6.35	3.81	3.81	25.4	6.35	50.8
Beam 18	381	152.4	5.08	6.35	3.81	3.81	25.4	6.35	63.5
Beam 19	381	152.4	5.08	6.35	3.81	3.81	25.4	6.35	25.4
Beam 20	381	152.4	5.08	6.35	3.81	3.81	25.4	6.35	12.7
Beam 21	381	152.4	5.08	6.35	3.81	1.905	25.4	6.35	38.1
Beam 22	381	152.4	5.08	6.35	3.81	.762	25.4	6.35	38.1
Bare $Steel_2$	381	152.4	5.08	6.35	3.81	-	-	-	-
Beam 30	381	152.4	-	6.35	3.81	-	-	-	-

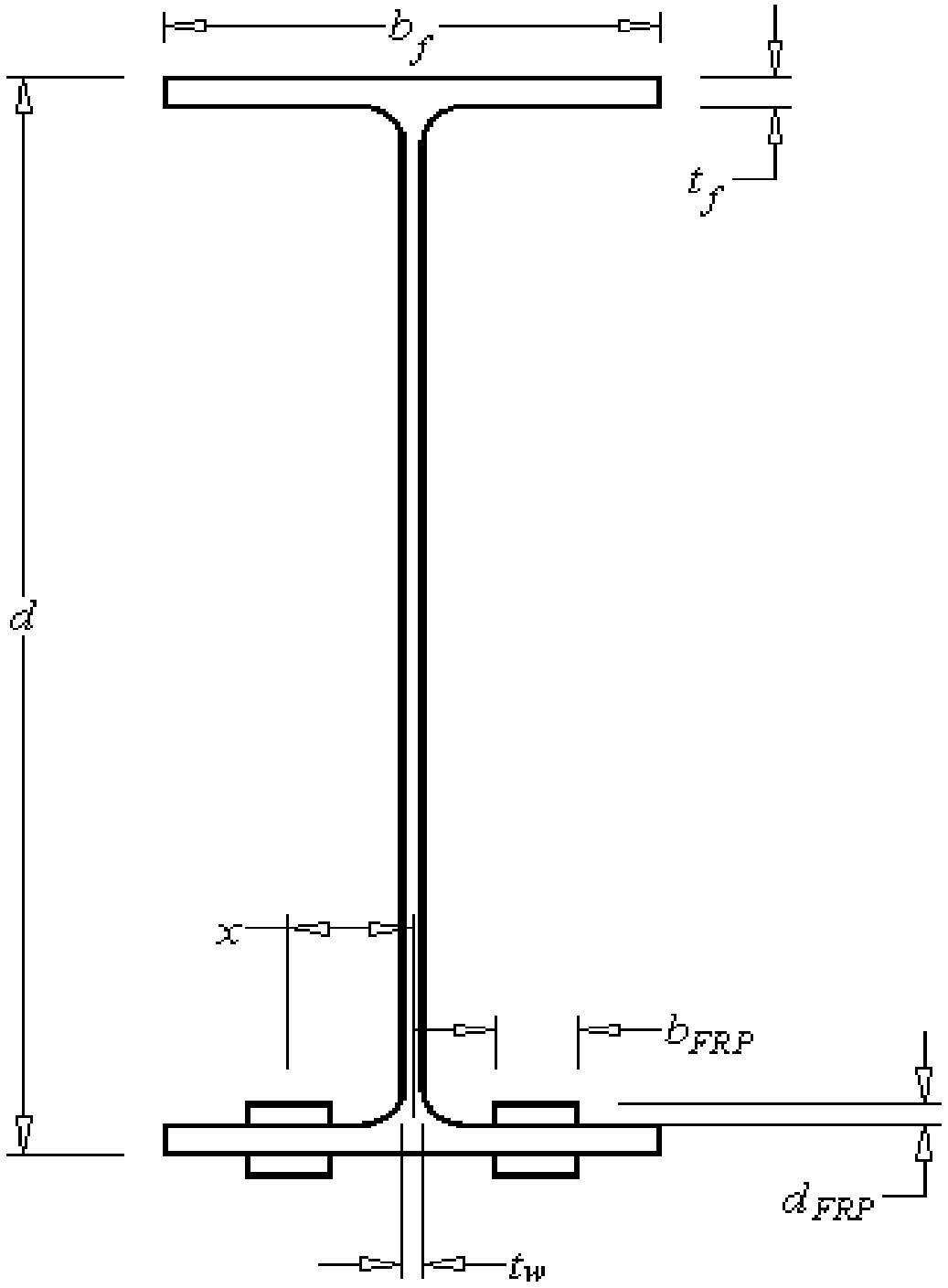

Figure 2.1 Schematic of Geometric Properties of Modeled Beams.

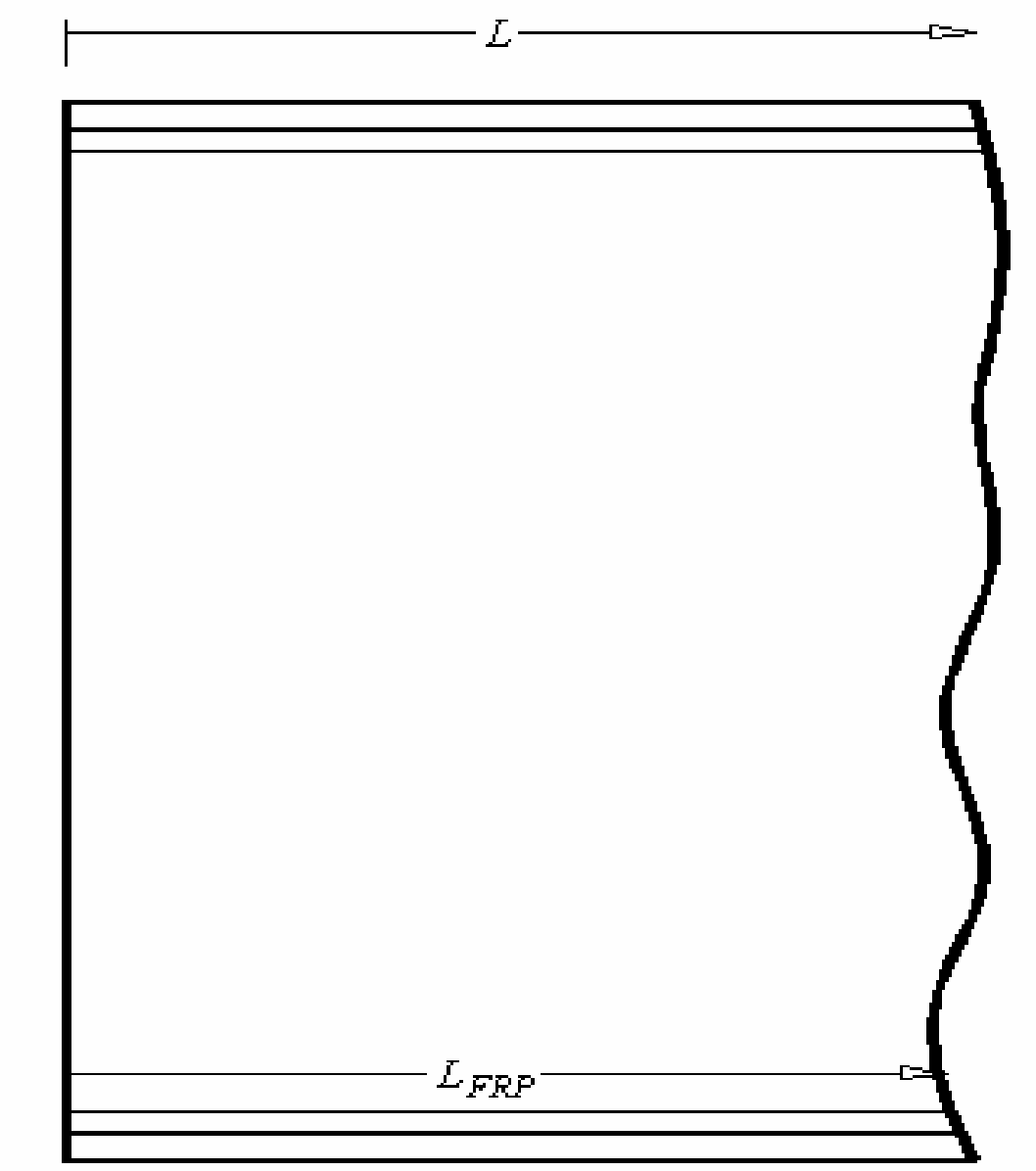

Figure 2.2 Elevation View Along Beam Length.

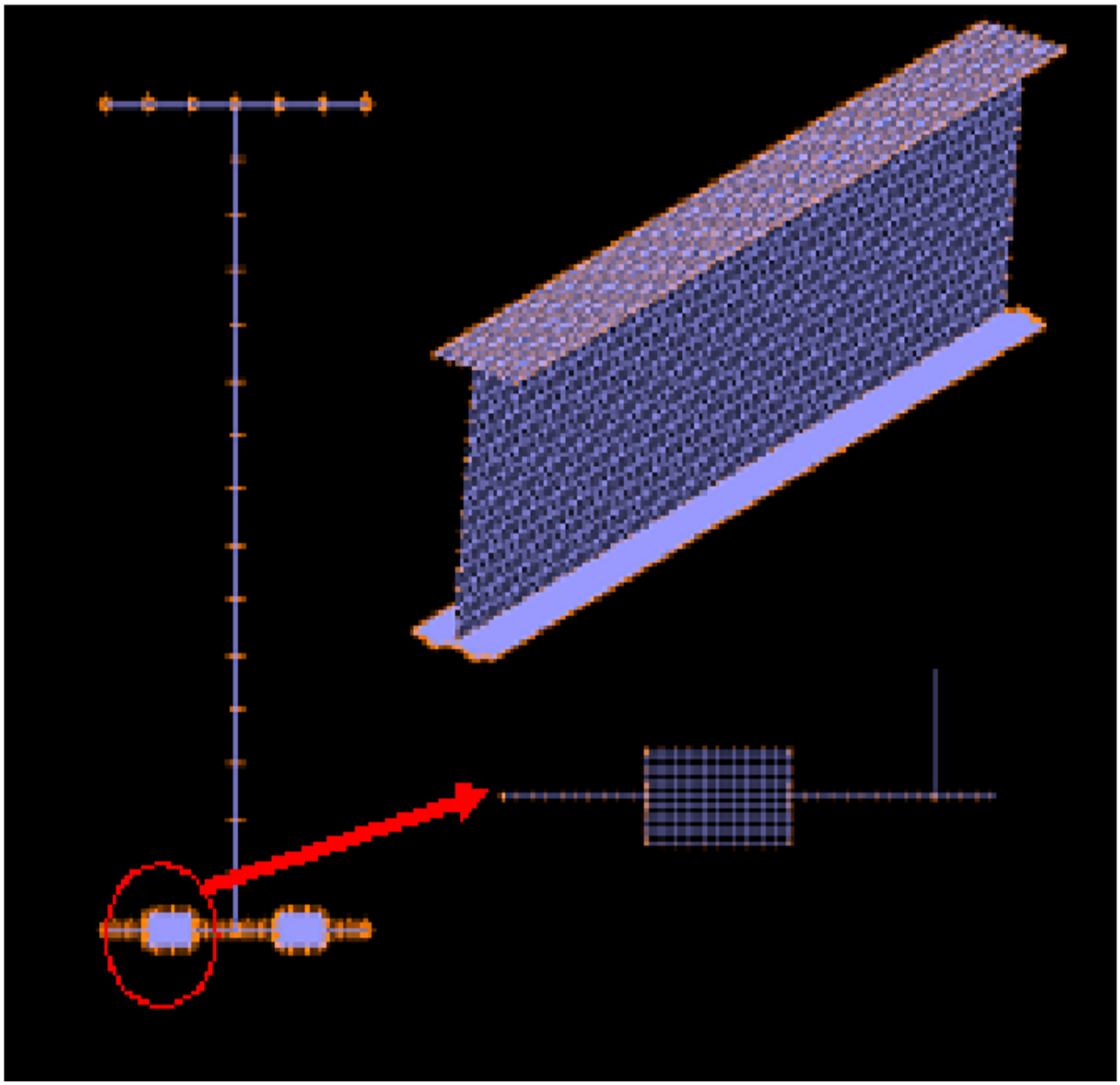

Figure 2.3 Depiction of Finite Element Modeled GFRP-Steel Composite Beam.

2.2 FINITE ELEMENT ANALYSIS

2.2.1 Finite Element Modeling Approach and Assumptions

The finite element method forms the basis for the research program reported on herein. Specifically, the commercially available software package, ADINA (ADINA 2003), is used in the current work. All models reported on herein consider both geometric (large rotation / small strain) and material (multi-linear plasticity) nonlinear effects. The nonlinear solution strategy used in all modeling reported on in this thesis is based on a combined method of load and displacement control wherein the spherical constant arc-length method (Crisfield 1981) is used in regions along the equilibrium path far from critical points, and a scheme based on constant increments of external work are employed within regions along the equilibrium path that are close to critical points (Bathe and Dvorkin 1983).

Given that the study is primarily interested the manifestation of local buckling in the steel section during plastic hinging, and the use of GFRP to prevent this buckling mode, a robust modeling strategy is adopted for the current work so as to properly account for the effects of distributed plasticity as well as local buckling effects. Figure 2.4 depicts the finite element modeling representations of the cantilever beam geometry treated. The boundary conditions and loading conditions used were chosen so as to create an accurate model of a cantilever beam subjected to a concentrated load. The fixed end of the beam was fully fixed along all lines and surfaces. The free end of the cantilever was left completely free except for lateral bracing of the web to prevent out of plane movement at the beam end. A concentrated force was applied to the free end of the cantilever at the lower flange-web junction (see Figure 2.4)

For the mesh of the steel I-section 4-node ADINA MITC4 shell finite elements were employed. This shell employs an assumed strain approach to improve its ability to properly model shearing effects within the element; especially as the shell element becomes thin. 2-node rigid beam elements were placed along plate centerlines of the cross-section at the free end of the cantilever to ensure proper load transfer from the load point to the entire beam cross-section (i.e. to reduce any effects due to shear-lag along the member length by fully activation the cross-section at the load point). Fully integrated 8-Node continuum finite elements were used to model the volumes of the GFRP and the interface material. The 2-node beam element and the 8-node continuum element were chosen to compliment the linear interpolation order used in the MITC4 shell finite elements.

Finite element models of the steel portion of the beam were created from meshes of nonlinear shell finite elements whose mechanical properties were assigned so as to be consistent with A36 steel. To obtain these material properties the stress-strain relationship of A36 steel (see Table 2.2) was directly inputted into the ADINA program. The exact material properties of the GFRP and the interface material were not as unambiguous due to the variety of materials that could be used. The GFRP was modeled to match the material properties found through lab tests performed by Yulismana in 2005 at the University of Pittsburgh (Yulismana, 2005). These results indicated that the GFRP material had a modulus of approximately 4000ksi. The interface material was also modeled as an isotropic elastic material with a modulus of approximately ¼ that of the GFRP material. This interfacial stiffness number was approximated as an upper bound from the average modulus values for adhesives as found in the manufactures brochures for FYFE Co. LLC. Both the GFRP and the interface material were assumed to be linear-elastic and perfect bond between all materials was assumed throughout the project.

To ensure that the beam follows the proper buckling path during loading imperfections were superimposed on the nonlinear models. To create the proper initial imperfections a linearized eigenvalue buckling analysis was performed on the beams to created buckling modes. The appropriate buckling mode was then selected (the first mode in the case of the present work). The imperfection from this mode was then scaled to factor of L/1000 (L= length of beam) and applied to the nonlinear model, creating an appropriate initial imperfection.

Table 2.2 Logarithmic Strain and True Stress of A36 Steel Inputted Into ADINA Program.

	True Stress (ksi)	**Logarithmic Strain**
Point 1	42.2704	**0.001433**
Point 2	43.7452	**0.016070**
Point 3	**75.0000**	**0.268881**

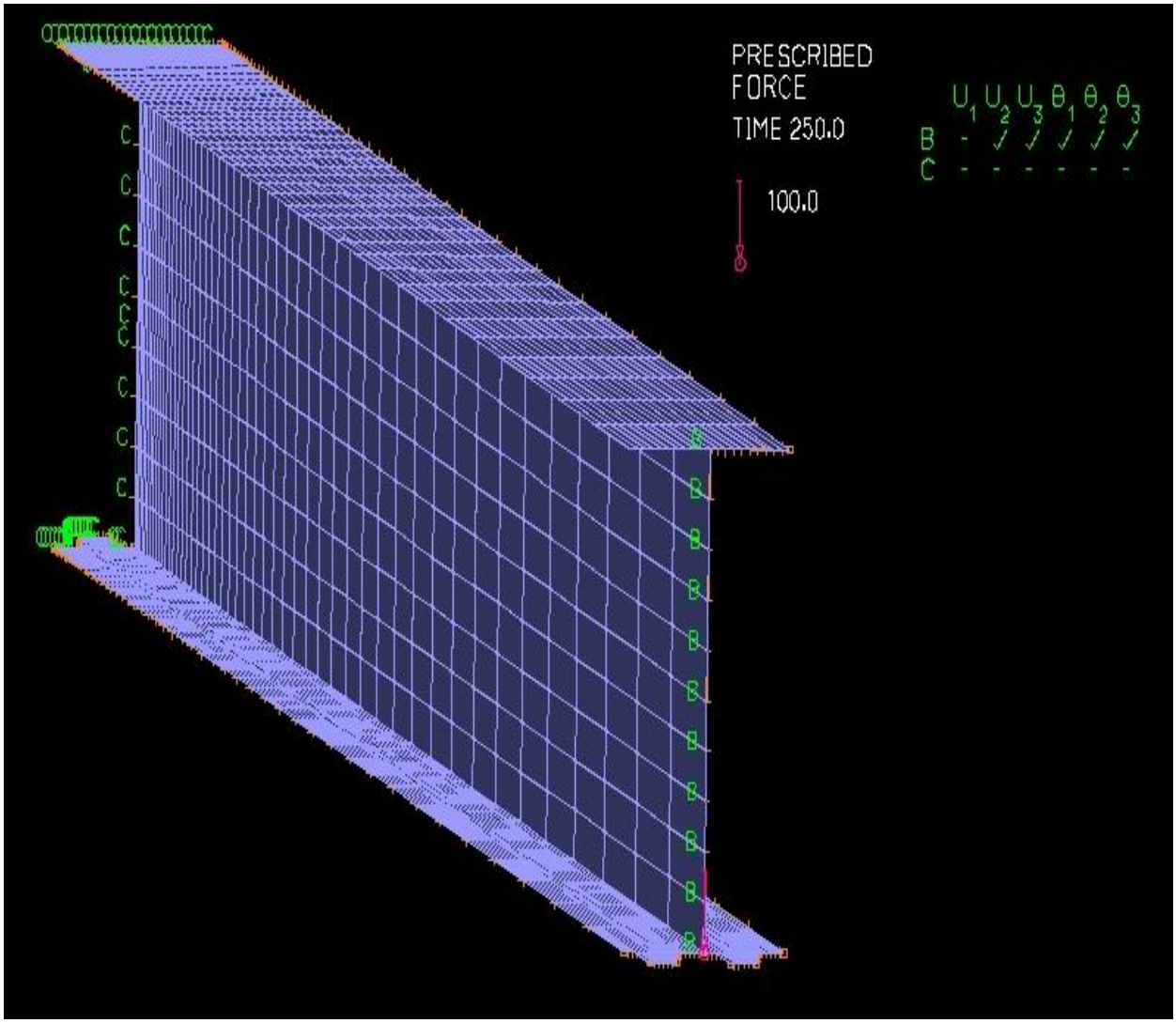

Figure 2.4 Finite Element Model Showing Loading and Boundary Conditions. (Check indicates a free condition)

2.2.2 Verification Study

To verify the accuracy of the ADINA-based nonlinear finite element modeling approach used in the current work, a validation study was conducted using a previously performed lab test found in the literature. Since both geometric and material nonlinearity are being considered in the present study, the lab test selected for the validation study had to involve significant nonlinear behavior in both of these domains. The experimental study selected from the literature for use in this regard was conducted by Lay and Galambos in 1965 at Lehigh University (Lay and Galambos, 1965). The test specimen from the study considered in the validation portion of the present study was specimen HT-28; a simply supported A242 8B13 I-section. The specimen was 1.473 m (58") long and was loaded at its midpoint with a concentrated load reaching 203 kN (45.6 kips) in magnitude. Lateral bracing and stiffeners were placed at the end-points and mid-point of the beam. The lab test beam layout can be seen in Figure 2.5. The dimensions of the beam are shown in Table 2.3.

The verification model was created using the ADINA finite element software system. The model was created using the nominal geometric proportions of the 8B13 shape used in the physical test. The simply supported boundary conditions were modeled using a pin and a roller condition by constraining a line of nodal points spanning the bottom corner of the lower flange (measured width-wise) to be: fixed against translation in all degrees in all of the global directions, and all but in the longitudinal direction; respectively. The finite element model was braced laterally against out of plane movement at both ends and at the mid-point of the beam as was done in the lab test. The load was applied using a line load imposed width-wise across the top flange to the element nodes. The material properties of the beam used in the test were

simulated in the model by directly inputting an idealization of the stress-strain relationship for the A242 steel that was employed in the experimental study. This idealized stress-strain relationship was calculated through a multi-step process. First, the known stress and strain values for critical points in the A242 steel stress-strain relationship, that were reported on in the literature, were used to created an idealized engineering stress-nominal strain plot for the steel. The ADINA program requires that stress-strain information inputted in to the program must be in true stress and logarithmic strain format. To convert engineering stress and nominal strain to true stress and logarithmic strain two equations must be used. Equation 2.1 converts engineering stress to true stress and equation 2.2 converts nominal strain to log strain.

$$\sigma_{true} = \sigma_{nom}(1+\varepsilon_{nom}) \tag{2.1}$$

$$\varepsilon_{ln} = \ln(1+\varepsilon_{nom}) \tag{2.2}$$

Stiffeners, modeled using MITC4 shell elements and the same material properties as the beam, were placed at the end-points and mid-point of the beam. The stiffeners were modeled with a 6.35 mm (.25") plate thickness. Figure 2.6 shows a graphical depiction of the model used for the validation against the beam physical testing results. Initial imperfections were also imposed on this model using the linearized eigenvalue buckling analysis approach described in the previous chapter.

The results of the lab test compared to the ADINA model analogs are presented in Fig. 2.7. The graphs show moment and rotation values for the beams normalized by dividing the moment by the plastic moment (M_p), and the rotation (θ) by the corresponding rotation at the plastic

moment (θ_p) based on first-order theory. The values of for moment and rotation at each loading time step are taken directly from the ADINA post-processor and the M_p and θ_p values are calculated using equations based on theory. This process is explained in more detail in the results chapter. As the normalized moment-rotation graph shows the ADINA finite element program can accurately and effectively produce results comparable to those found through physical testing.

A simply supported beam test was used to verify the validity of the ADINA modeling program. The verification of the simply supported beams was used as verification for the cantilevered beams in the study, because, in theory the geometry and moment gradient of half of a simply supported beam is similar to that of a cantilever.

Table 2.3 Geometric Properties of Verification Beam.

	d (mm)	b_f (mm)	t_f (mm)	t_w (mm)	**L (m)**
Verification Beam	**202.1**	**101.6**	**6.4**	**6.4**	**1.5**

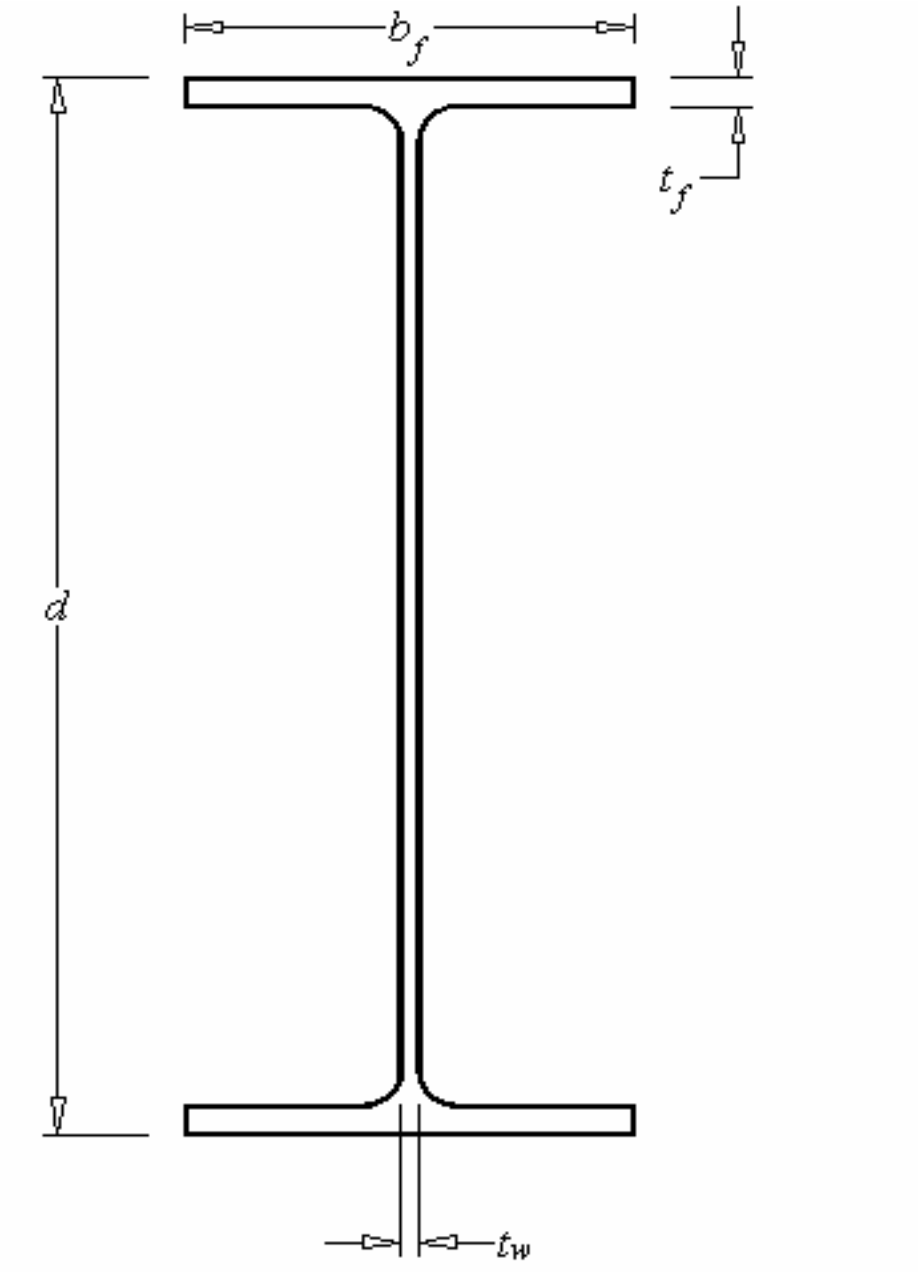

Figure 2.5 Schematic of Geometric Properties of Verification Beam.

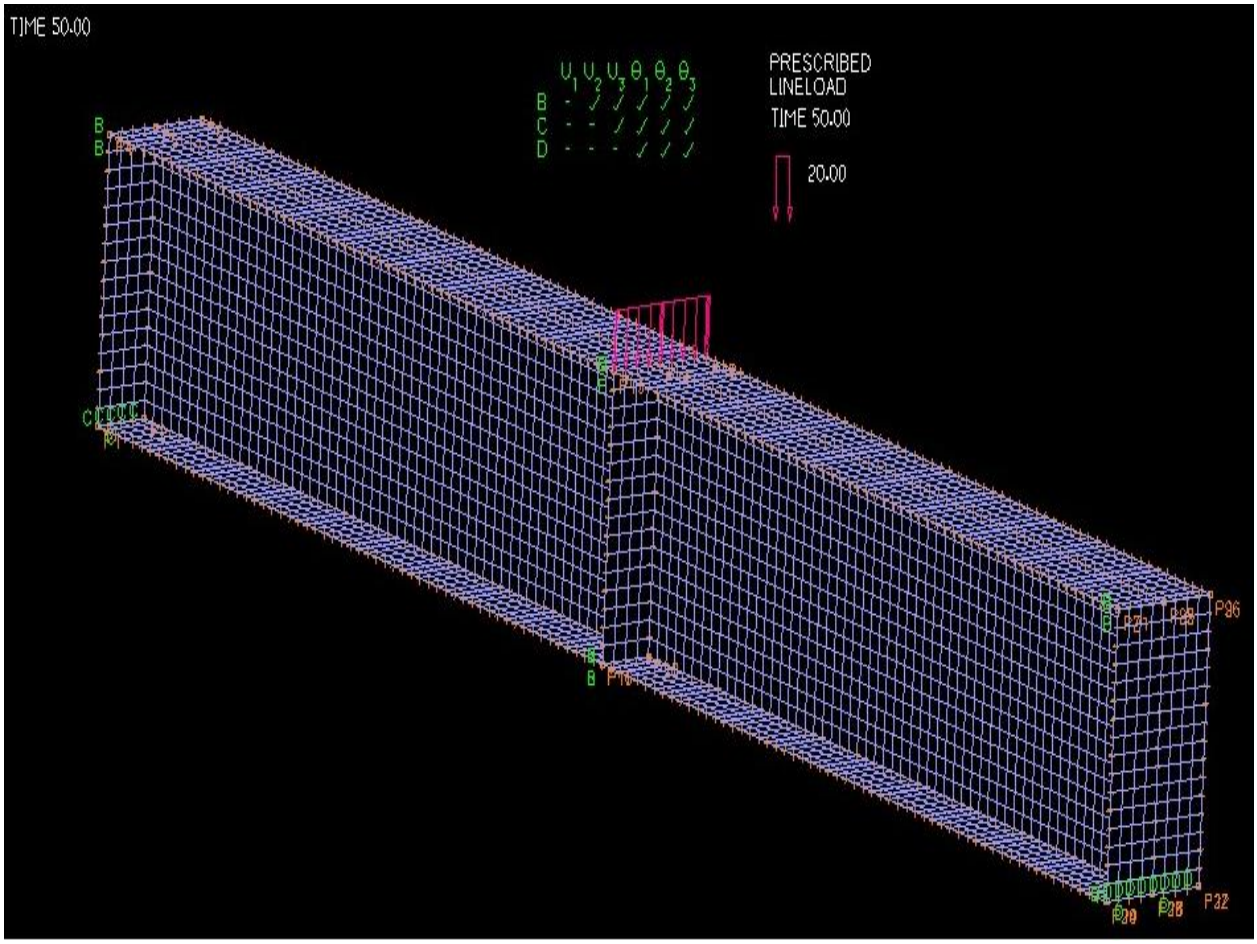

Figure 2.6 Finite Element Model of Verification Beam.

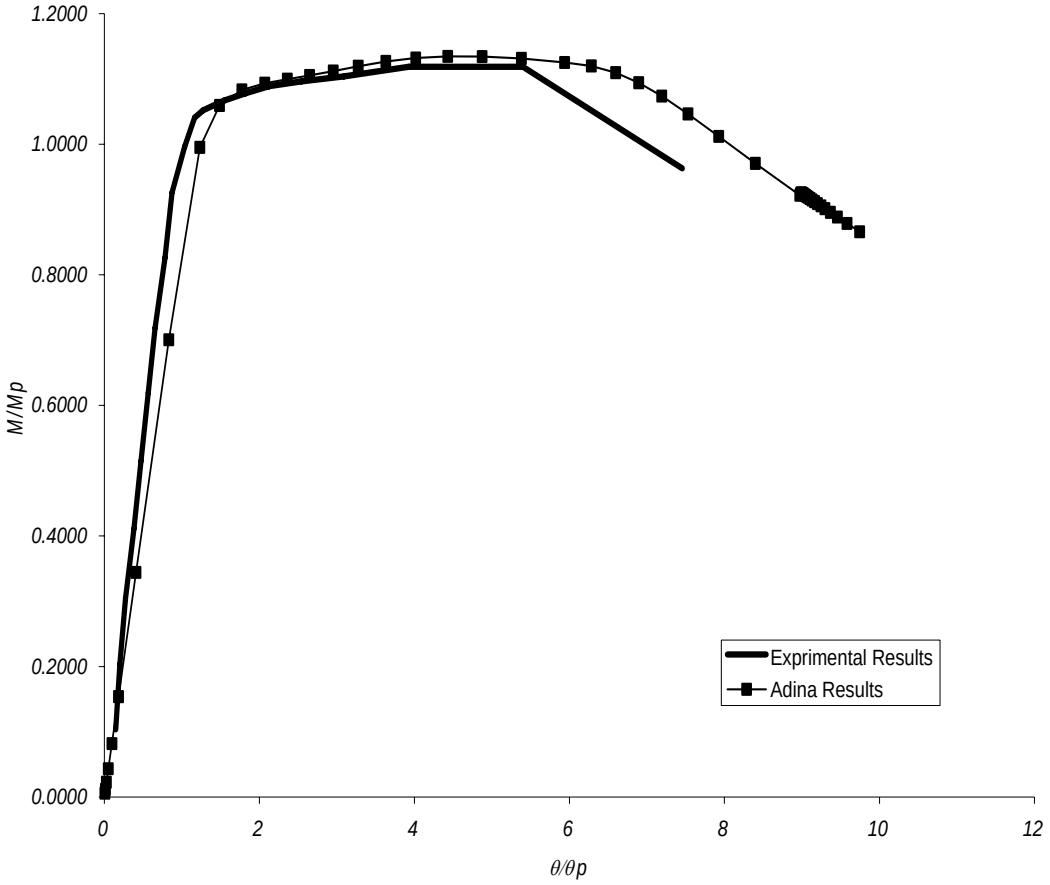

Figure 2.7 Plot Showing the Results of the Verification Study.

3.0 RESULTS

3.1 PRESENTATION OF RESULTS

The results of the study are presented in the form of load-deflection plots and moment-rotation plots. The load-deflection plots represent the concentrated load applied gradually to the free end of the cantilevered beams at the bottom flange-web junction. The deflection values in the plots represent the deflection of these same flange-web junction points. The moment-rotation plots represent the moment and rotation at the fixed end of the cantilevered beam.

Figure 3.1 shows the load-deflection plot for the beams which have a flange thickness of 10.16 mm (0.4”). The bare steel model is plotted with the steel-GFRP models so as to highlight the effects of varying the cross-sectional locations of the GFRP strips. Figure 3.2 shows the load deflection plot of the bare steel model and the models where GFRP strips were positioned at the centerline of the flange outstands while the length of the strips along the longitudinal axis (measured from the fixed end) was varied. Figures 3.6 and 3.7 show the moment-rotation plots for the same beam combinations described above. Figure 3.3 is a plot of a beam with GFRP strips placed along the centerline of the flanges; instead of the strips running full length they extend 1.905 m (75”) longitudinally as measured from the fixed end of the beam (Beam 15). The analysis results from this beam are plotted with the results from a beam which has no GFRP strips added (Beam 30). In place of GFRP strips Beam 30’s compression flange thickness is increased by a factor of 1.5 (15.24 m total thickness); 6”). This section of thicker flange extends for the width of the beam as well as for a length of 1.905 m (75”) longitudinally; as measured from the fixed end of the beam.

Figures 3.4 and 3.5 show the load-deflection plots for Beams 10, 17, 18, 19, 20, 21, 22 and Bare Steel 2. These beams have similar geometrical properties and GFRP strip layouts to the beams described above except their flange thickness is reduced to 5.08 mm (0.2"). Figures 3.8 and 3.9 show the moment-rotation plots for these beams with a flange thickness 5.08 mm (0.2"). The load-deflection plots are created by using the ADINA post-processing program to output response values from the model. To execute this step the node of interest (bottom flange-web junction of the free end of the cantilever) is chosen, and the variables to be listed are chosen (Y-deflection, Y-prescribed force). The ADINA post-processor then returns values for these variables at the given node, for each loading time step. These values are then imported into a spreadsheet program to produce the load-deflection graphs.

The moment-deflection plots are also produced using the ADINA post-processor; as described above. The same Y-prescribed force and Y-deflection values at the same node are used to generate these results. These load and deflection values are then used to find moment and rotation values at each loading time step. Equation 3.1 uses the Y-prescribed force (P) value applied at the free end of the beam, in conjunction with the length of the beam, to calculate the moment experienced at the fixed end of the beam. Equation 3.2 uses the Y-deflection (Δ) value at the free end of the beam, and the length of the beam, to compute the rotation at the fixed end of the beam.

$$M = PL \tag{3.1}$$

$$\Theta = \arctan(\Delta/L) \tag{3.2}$$

The moment and rotation values are then normalized using the plastic moment M_p and the corresponding plastic rotation θ_p. M_p is calculated using equation 3.3.

$$M_p = ZF_y \tag{3.3}$$

where

F_y = 289579.92 kPa (42 ksi); for A36 steel)

$$Z = 2\{t_w[(d/2)-t_f]^2(1-2)+b_f\, t_f(d/2-t_f/2)\} \tag{3.4}$$

θ_p is calculated using Equation 3.5.

$$\theta_p = M_pL/2EI \tag{3.5}$$

where

L = length of beam 3.81m (150")

E = 203395420 kPa (29500 ksi)

$I = 1/12(t_w*(d-2t_f)^3)+1/6(b_f*t_f^3)+2((t_f*b_f)*(d/2)^2)$

From the moment-rotation graphs shown below, the rotational capacity (R) can be calculated for all beams considered in the present work. In plastic analysis the full cross sectional capacity of the beam is able to be utilized through the formation of the plastic hinge. The plastic hinge occurs at the location where the beam cross-section has become fully plastic and can no longer accommodate any increase in applied load. The beam continues to rotate, but the plastic moment (M_p) stays constant. To ensure proper moment redistribution, the beam must be ductile enough

to continue rotation while maintaining the cross-sectional plastic capacity in order for the moment to be redistributed within the context of a statically indeterminate system. A good measure of this ductility is the rotation capacity, which is defined by Equation 3.7.

$$R = \{(\theta_2 / \theta_1) - 1\} \tag{3.6}$$

θ_2 is the rotation when the moment capacity drops below M_p on the unloading branch of the M-θ plot and θ_1 is the theoretical rotation (based on linear elastic theory) at which the full plastic capacity is achieved. Rotation capacity values for the beams tested are tabulated in Table 3.1

Table 3.1 Rotations and Rotational Capacities for Modeled Beams

	θ_1	θ_2	**R**
Bare Steel 1	1	2.2	**1.2**
Test 9	1	6.7	**5.7**
Test 11	1	8	**7**
Test 12	1	8	**7**
Test 13	1	5.1	**4.1**
Test 14	1	4.5	**4.5**
Test 15	1	6.5	**6.5**
Test 16	1	4.7	**3.7**
Bare Steel 2	1	1.1	**0.1**
Test 10	1	4.6	**3.6**
Test 17	1	5.7	**4.7**
Test 18	1	6.5	**5.5**
Test 19	1	3.7	**2.7**
Test 20	1	3.5	**2.5**
Test 21	1	4.3	**3.3**
Test 22	1	2.8	**1.8**
Test 30	**1**	**7**	**6**

The ADINA finite element analysis program creates porthole files which can be used to view the modeled beams during and after testing. The beams can be viewed at each loading time step

to give an idea of the physical behavior of the beam during the loading process. This post-processor also allows band plots to be created to illustrate stress, deflection, etc., in a graphical context.

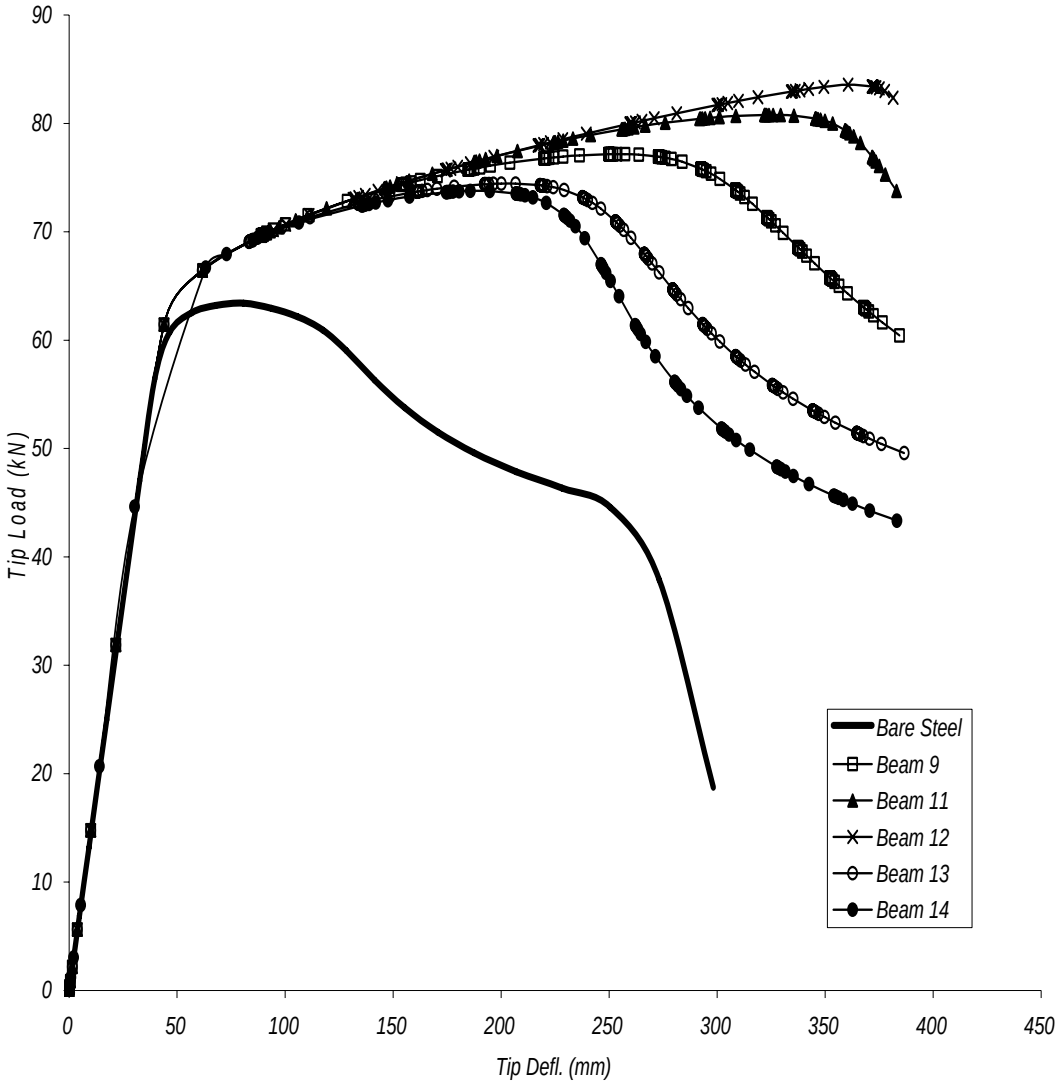

Figure 3.1 Load-Deflection Plot Showing Results as GFRP Strips are Moved Along the Width of the Compression Flange. ($t_{f=}$ 10.16mm)

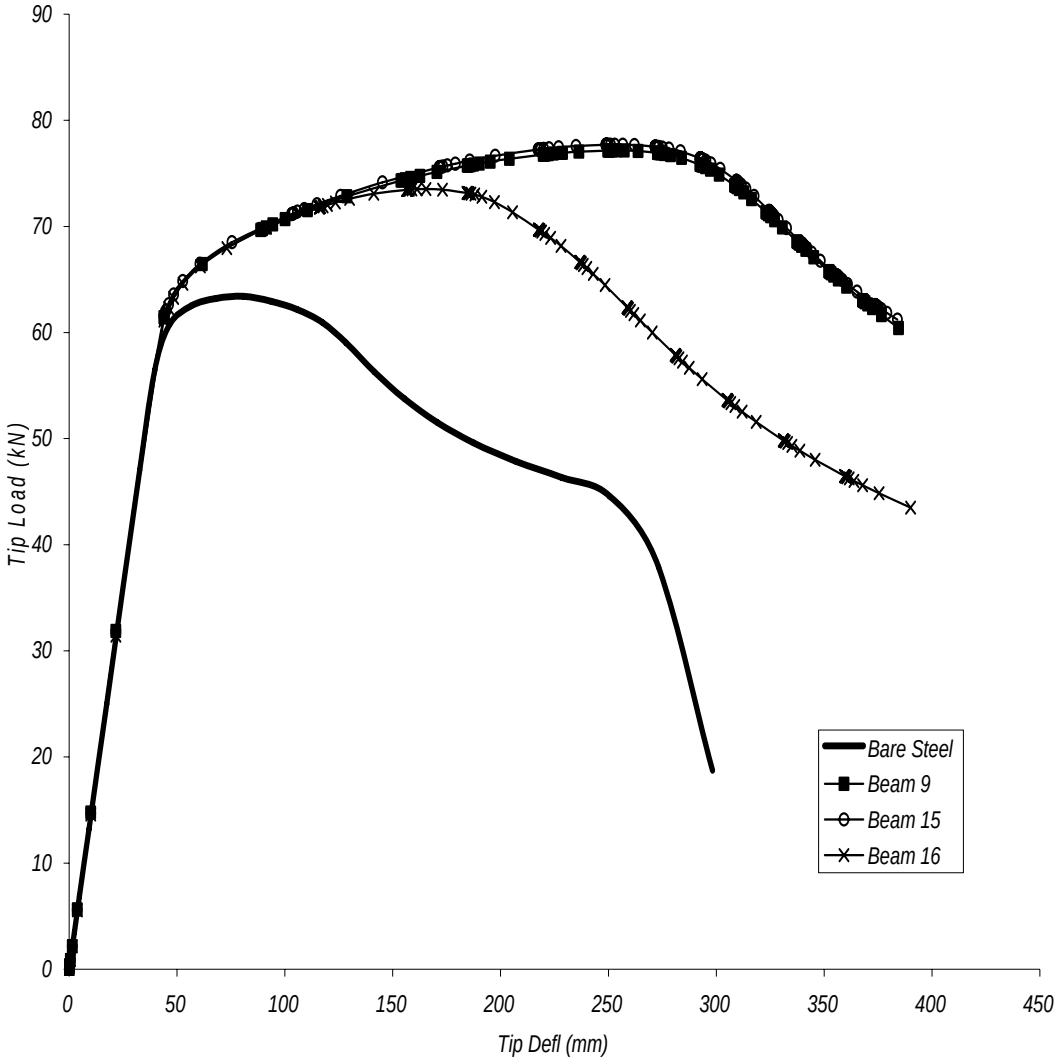

Figure 3.2 Load-Deflection Plot Showing Results as GFRP Strip Longitudinal Lengths Are Varied Along the Compression Flange. ($t_{f=}$ 10.16 mm)

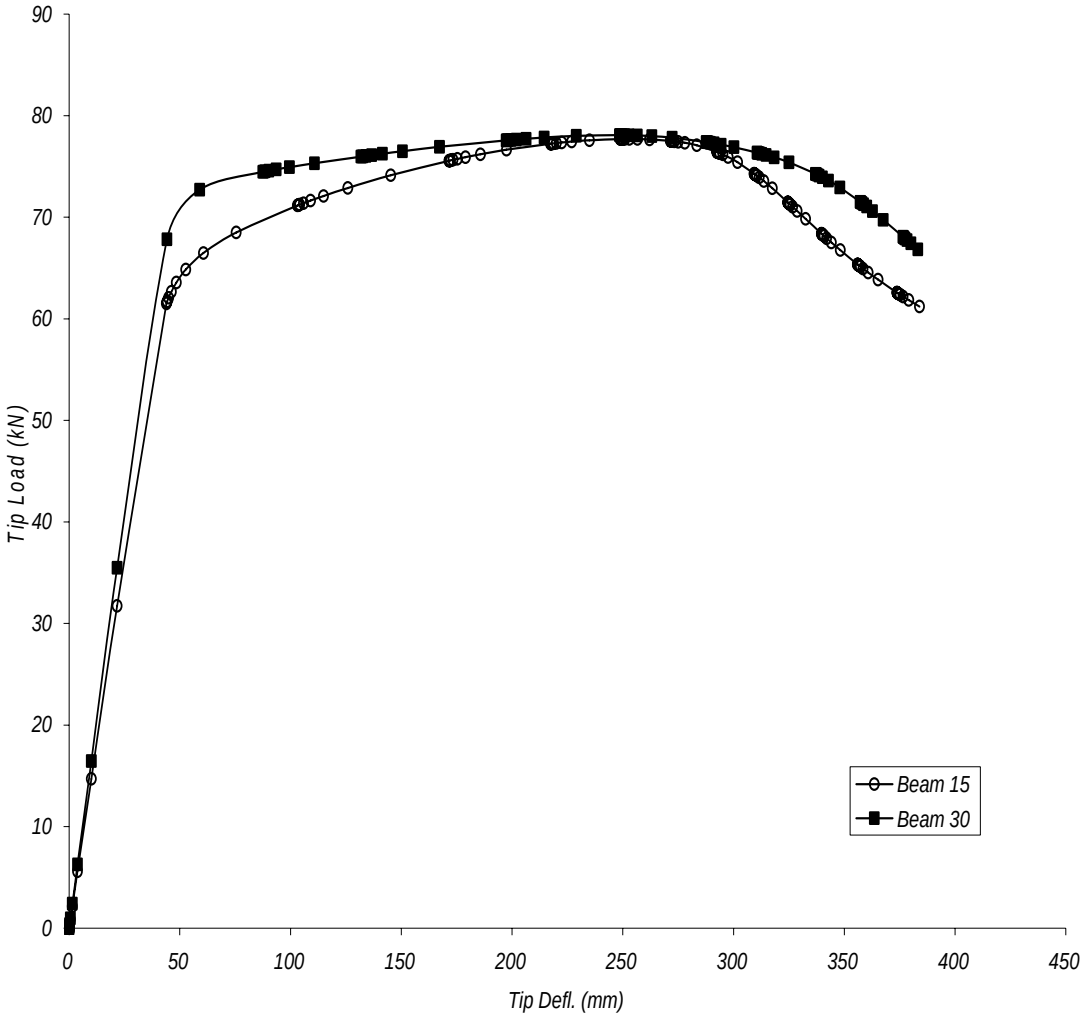

Figure 3.3 Load-Deflection Plot Showing Similarities Between A Beam With GFRP Strips and A Beam With An Increased Compression Flange Thickness.

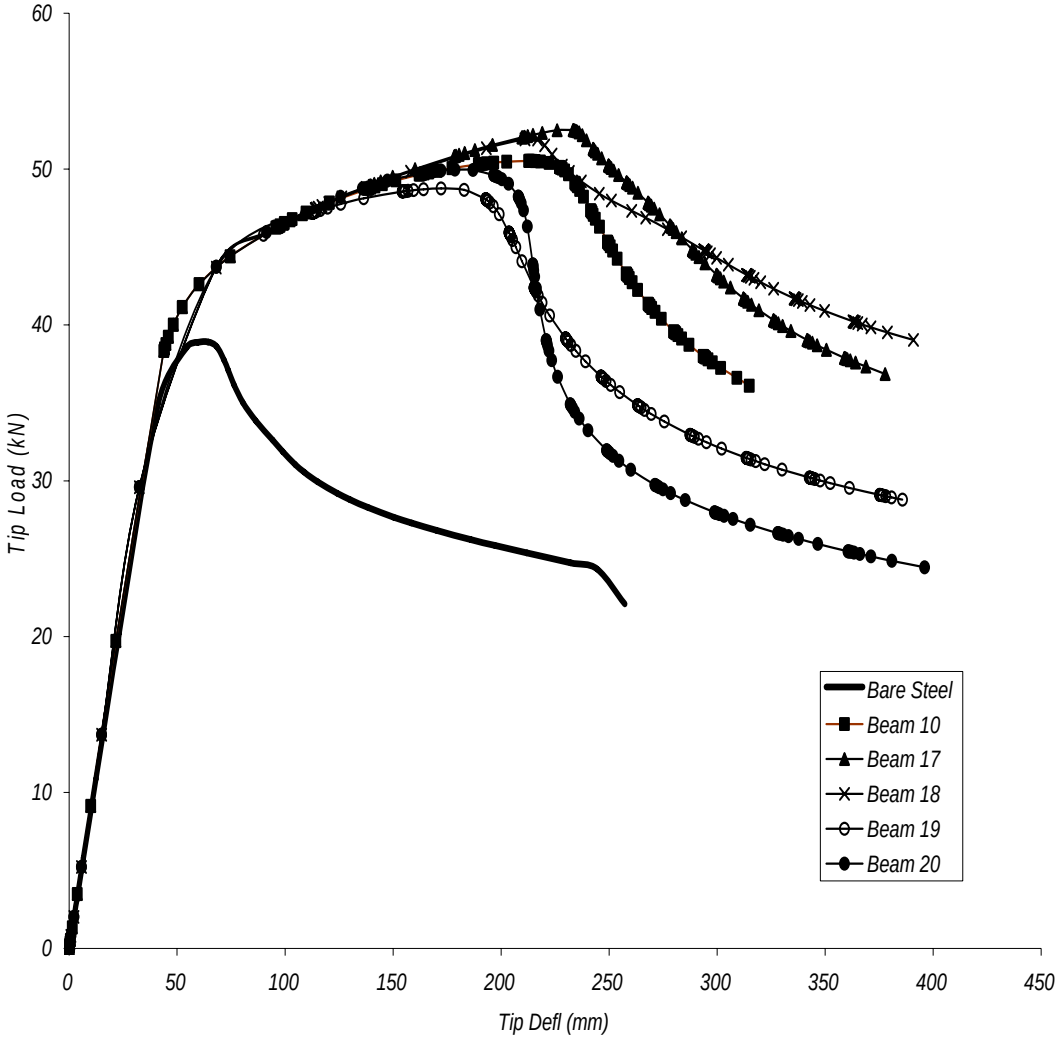

Figure 3.4 Load-Deflection Plot Showing Results as GFRP Strips are Moved Along the Width of the Compression Flange. (t_f = 5.08 mm)

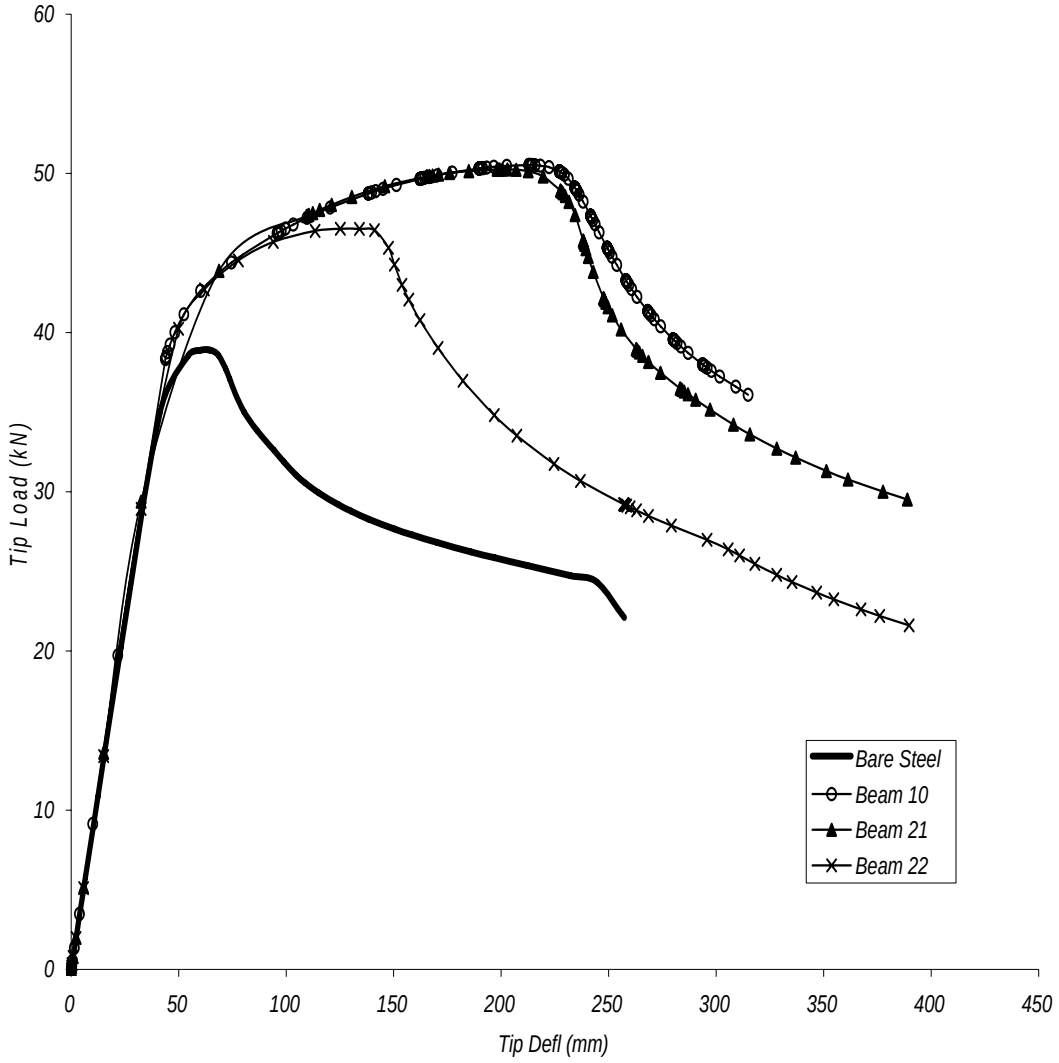

Figure 3.5 Load-Deflection Plot Showing Results as GFRP Strip Longitudinal Lengths Are Varied Along the Compression Flange. (t_f = 5.08 mm)

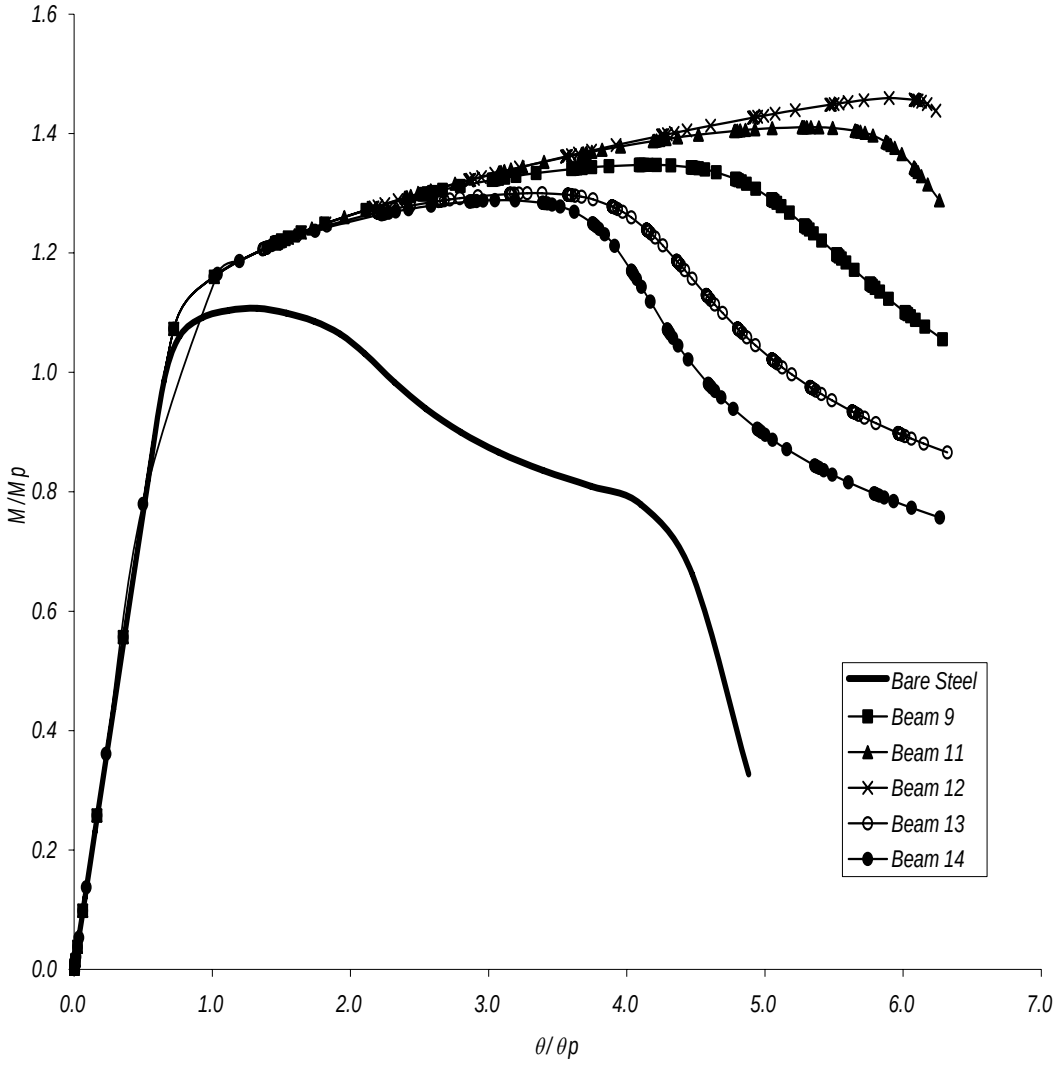

Figure 3.6 Moment-Rotation Plot Showing Results as GFRP Strips are Moved Along the Width of the Compression Flange. ($t_{f=}$ 10.16 mm)

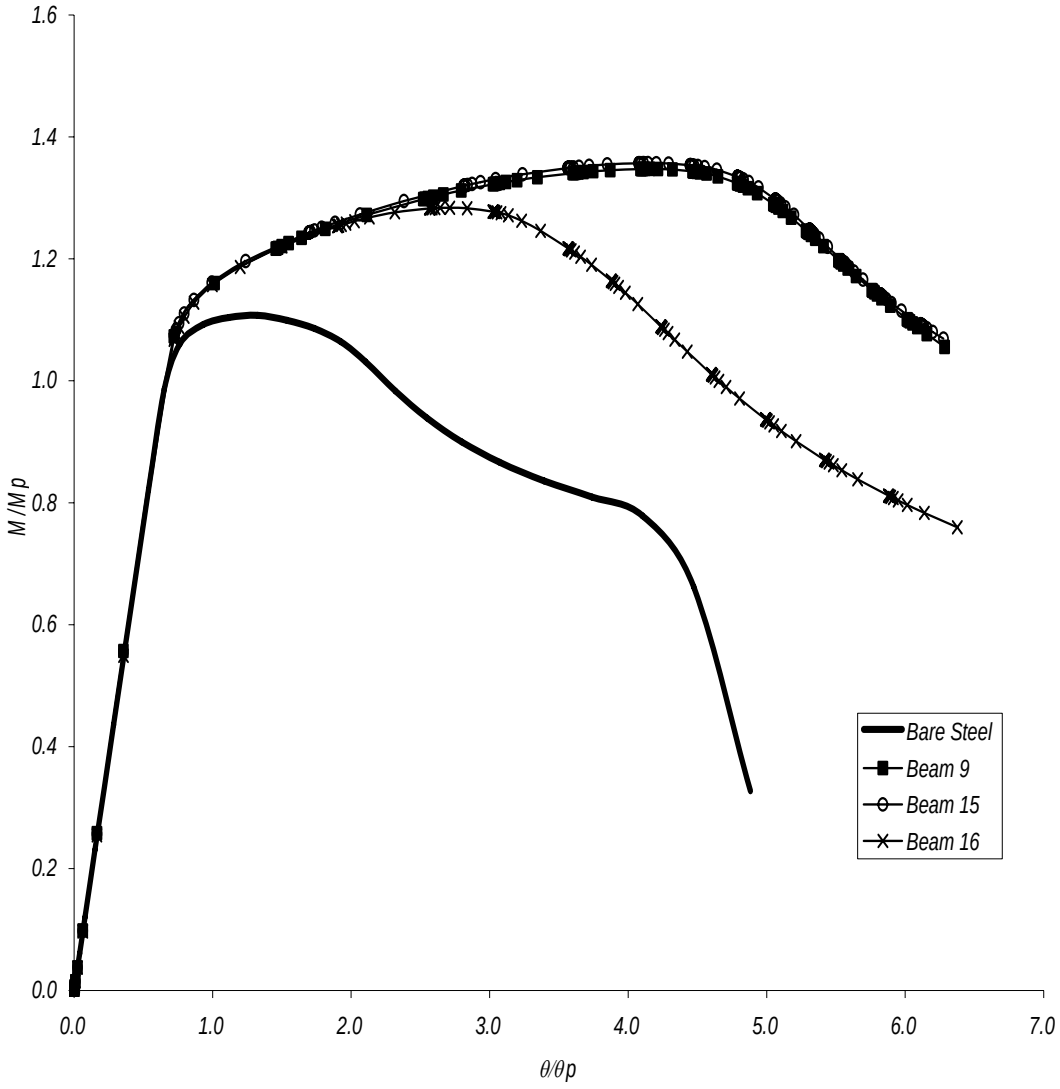

Figure 3.7 Moment-Rotation Plot Showing Results as GFRP Strip Longitudinal Lengths Are Varied Along the Compression Flange. ($t_{f=}$ 10.16 mm)

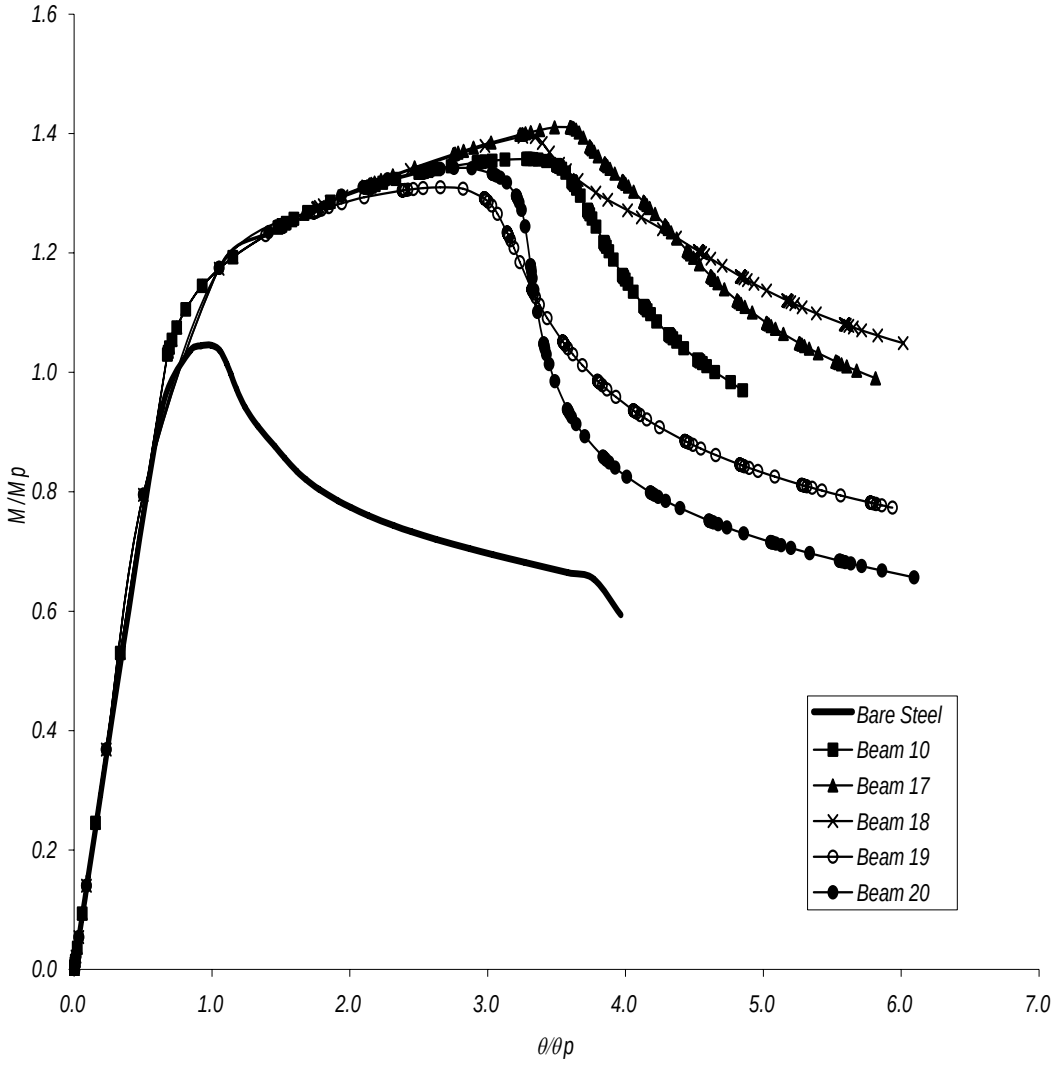

Figure 3.8 Moment-Rotation Plot Showing Results as GFRP Strips are Moved Along the Width of the Compression Flange. (t_f = 5.08 mm)

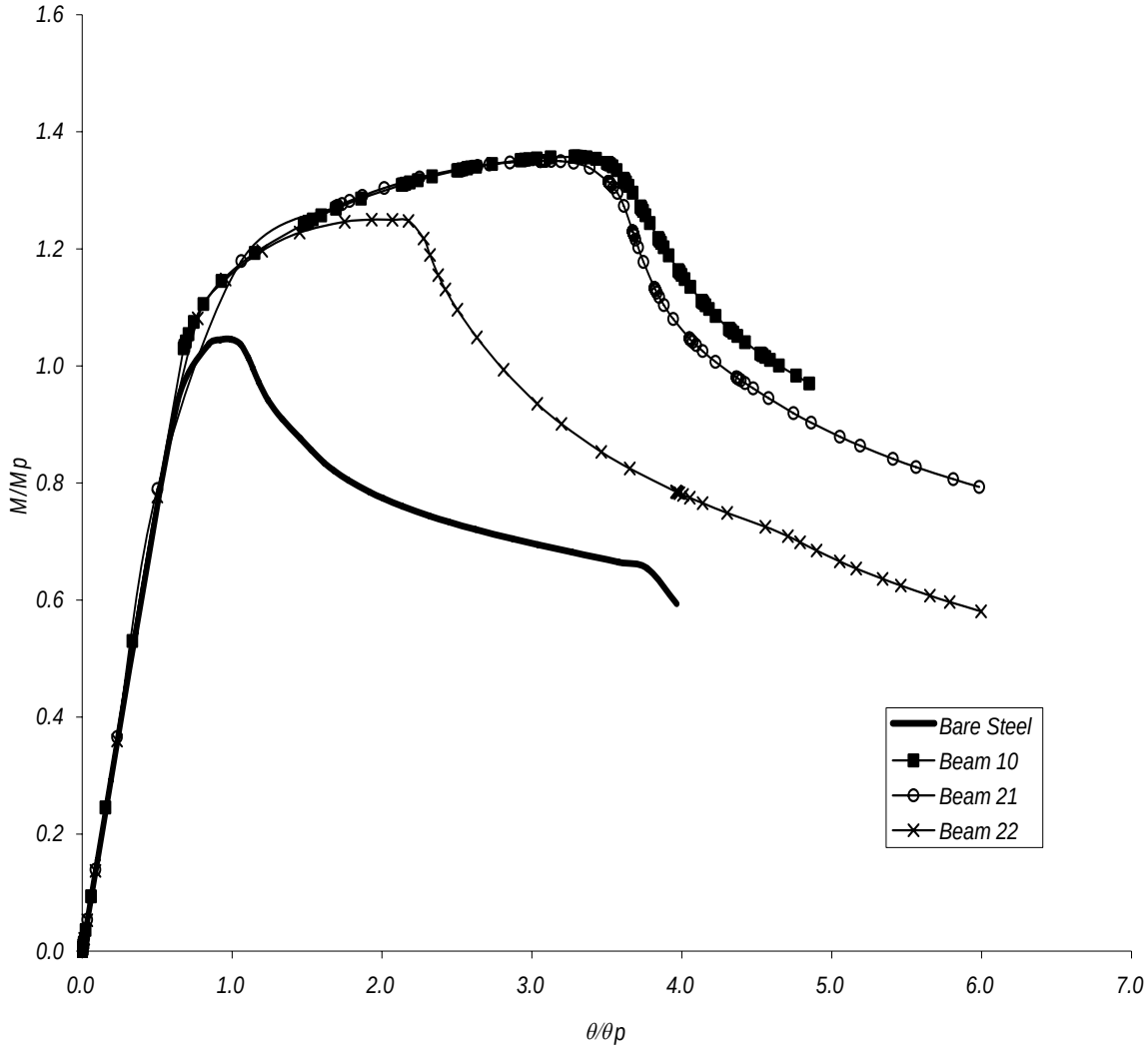

Figure 3.9 Moment-Rotation Plot Showing Results as GFRP Strip Longitudinal Lengths Are Varied Along the Compression Flange. ($t_{f=}$ 5.08 mm)

Figures 3.10-3.13 depict Beam 9 in four different views, all of the views show the beam at the load step where unloading begins. Figure 3.10 depicts the meshed beam in a view that looks from the bottom of the beam (i.e. looking up at the compression flange) down the length of the beam. Figure 3.11 show an elevation view of the mesh beam with a band plot superimposed which depicts the effective stress (i.e. von Mises stresses) in the beam. Figure 3.12 shows a closer view of the region of the plastic hinge, where the stress in the GFRP, interface material, and steel can all be seen. Figure 3.13 shows a view looking down on the bottom of the beam where the stresses in the GFRP can be seen. The views described above, for all of the beams used in the current research project, can be found in Appendix A. The legend depicting the intensity of the effective stresses in the beam is show in Figure 3.11. This legend holds true for Figures 3.12 and 3.13. Likewise the Figures in Appendix A have a representative legend displayed on the first effective stress band plot of each beam.

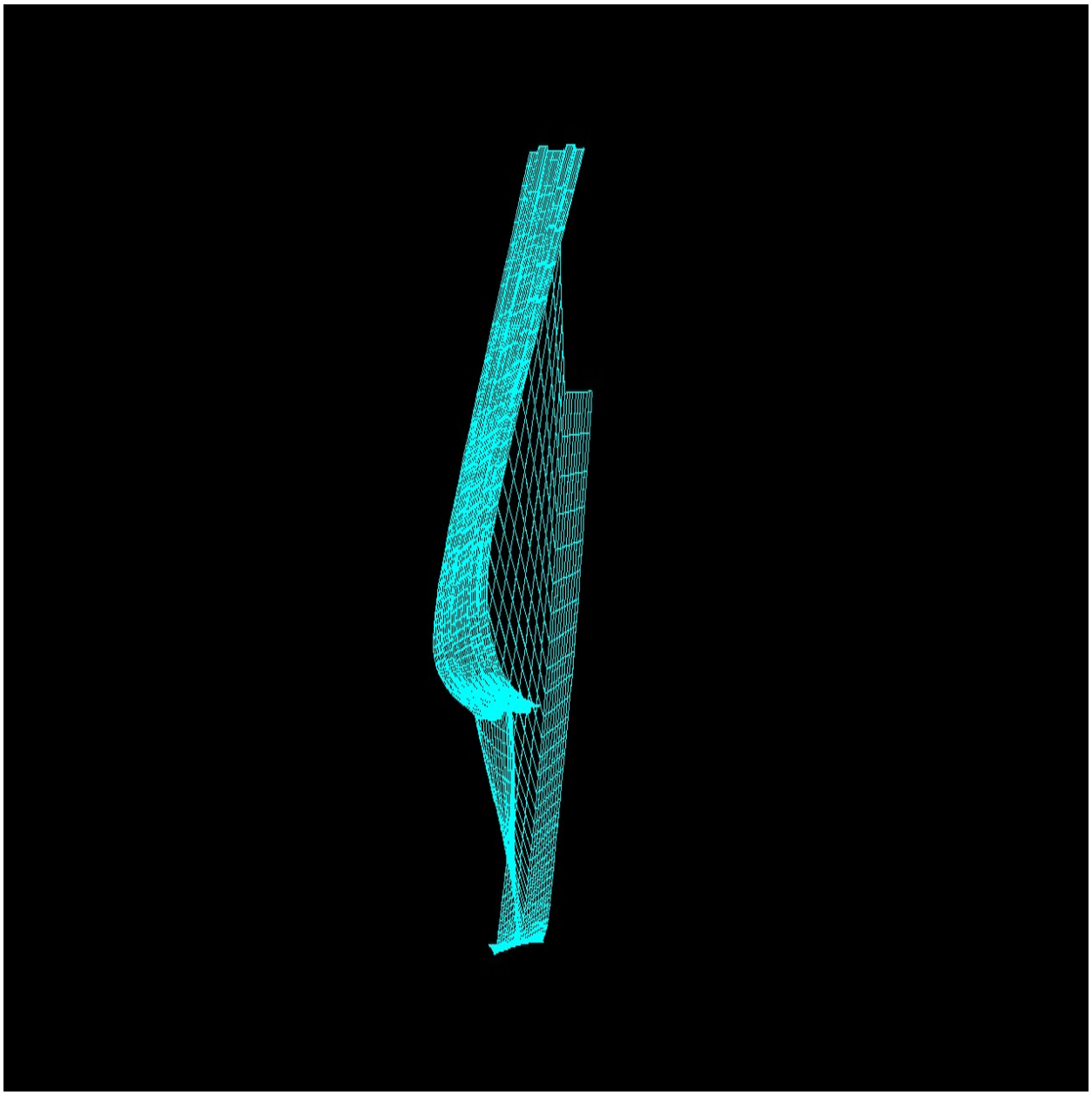

Figure 3.10 Depiction of Deflection and Twist of Beam 9. (Fixed End Forground)

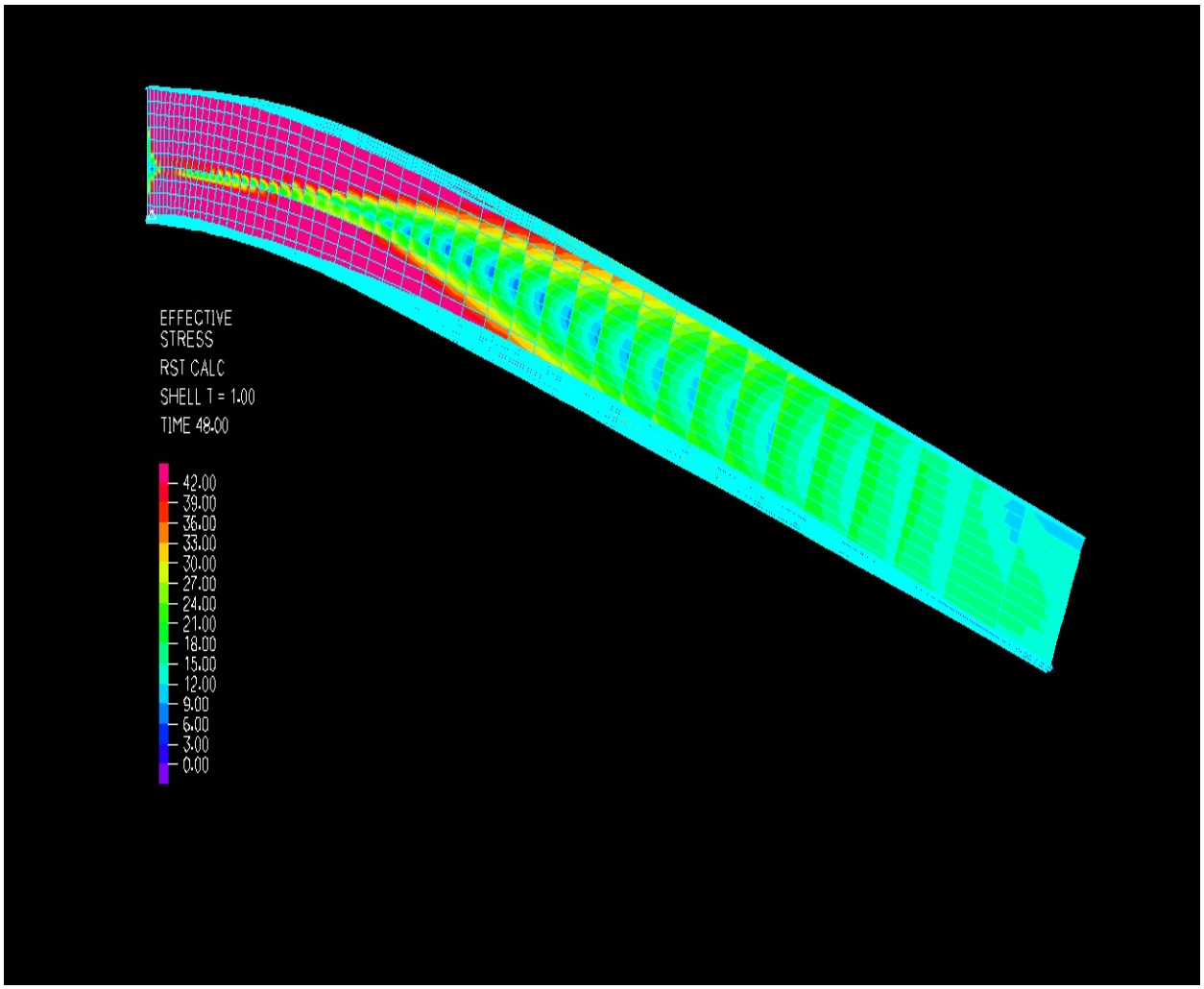

Figure 3.11 Depiction of the Effective Stress on Beam 9.

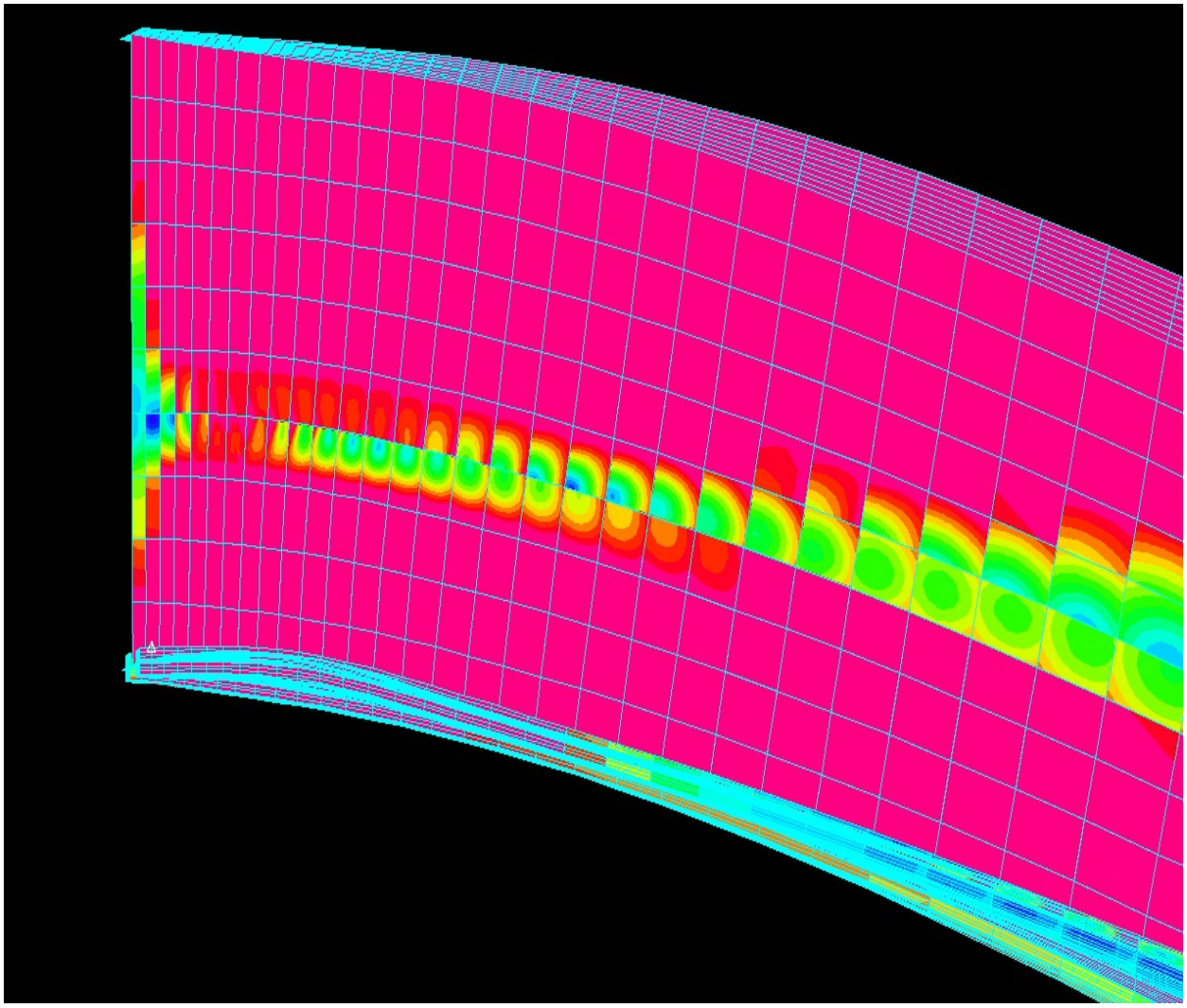

Figure 3.12 Depiction of the Effective Stress in the Plastic Hinge Region of Beam 9

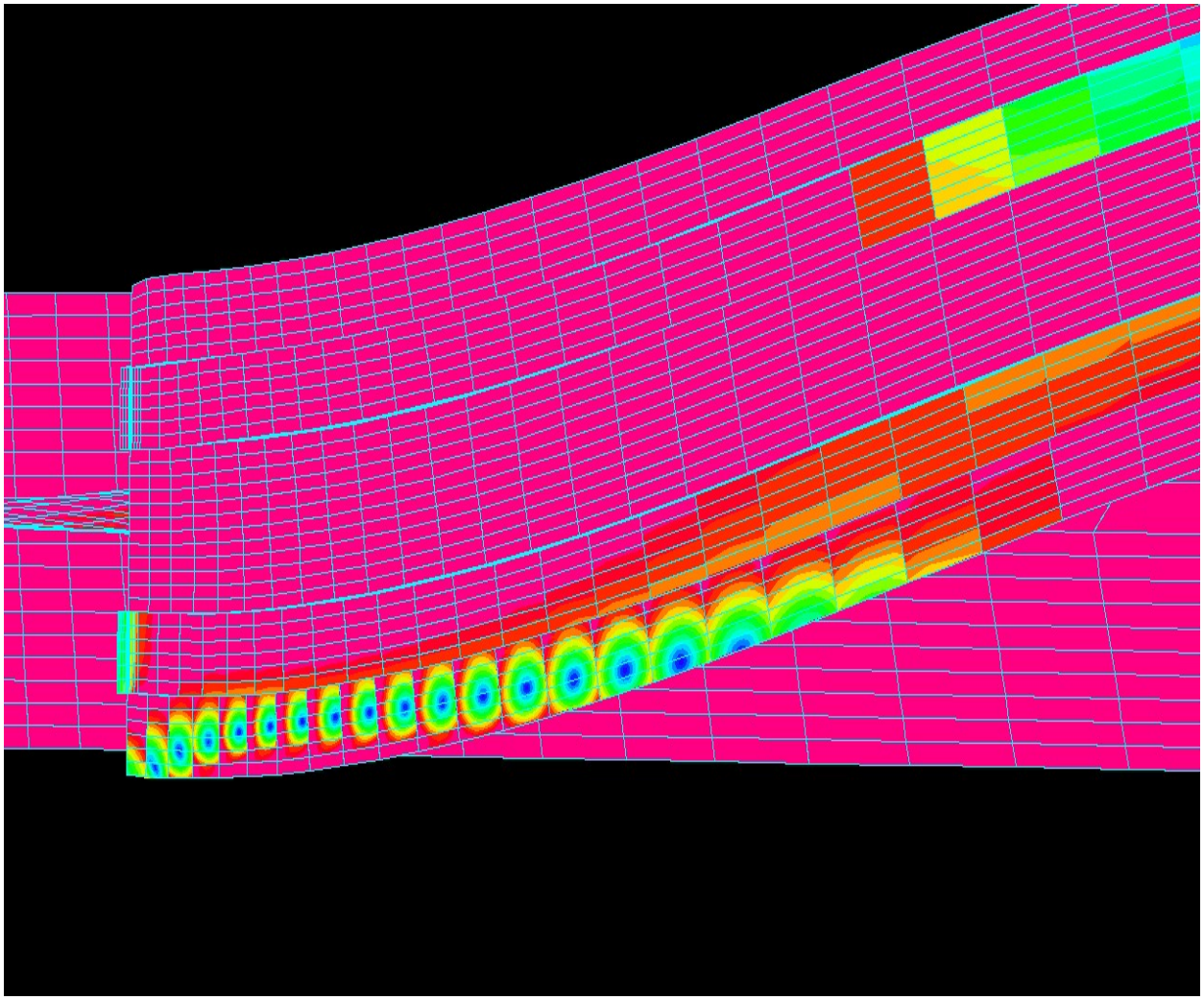

Figure 3.13 Depiction of the Effective Stress in the Bottom of the Compression Flange and GFRP Strips of Beam 9.

4.0 DISCUSSION

The results presented in Chapter 3 show significant improvements in the structural behavior of steel beams with the addition of GFRP strips to the compression flange. The GFRP reinforced steel beams modeled in the research show improvement in strength and, especially, ductility compared to bare steel beams.

4.1 PHYSICAL BEHAVIOR

The bare steel beams modeled in the current research display a much different physical behavior than that of the GFRP reinforced steel beam models. The bare steel models for both the 10.16 mm and 5.08 mm flange widths experienced severe compression flange local buckling in the plastic hinge region of the beam. The onset of the local buckling in the compression flange prompted local buckling in the adjacent web-portion in compression. However, the bare steel beams did not experience significant lateral deflections in the compression flange. This is precisely the opposite behavior from what was displayed in the GFRP reinforced cases as discussed subsequently. The behavior of the bare steel models can be seen in Figures A1-A4 and Figures A33-36 of appendix A. The stress band plots of these bare steel models show that the beam cross section material response is fully plastic indicating a phenomenological agreement with the notional idealization of a plastic hinge. The stress band plots also show that the stress in the beam outside the region of the plastic hinge is significantly lower; once again supporting the theoretical assumption of finite plastic hinge articulation while the rest of the member displaces largely as a rigid body.

The GFRP reinforced members with 10.16 mm flange widths and full length GFRP strips (Beam 9, Beam 11, Beam 12, Beam 13, and Beam 14) exhibited much different physical

behavior during loading (Figures A5-A24). These beams did not experience local buckling; throughout the analyses of these cases, no sign of local buckling was observed in the GFRP reinforced beams. At loads approaching ultimate, the beams began to deflect laterally and twist (as the Figures 3.10-3.13 indicate). The stress plots of these GFRP reinforced beams show that a significant elastic core exists proximally with the neutral axis. This core zone of elasticity persists throughout the test indicating that a constrained plastic hinging is occurring with a dominant flexural response persisting. In the case of the bare steel beam a more uniformly distributed zone of plasticity developed throughout the beam (as seen in the band plots) as a result of the flexural nature of the problem being destroyed by the decaying cross-sectional integrity accompanying large compression flange local buckling deformations. The band plots associated with the GFRP reinforced models also show that the neutral axis of the beam is shifted down, towards the GFRP reinforced compression flange, as would be expected in a case where significant structural benefit were derived from a reinforcing strategy.

Beam 15 (GFRP strips on half of the beam length) displays physical behavior very similar to that of the beams with full length GFRP strips (Figures A25-A28). Beam 16 (GFRP strips .762m (30") long) has similar behavior to the other GFRP reinforced beams for early loading. However as loads get higher, a plastic hinge begins to form in the area where the GFRP strips end (FiguresA29-A32). Tests with GFRP strip lengths between those in Beams 15 and 16 also failed to match the performance of Beam 15 (not shown). These beams are thus acting in a fashion consistent with a reduced beam section (RBS) moment connection approach sometimes achieved with so-called "dog-bone" compression flange width reduction strategies used to force plastic hinges, and their concomitant ductility demands, away from column faces in moment frame connections. This is a very interesting response feature to note.

Bare Steel 2, the bare steel model with 5.08mm flange thickness, exhibits behavior similar to that of the more compact bare steel model (Figures A33-A36). The beam forms a plastic hinge and local buckling of the compression flange and web take place within the zone of the plasticity associated with hinge formation. Very little lateral movement of any portion of the beam cross-section is observed. The beams with 5.08 mm (0.2") flange thickness and full length GFRP strips (Beams 10, 17, 18, 19, and20) show a combination of the behaviors seen in the bare steel models and the more compact sections. The beams begin to undergo moderate compression flange local buckling and lateral buckling of the compression flange dominates the response at ultimate (as seen in Figures A37-A56).

The two beams with 5.08 mm (0.2") flange thicknesses and GFRP strips not running full length (Beams 21 and 22) exhibit behavior similar to the respective more compact sections with similar reinforcement (Figures A57-A64). Beam 21 displays behavior nearly identical to the full length GFRP strip models. Beam 22 shows early behavior similar to the other beams but begins to fail locally at the end of the GFRP strip region as loads increase.

The physical behaviors of the beams seen in the post-processing figures produced by ADINA indicate significant improvements with the addition of the GFRP strips. In the more compact sections (10.16 mm flange thickness) the bare steel model is observed to experience local buckling of the compression flange and web. The addition of the GFRP strips to these beams appears to brace the compression flange against local buckling, forcing the beam into a higher buckling mode, which appears to be similar to lateral-torsional buckling in nature.

The beams with 5.08 mm flange thickness show local buckling of the compression flange in the bare steel model. The addition of the GFRP strips reduces the severity of the local buckling while introducing moderate lateral buckling. This behavior indicated that the GFRP strips are

bracing against true local buckling and forcing the beam into a combination mode involving both local and lateral-torsional buckling.

4.2 LOAD-DEFLECTION PLOTS

The load-deflection plots gleaned from the current finite element modeling effort show that a higher ultimate load is achieved with the addition of GFRP strips to the bare steel (Figures 3.1-3.5). In addition the plots indicate that the effectiveness of the GFRP reinforcing can be optimized by strategic placement and sizing of the GFRP strips.

Both sets of beam flange thicknesses tested showed similar trends in the load-deflection and moment-rotation plots with the more compact beams (10.16 mm flange thickness) simply shifted to higher force values than the beams with 5.08 mm flange thicknesses.

The improvements in ultimate load resulting from the GFRP reinforcing strategy, as observed in both sets of beams, were significant. As Figure 3.1 and 3.4 indicate, all of the beams reinforced with full length (3.81 m) GFRP strips showed large ultimate strength gains in comparison to the associated bare steel model. The plots show that the strength improvements increased as the GFRP strips moved outward toward the flange tips. The beams with GFRP strips closest to the web showed the smallest ultimate strength gains while the beams with GFRP strips aligned with the flange tips showed the greatest improvements. Table 4.1 shows the increase in ultimate load (as a percentage) for each modeled beam; as compared to the associated bare steel models.

Table 4.1 Ultimate Load and Increase in Ultimate Load (%) Compared to Bare Steel.

	Ultimate Load (kN)	**% increase**
Bare Steel 1	64	**-**
Beam 9	77	**20**
Beam 11	81	**27**
Beam 12	84	**31**
Beam 13	75	**17**
Beam 14	74	**16**
Beam 15	77	**20**
Beam 16	73	**14**
Bare Steel 2	39	**-**
Beam 10	50	**28**
Beam 17	52	**33**
Beam 18	52	**33**
Beam 19	49	**26**
Beam 20	49	**26**
Beam 21	50	**28**
Beam 22	47	**21**
Beam 30	**78**	**22**

The increase in effectiveness in bracing against local buckling modes, as the GFRP strips are moved toward the flange tips, is consistent with manifestation of compression flange local buckling (Figures 3.1 & 3.4). In the bare steel models the compression flange local buckle

evolved in the classical form of a sinusoidal wave. In such a buckling mode, the maximum deflection and intensity of the wave occurs at the flange tips. The introduction of the GFRP strips to the steel beam effectively imposes nodal line bracing along the longitudinal axis of the strips coinciding with the given cross-sectional position assumed along the flange outstands. The closer this bracing can be applied to the point of maximum intensity of the local buckling, the more effectively it can control or arrest it. Therefore, the GFRP strips placed closest to the flange tips are most effective in bracing against local buckling and therefore provide the greatest ultimate strength gains.

The models tested with GFRP strips placed at the center of the flange widths, and with GFRP strip lengths of .762 m (Beams 16 and 22) and 1.905 m (Beams 15 and 21), also showed similar behavior for both flange thicknesses. The load-deflection plots (Figures 4.2 & 4.5) indicate that the beams reinforced with 1.905 m GFRP strips behaved nearly identically with the similar beams possessing full length GFRP strips. The beams with .762 m GFRP strips performed better than the bare steel models but failed to achieve the same improvements of the half and full length strips.

These results indicate that the GFRP strips of length 1.905 m are of sufficient length to effectively brace the beam against local buckling; presumably because of the fact that the stresses in the beam are comparatively low at the length were the strips stop. The .762m GFRP strips, however, are able to brace against local bucking initially but as stresses are redistributed the stresses at the location where the GFRP strips end are too great and thus the beam undergoes local buckling at this point.

4.3 MOMENT-ROTATION PLOTS

The moment-rotation plots presented in the previous chapter provided data which allowed for the calculation of rotational capacity values (R). The rotational capacity values are significant because they are a measure of the beam's ductility in a structural sense (i.e. the beam's ability to undergo large plastic hinge rotations while maintaining a significant load carrying capacity). Improvements in ductility with the addition of GFRP strips will allow the beam to more effectively redistribute moment within the statically indeterminate structure by virtue of the beam being able to sustain continued plastic hinge rotation while maintaining a strength greater than the plastic moment, M_p.

As described in previous chapters the calculation of R values is performed using Equation 3.6. Theoretically, the value of θ_1 should equal one due to the fact that at the point where the plastic moment (M_p) is achieved, the corresponding θ_p value should also be reached by definition. This is illustrated in Figure 4.1. However, since the model beams are cantilever beams their true rotation is difficult to calculate due to the nature of the fixed boundary conditions and as a result the modeled beams appear stiffer than they truly are giving $\theta_p < 1$ when $M_p = 1$(Seen in Figures 3.6-3.9). Therefore, the rotational capacity values given in table 3.1 are calculated by conservatively using the value of $\theta_p = 1$. The values for Beam 11 and Beam 12 are estimated because their tests ended before a value of θ_2 was reached as a result of the very large structural ductility observed by these cases.

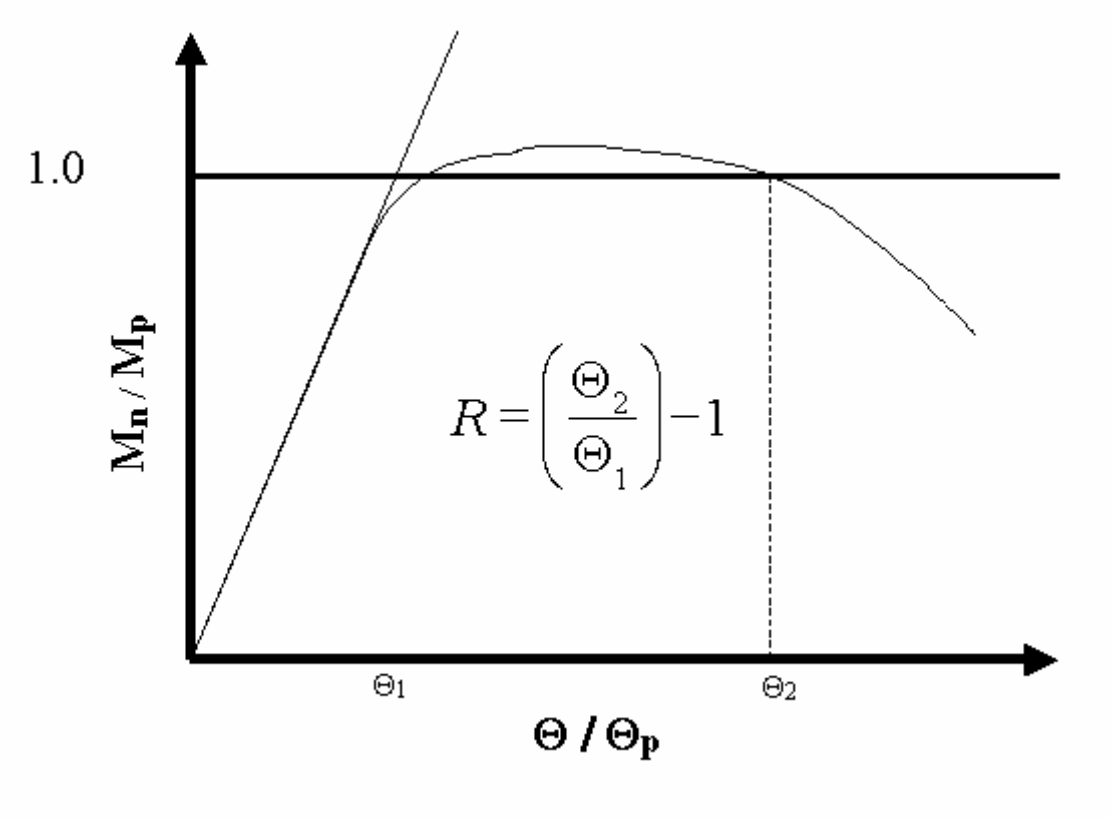

Figure 4.1 Plot of Normalized Theoretical Moment-Rotation Curve.

The results of the rotational capacity values found in Table 3.1 show that significant improvements were made in the rotational capacity of all test beams that employed the current strategy for the use of GFRP strips. The rotational capacity values follow the same trends seen in the load-deflection improvements. The improvements are greater the closer the GFRP strips are placed to the flange tips. The improvements are nearly identical for the 1.905 m long strips and full 3.81 m strips; while the .762 m strips showed improvement over bare steel but failed to achieve the results of longer strips. The apparent causes of these trends are fully described in section 4.2.

4.4 BEAM 30

The addition of GFRP strips to the compression flange of a cantilevered beam has been shown to improve the beam's structural behavior by bracing against local buckling and improving ultimate strength and ductility. The imposition of the GFRP strips should, in effect, give the same behavior as would be realized if the thickness of the compression flange of the member were to be increased so as to eliminate local buckling. To test this theory an additional beam (Beam 30) was modeled as a part of the current research. Beam 30 is a bare steel model with geometrical properties similar to that of Bare Steel 1. The only difference in Beam 30 is that a portion the compression flange is increased in thickness by a factor of 1.5; thus endowing it with a total thickness of 15.24 mm. This thicker portion of the compression flange was realized along the entire width of the beam; starting at the fixed end and running half of the beam length (1.905 m). This case was thought to be similar to Beam 15 where the GFRP strips run for half of the length of the beam.

The results from the finite element modeling of this case all indicate that the theory, about the addition of GFRP strips to the compression flange being somewhat equivalent to increasing the thickness of the compression flange, appears reasonable. Figures A65-A68 show that the physical behavior of the beam with enhanced steel compression flange thickness is very similar to the physical behavior of the GFRP reinforced beams lesser compression flange thickness. The beam appears to buckle by lateral-torsional buckling instead of local buckling. Figure 3.3 shows that the load deflection plot of Beam 30 is similar to that of Beam 15 and Tables 3.1 and 4.1 show that the Beam 30 showed similar increases in ductility and ultimate load to Beam 15.

5.0 CONCLUSIONS

The results of the study reported herein conclude that the addition of GFRP strips to the compression flange of cantilevered beams serves to brace against local buckling of the flange and therefore increases the ductility and ultimate load of the beam. The study also concludes that strategic placement and length selection of the strips can significantly improve the effectiveness and efficiency of the GFRP-steel system, and that the imposition of GFRP strips is equivalent to increasing the thickness of the compression flange in the region of the strips.

As discussed in Chapter 4 the addition of GFRP strips to the bare steel models tested showed significant improvements in several areas. The strips served to brace against local buckling of the compression flange and therefore forced the beams into higher buckling modes such as later-torsional and distortional buckling. The results of this bracing were seen in the increase of the ultimate load and ductility over that of the bare steel models.

The results also showed that by placing the GFRP strips closer to the flange tips their effects were greater due to the fact that the flange tips experience the greatest deflection during local buckling. Adjusting the lengths of the GFRP strips along the compression flanges showed that the strips do not need to be full length to be effective. Strips running half of the length of the beam proved to be just as effective as the full length strips. Strips running .762 m proved to be more effective than bare steel but not as effective as the half length strips.

APPENDIX A

DEFLECTION AND STRESS FIGURES

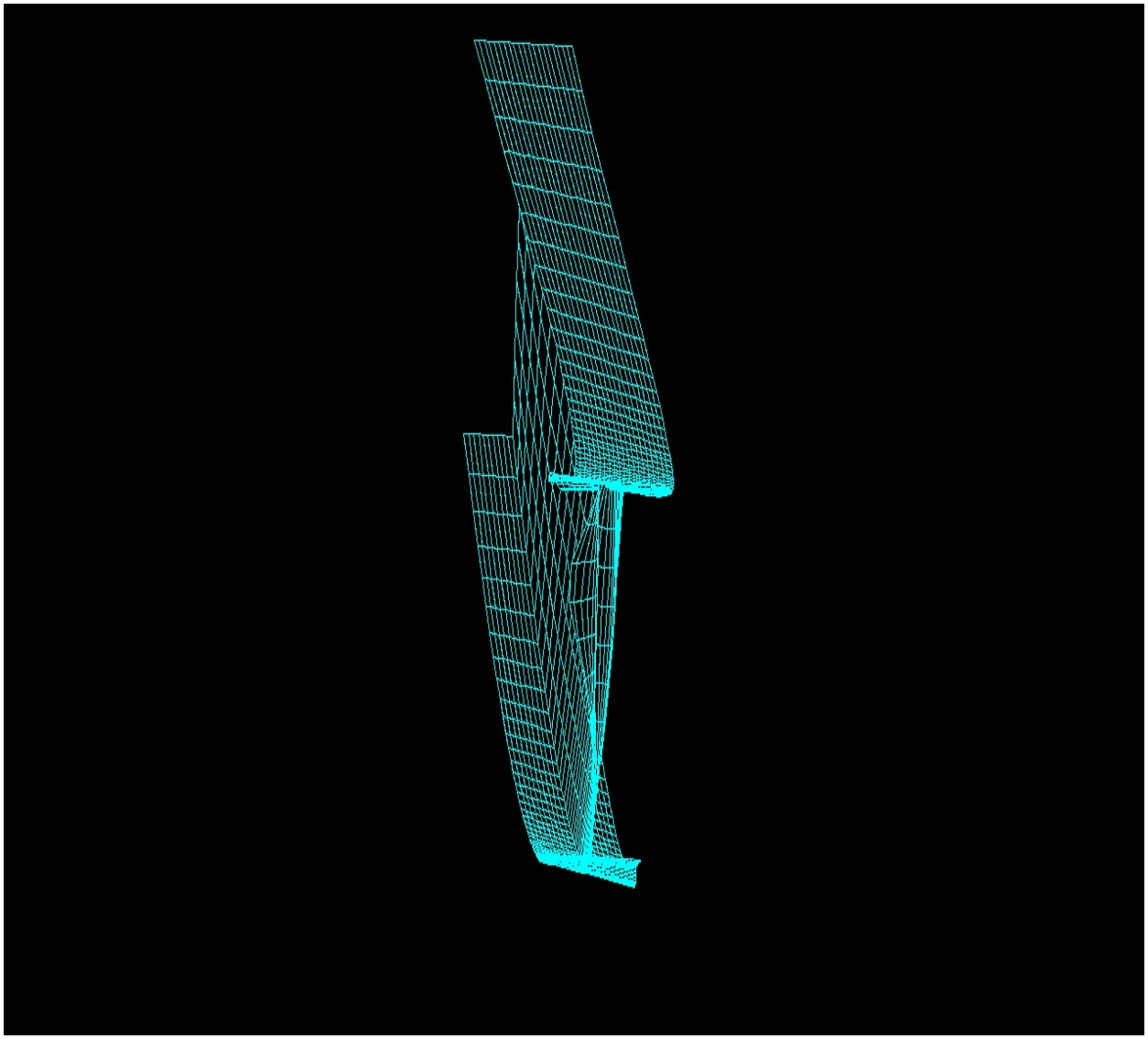

Figure A.0 Bare Steel 1

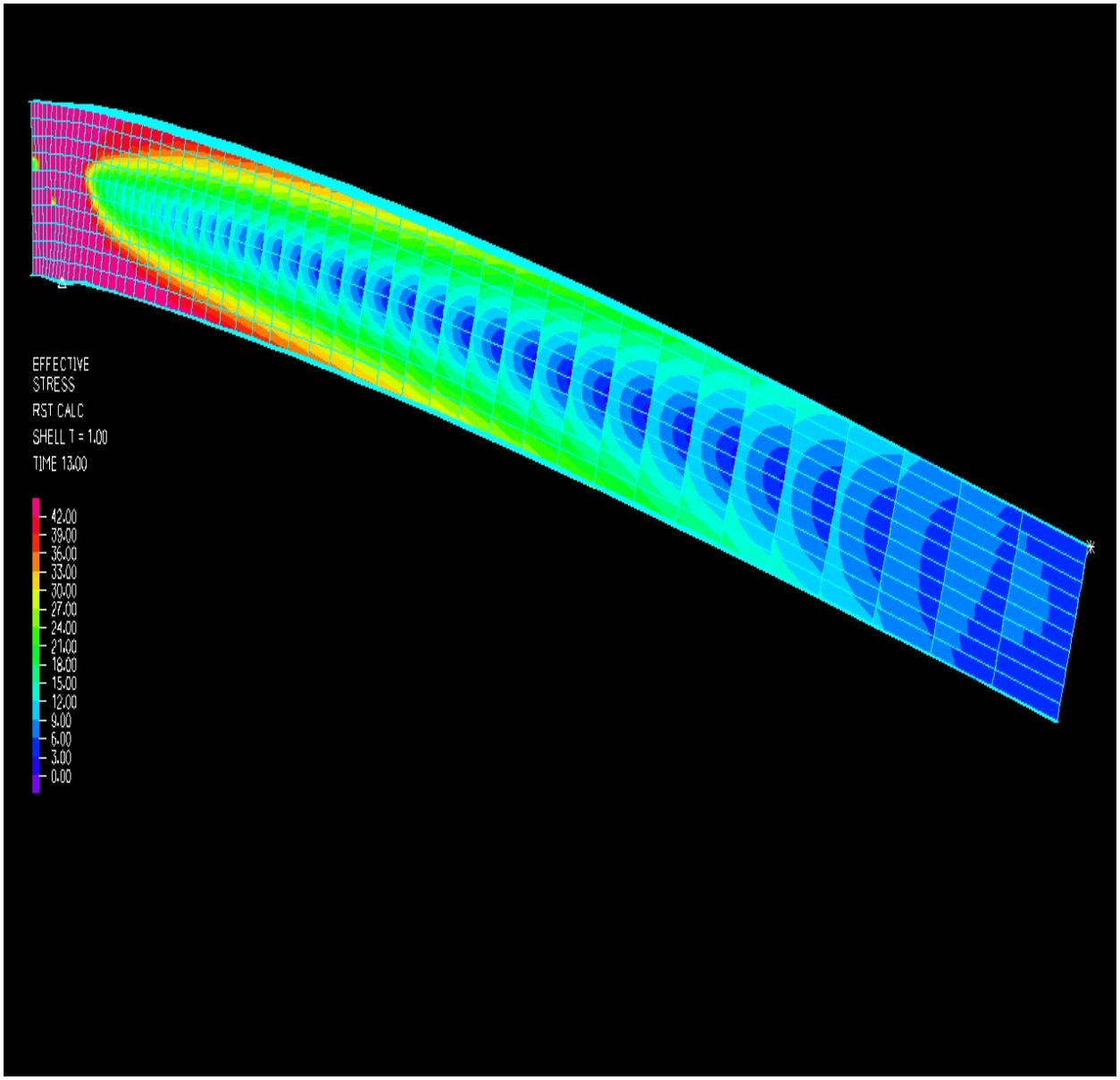

Figure A.1 Bare Steel 1

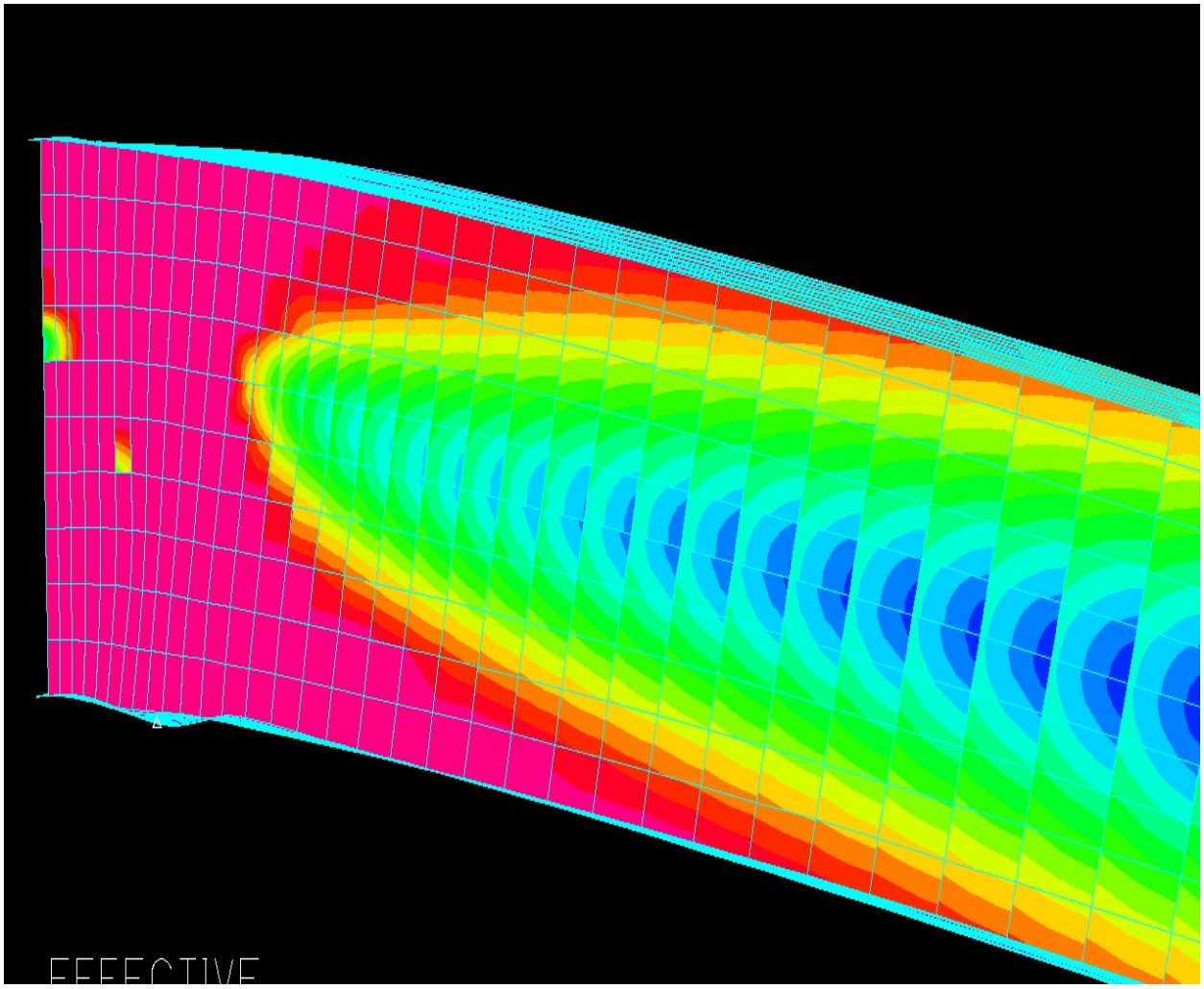

Figure A.2 Bare Steel 1

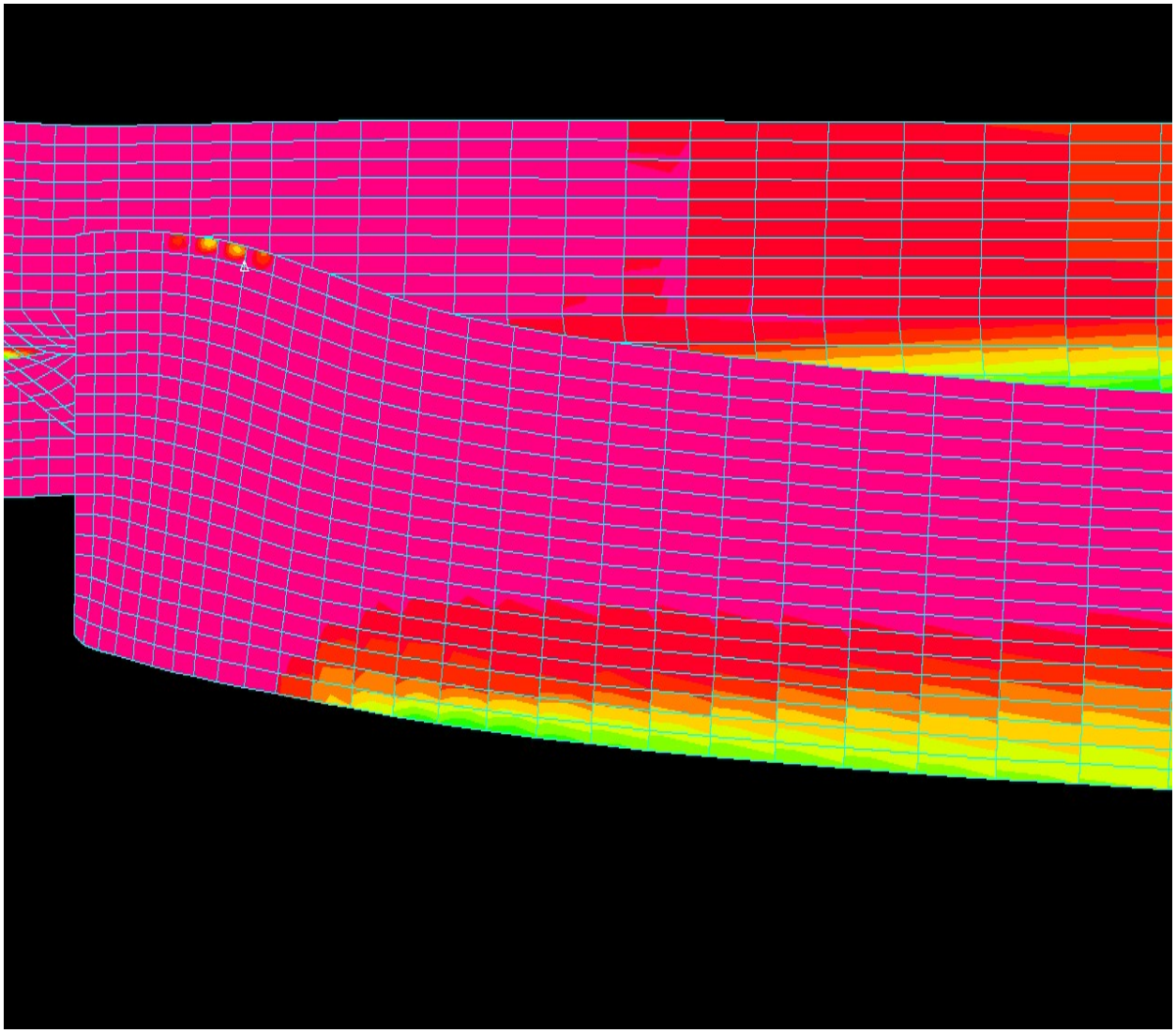

Figure A.3 Bare Steel 1

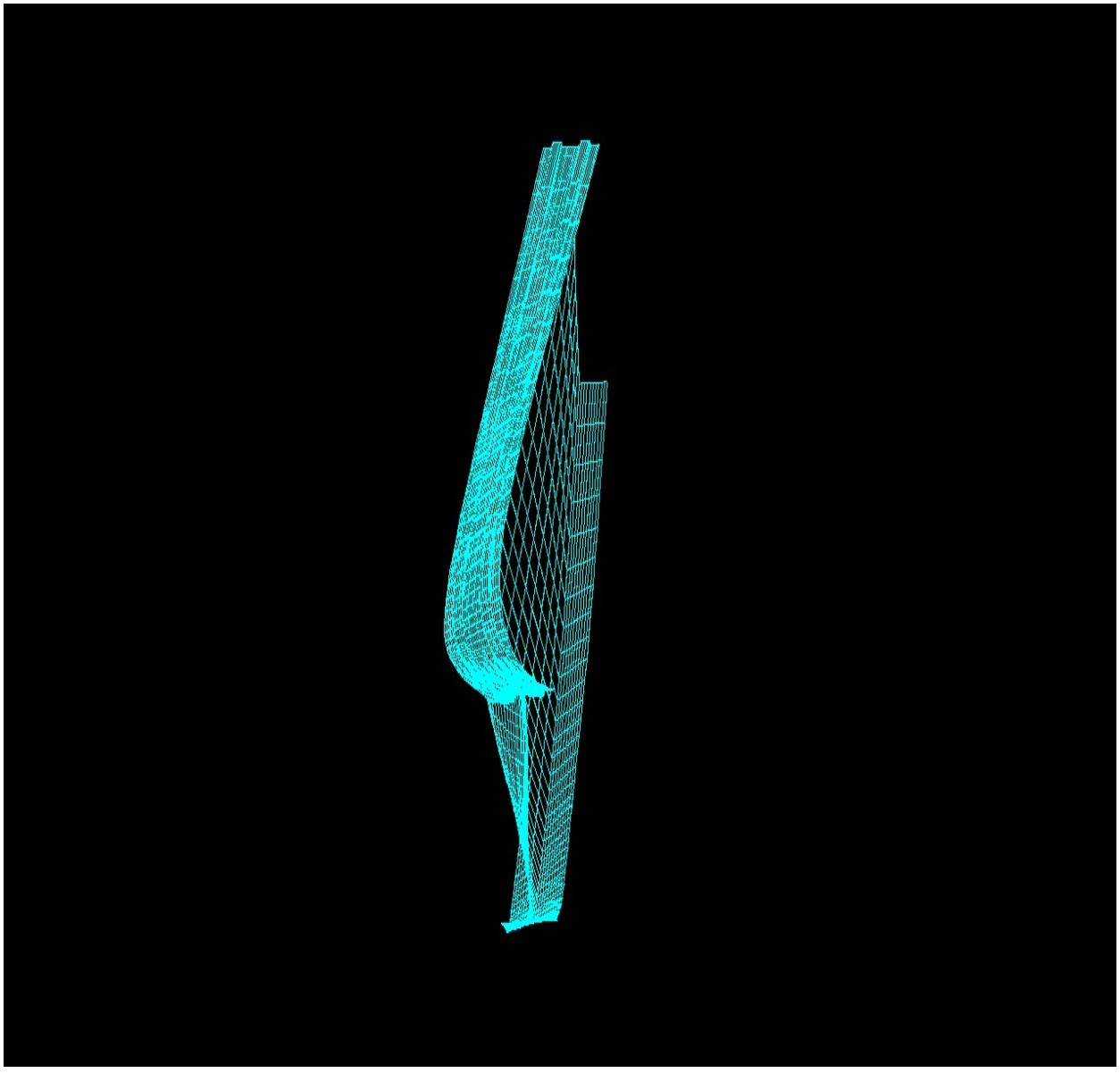

Figure A.4 Beam 9

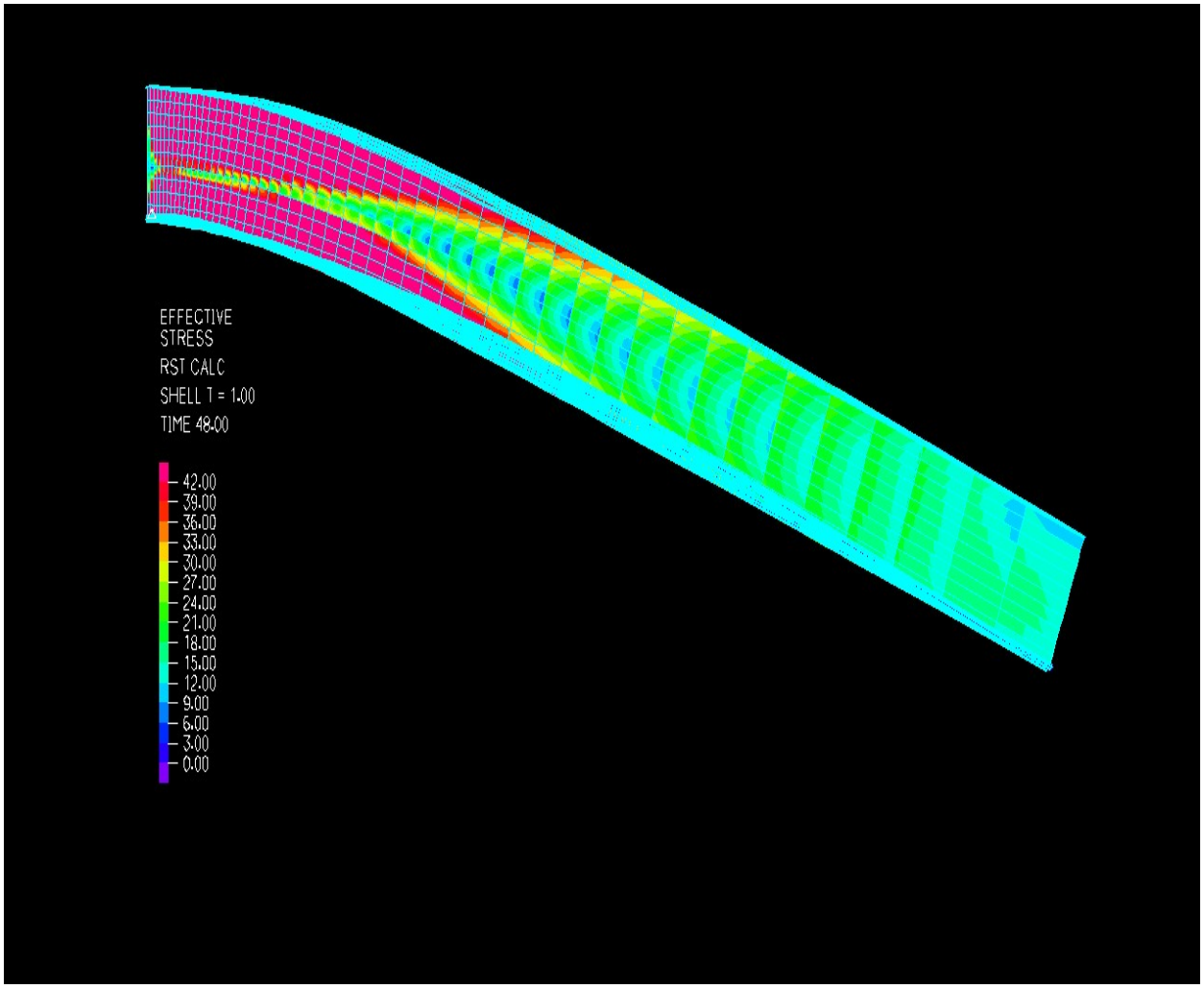

Figure A.5 Beam 9

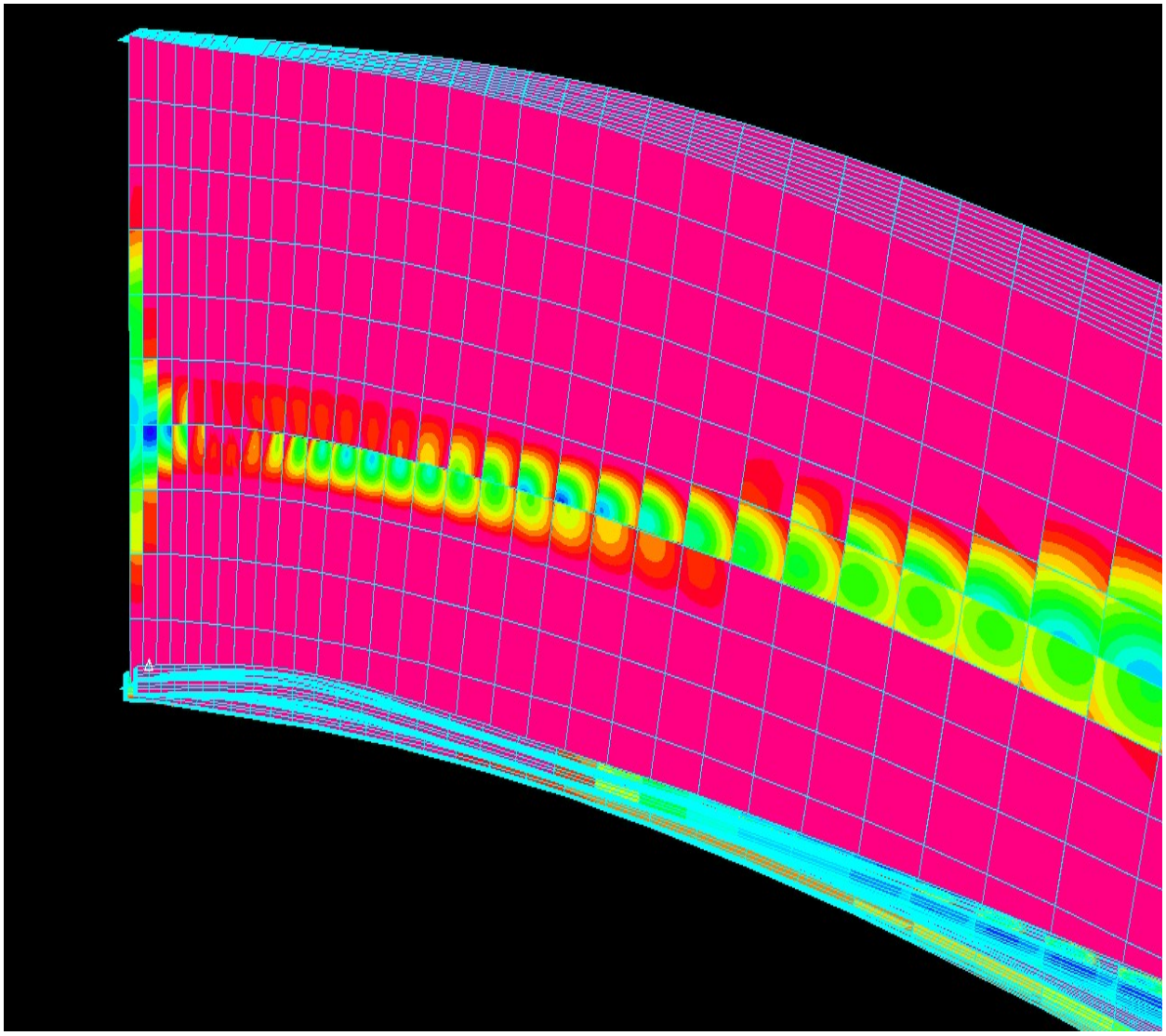

Figure A.6 Beam 9

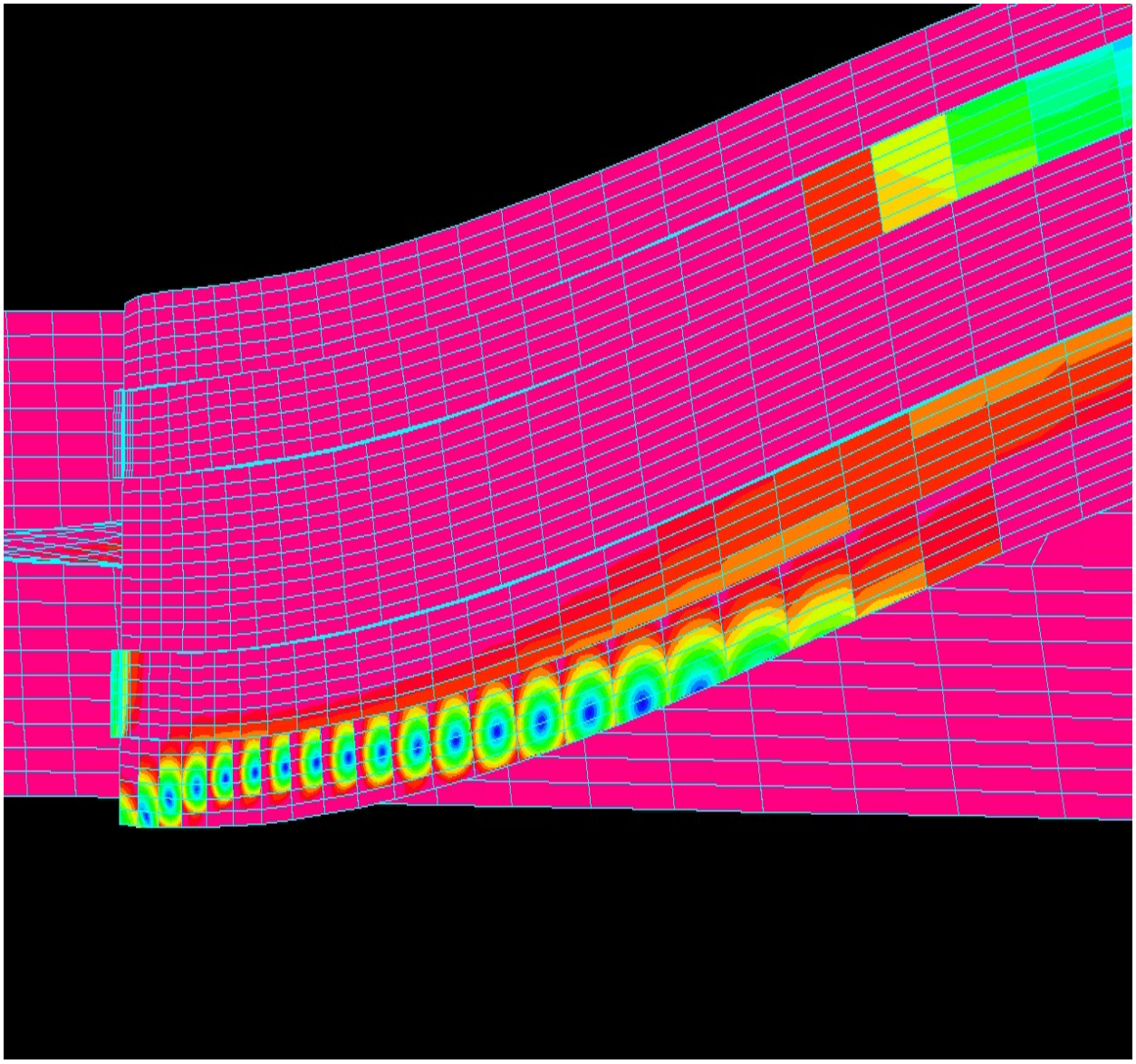

Figure A.7 Beam 9

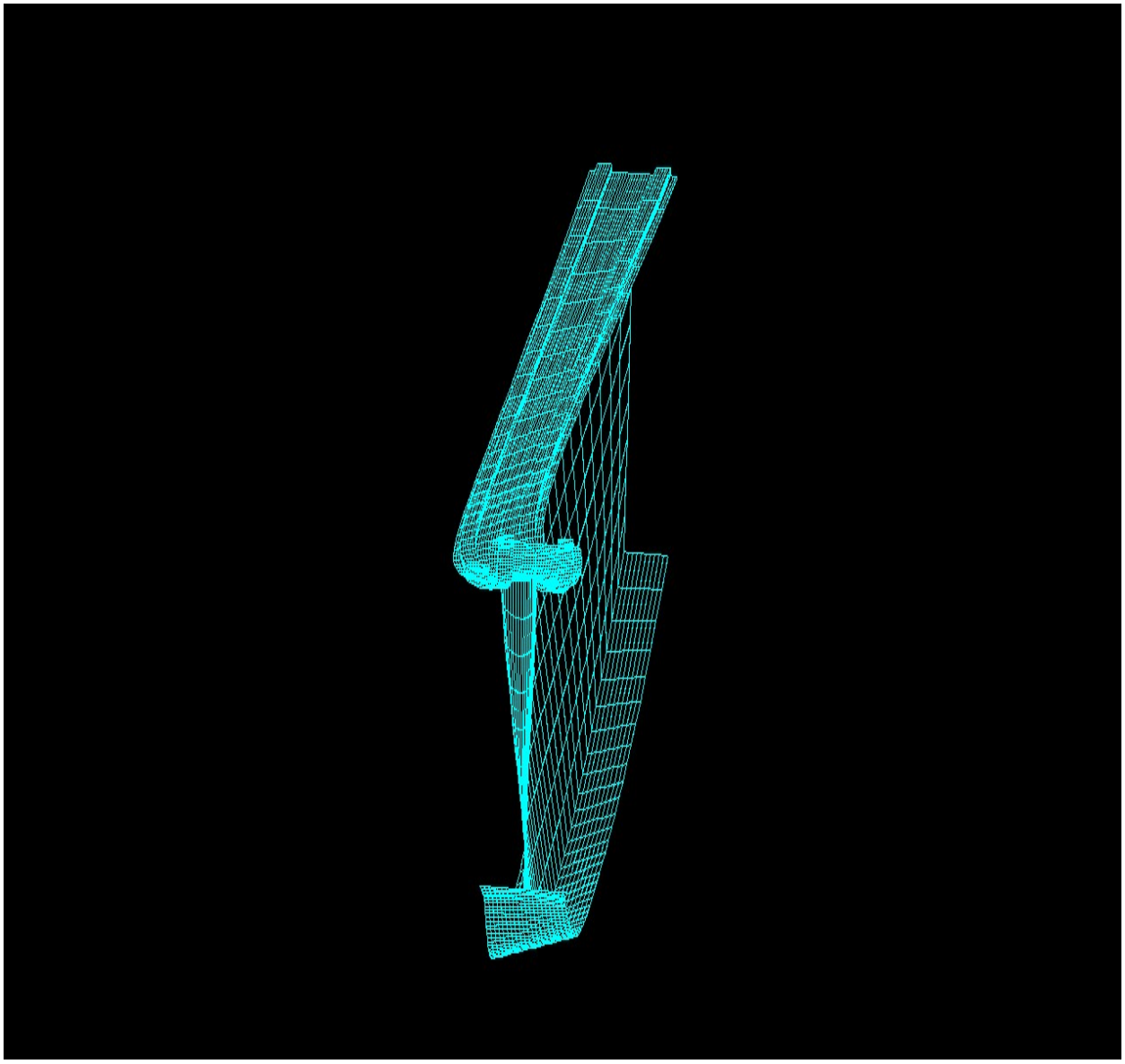

Figure A.8 Beam 11

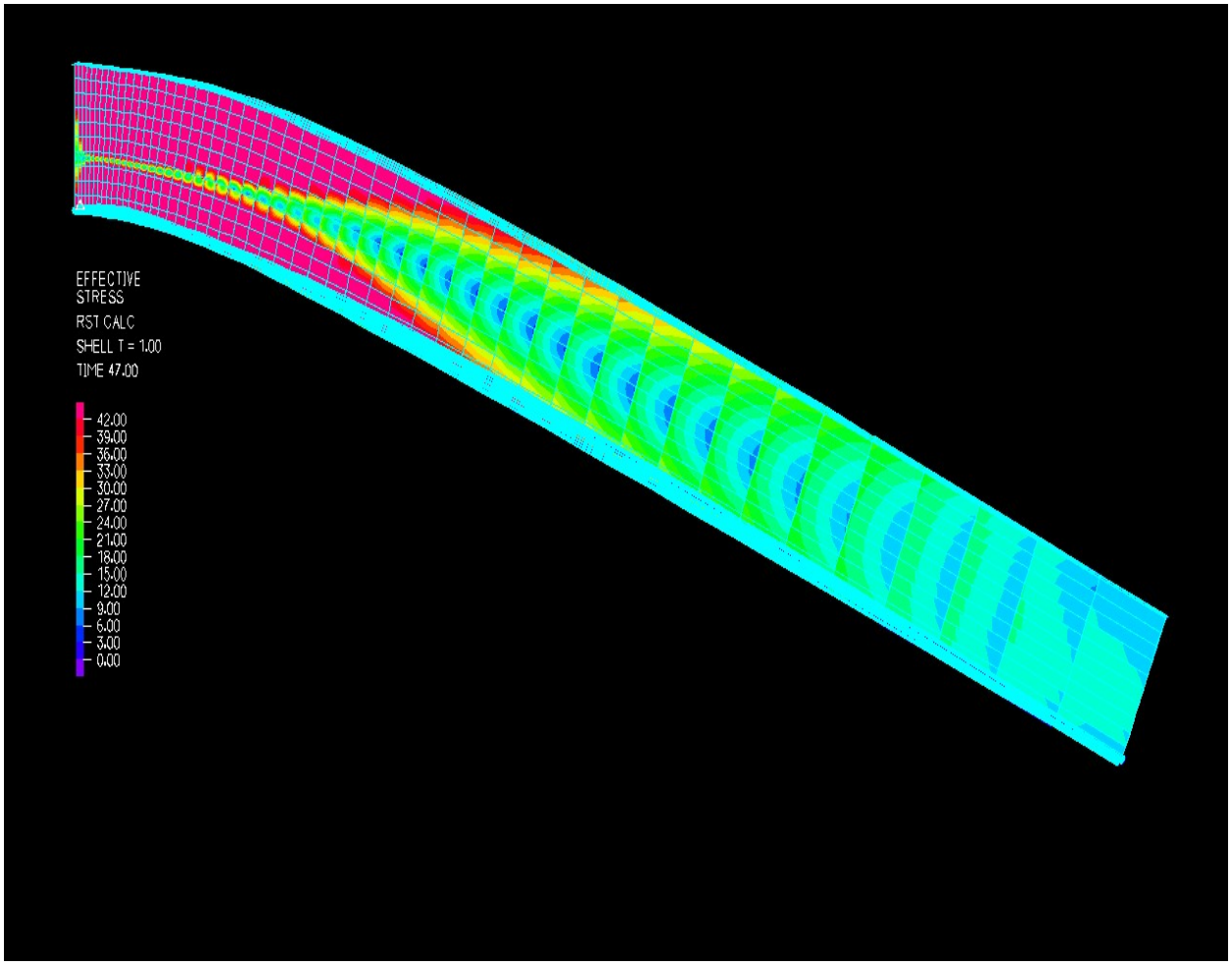

Figure A.9 Beam 11

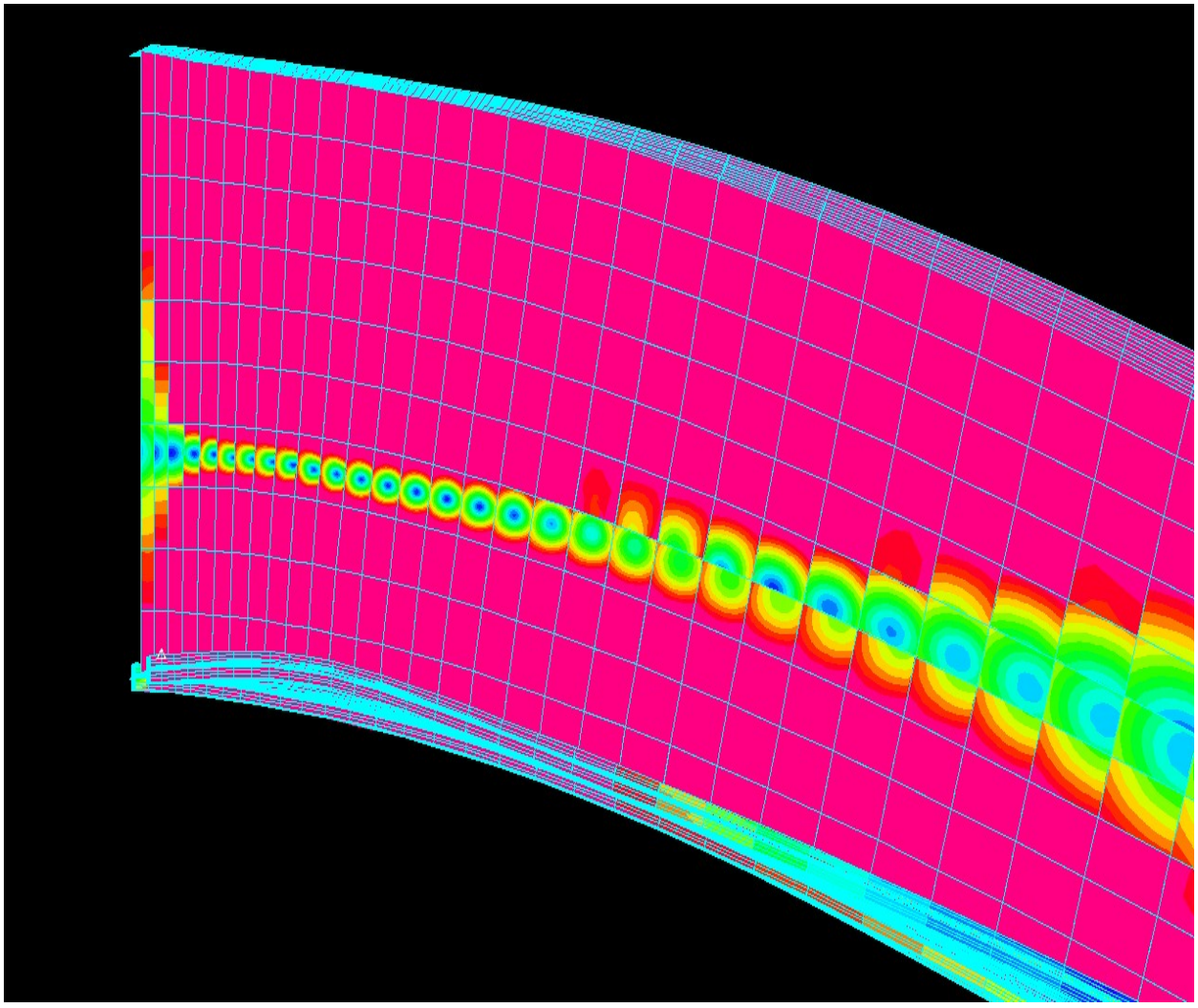

Figure A.10 Beam 11

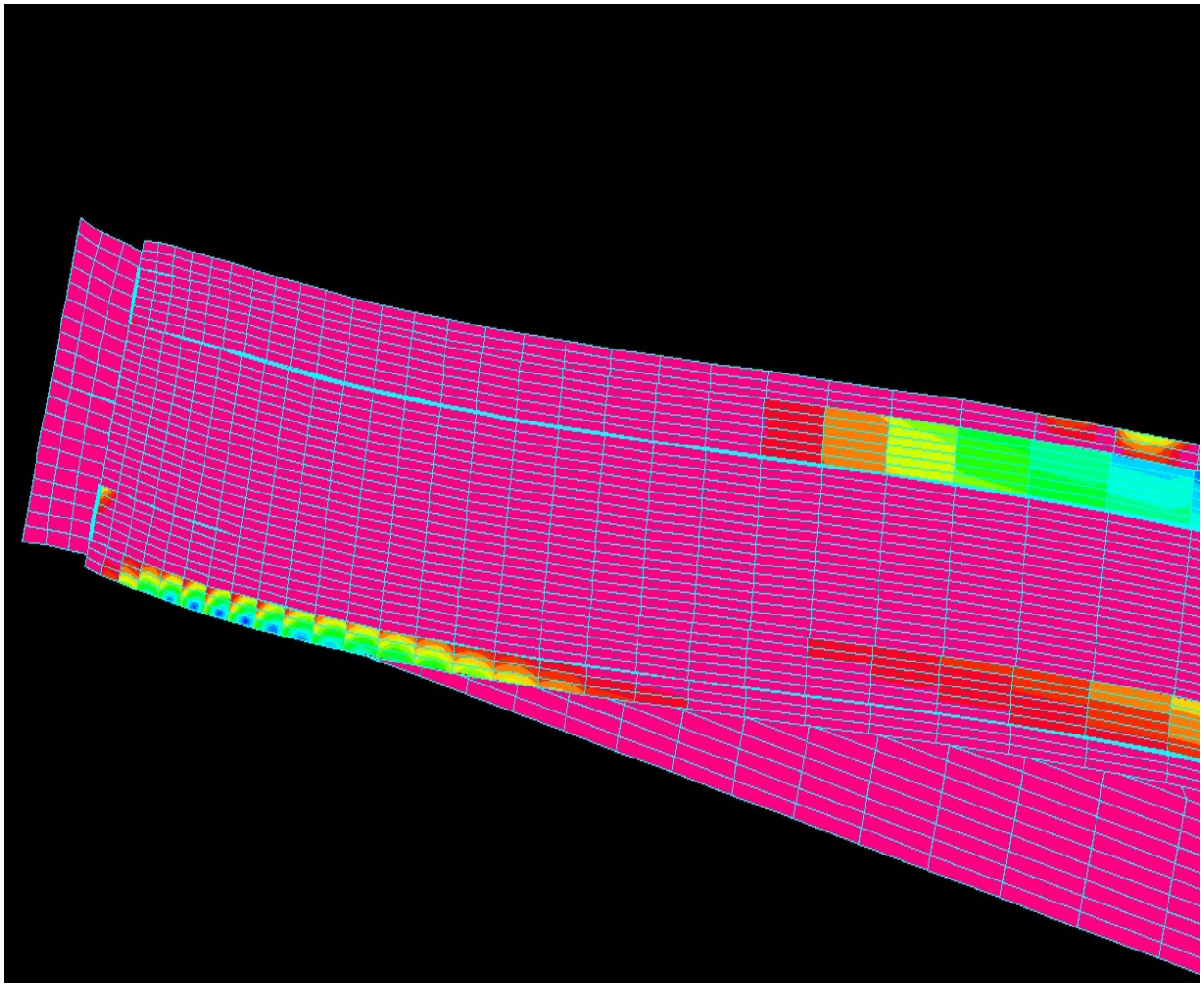

Figure A.11 Beam 11

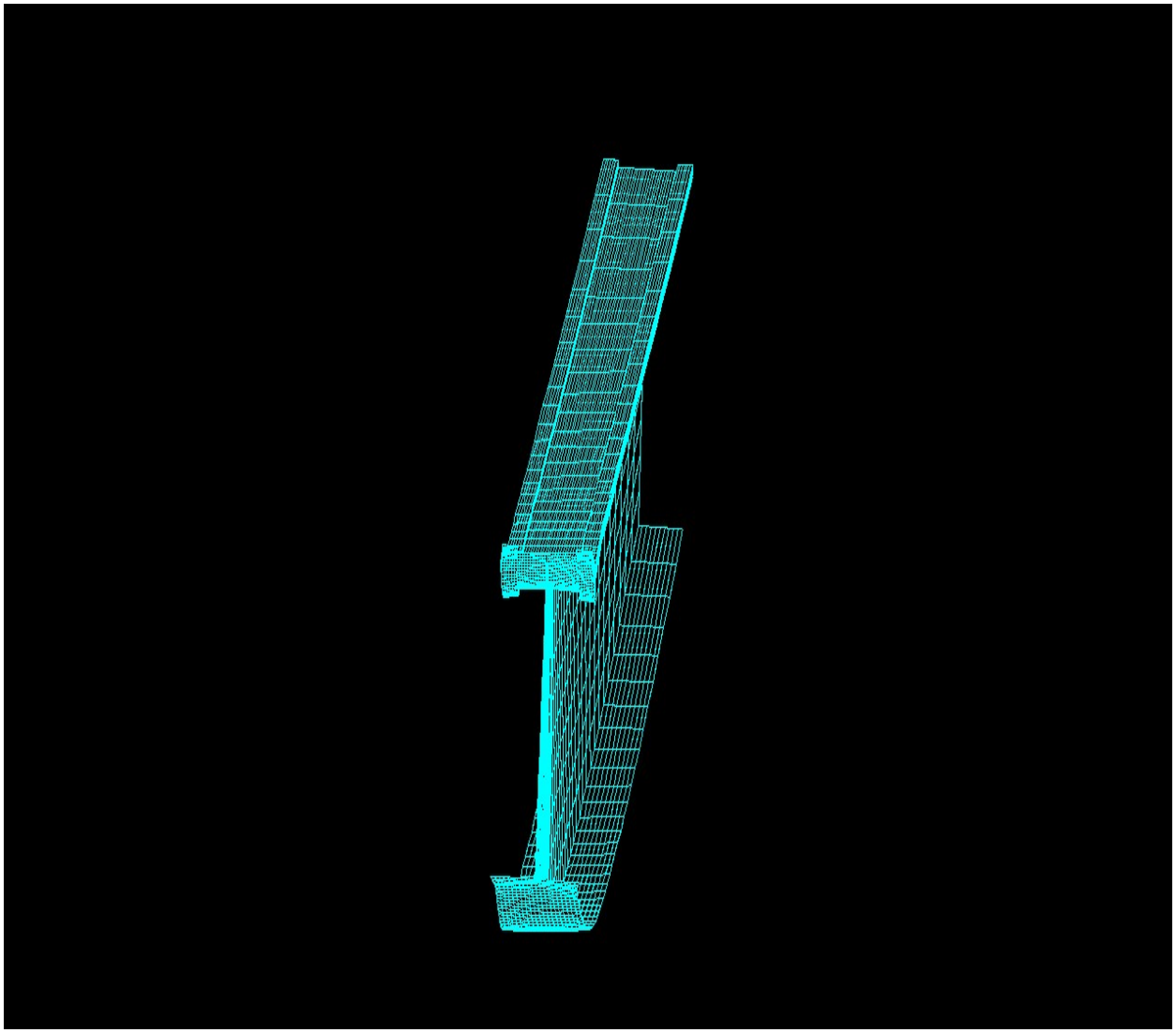

Figure A.12 Beam 12

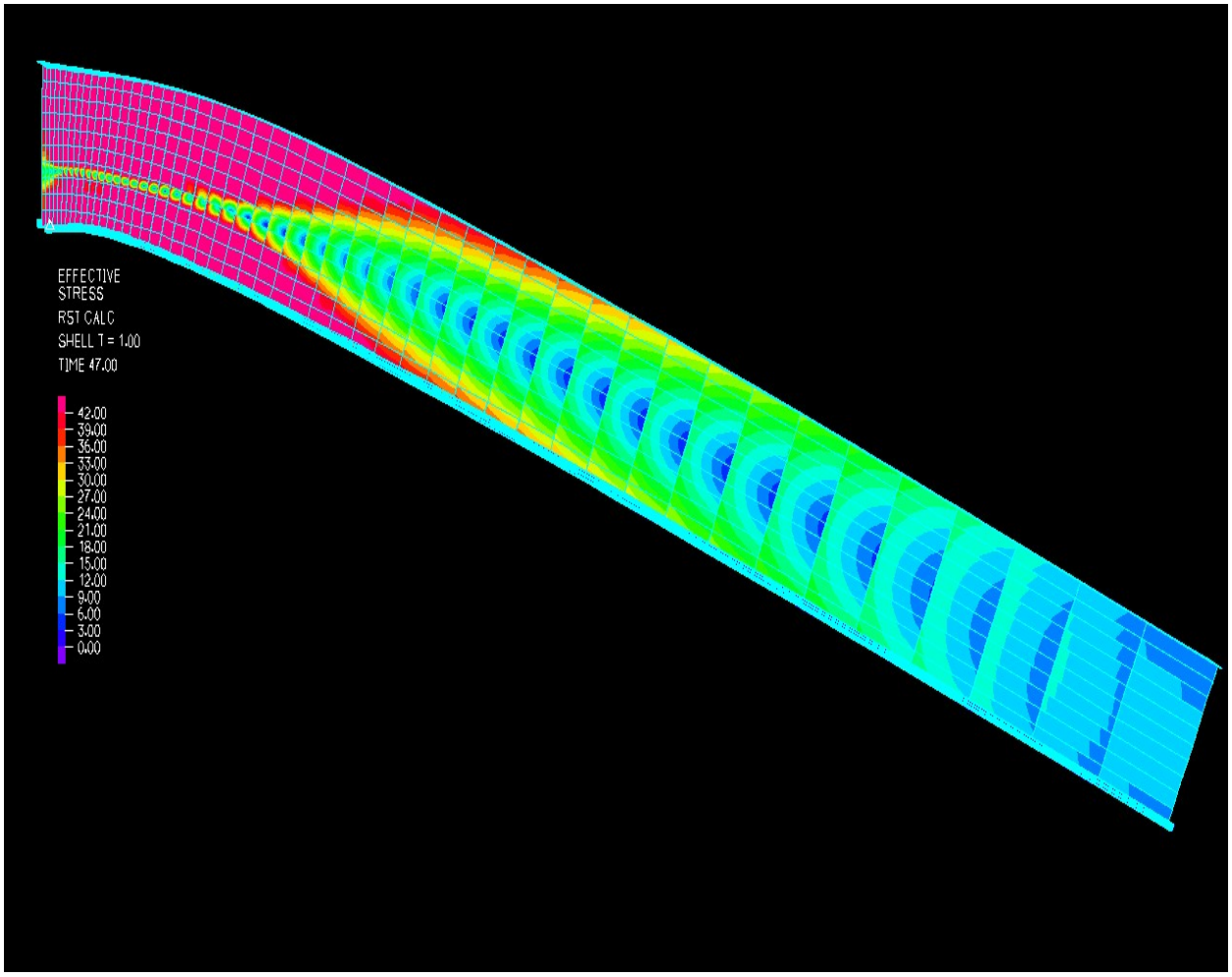

Figure A.13 Beam 12

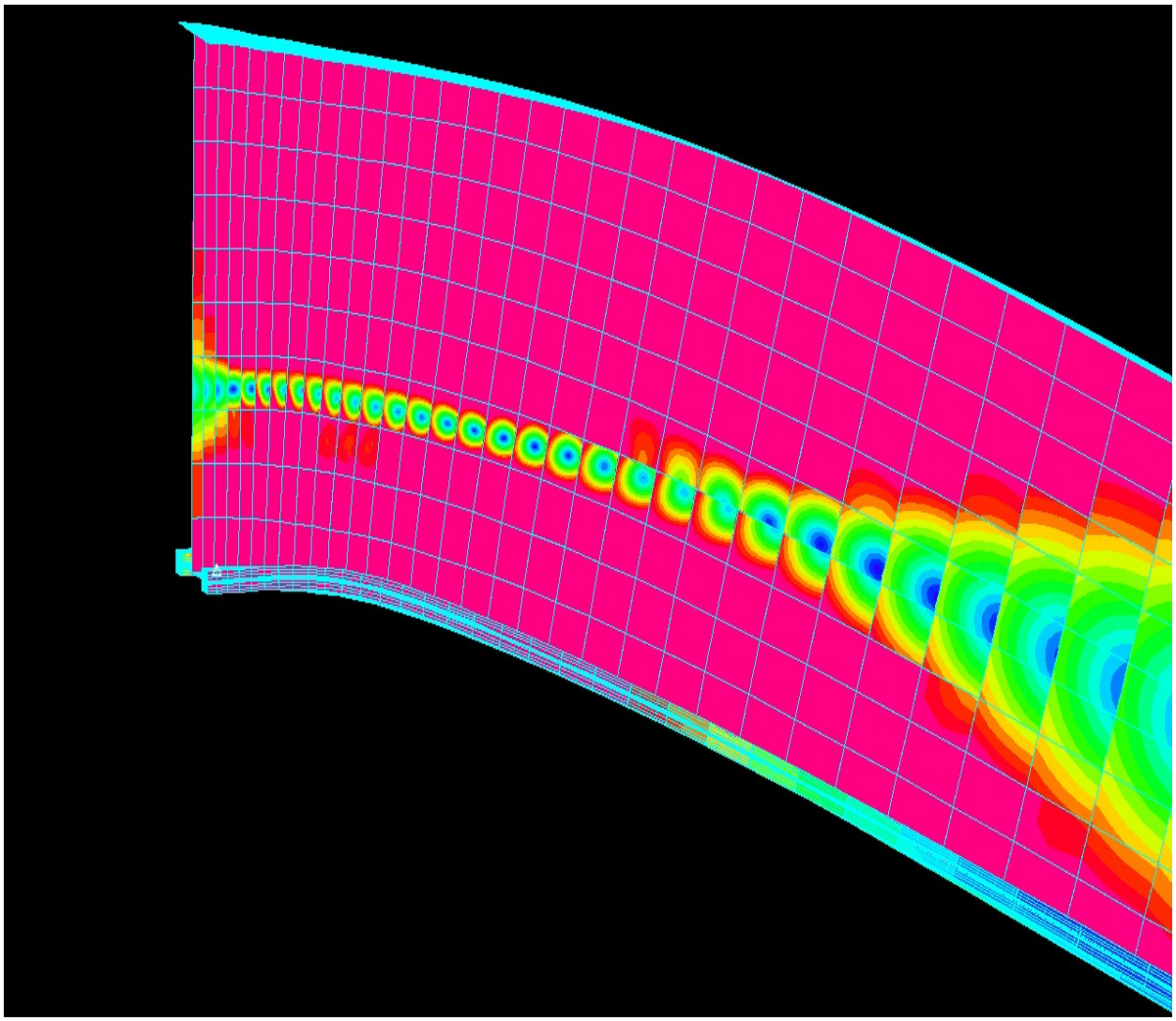

Figure A.14 Beam 12

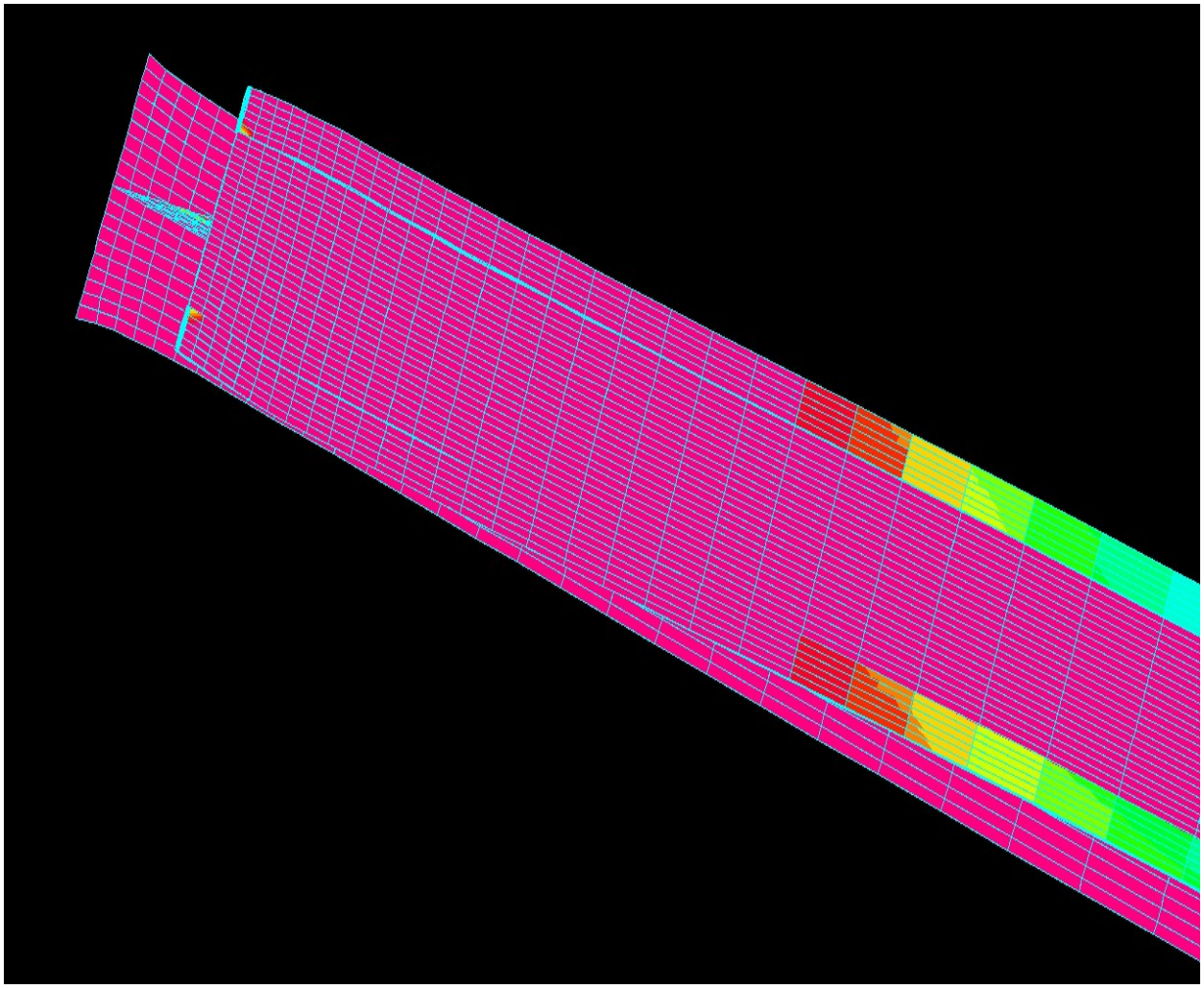

Figure A.15 Beam 12

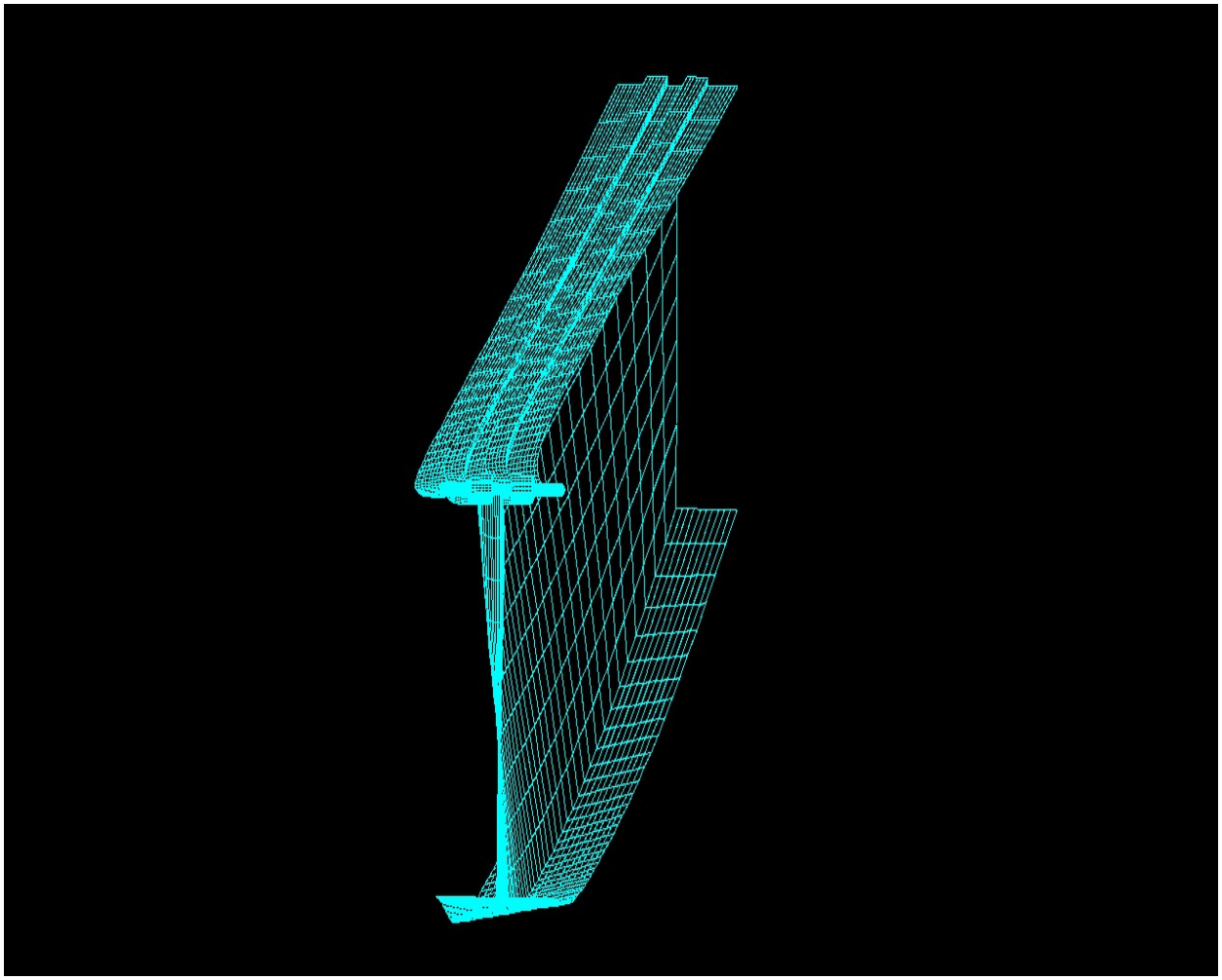

Figure A.16 Beam 13

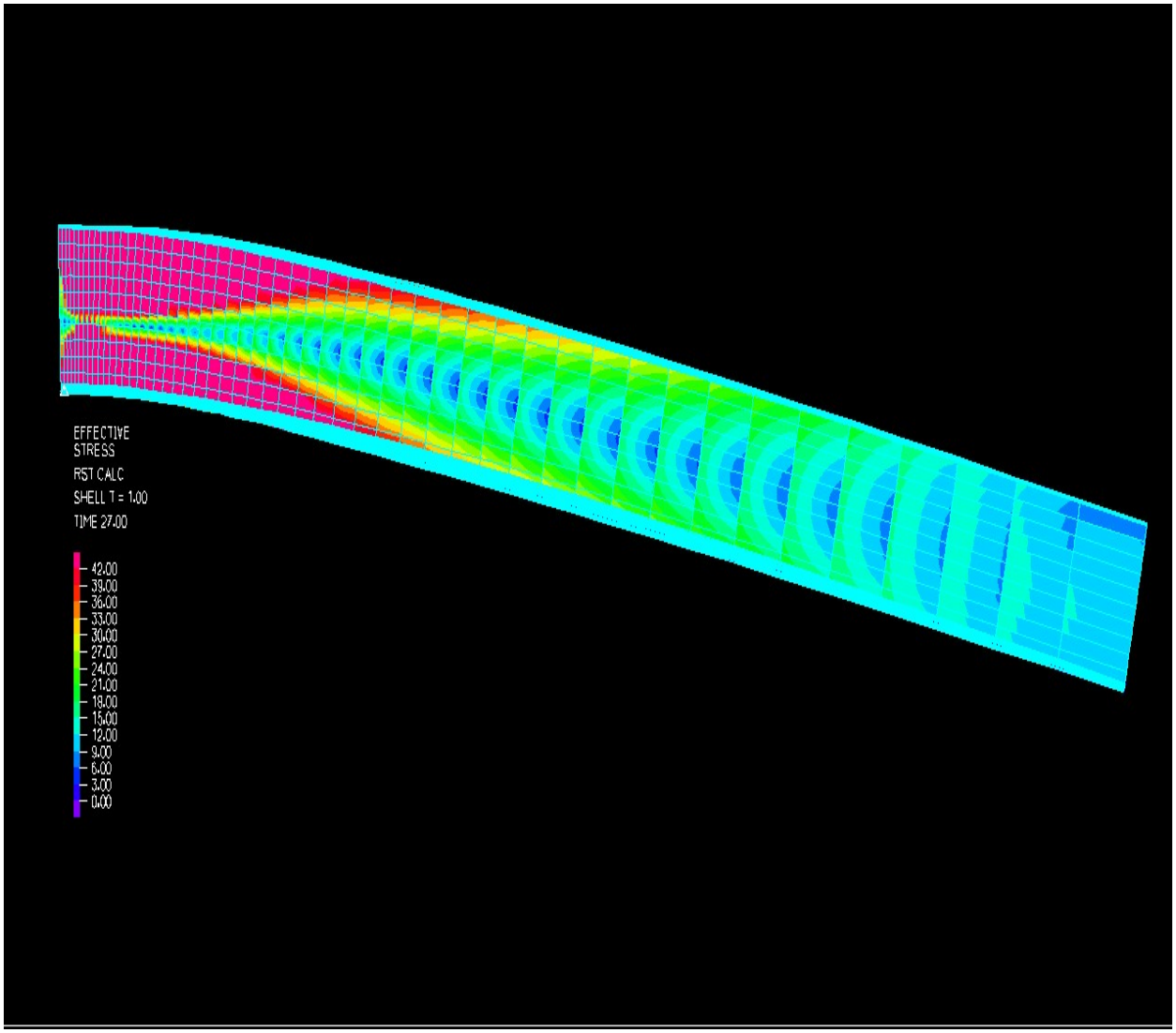

Figure A.17 Beam 13

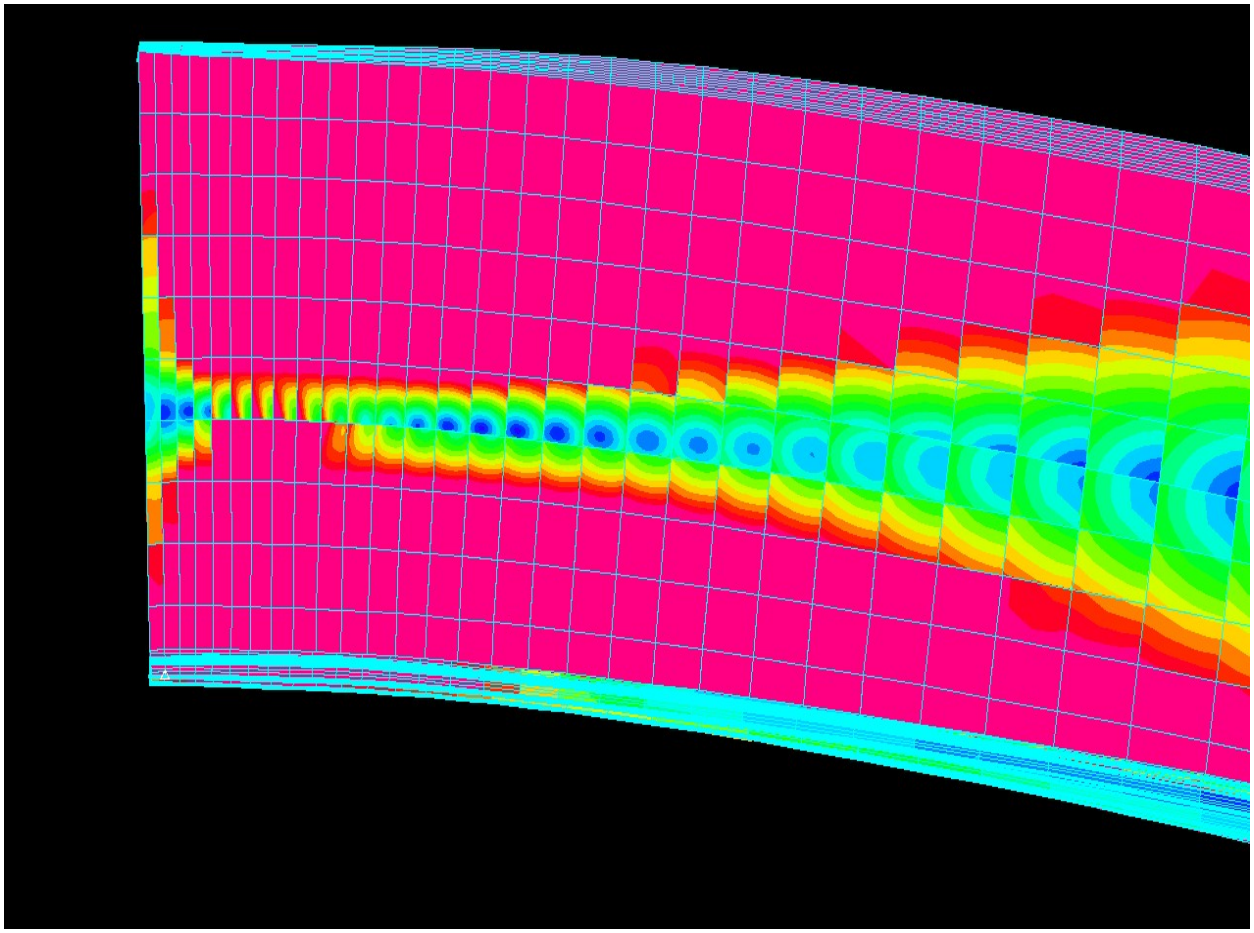

Figure A.18 Beam 13

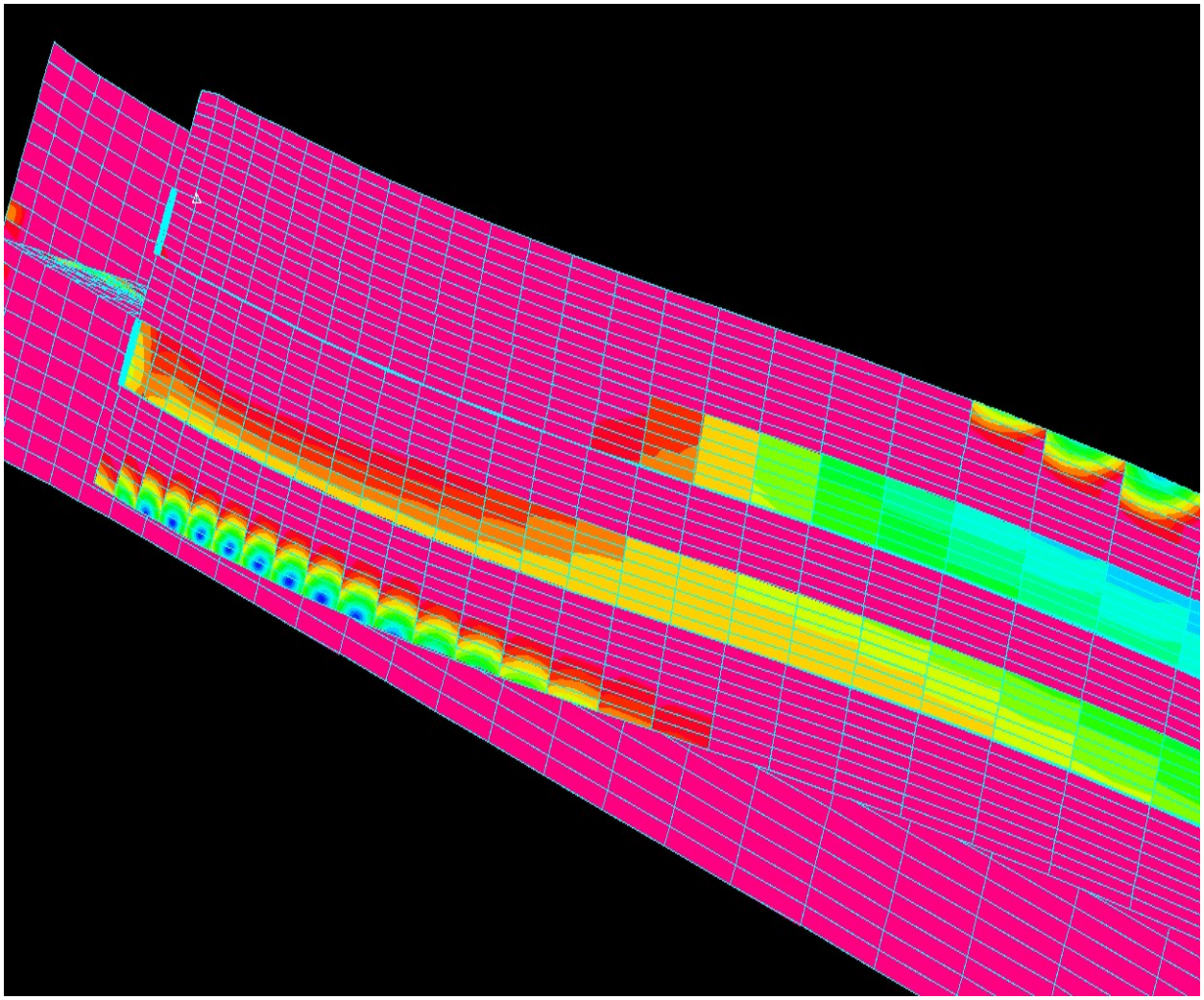

Figure A.19 Beam 13

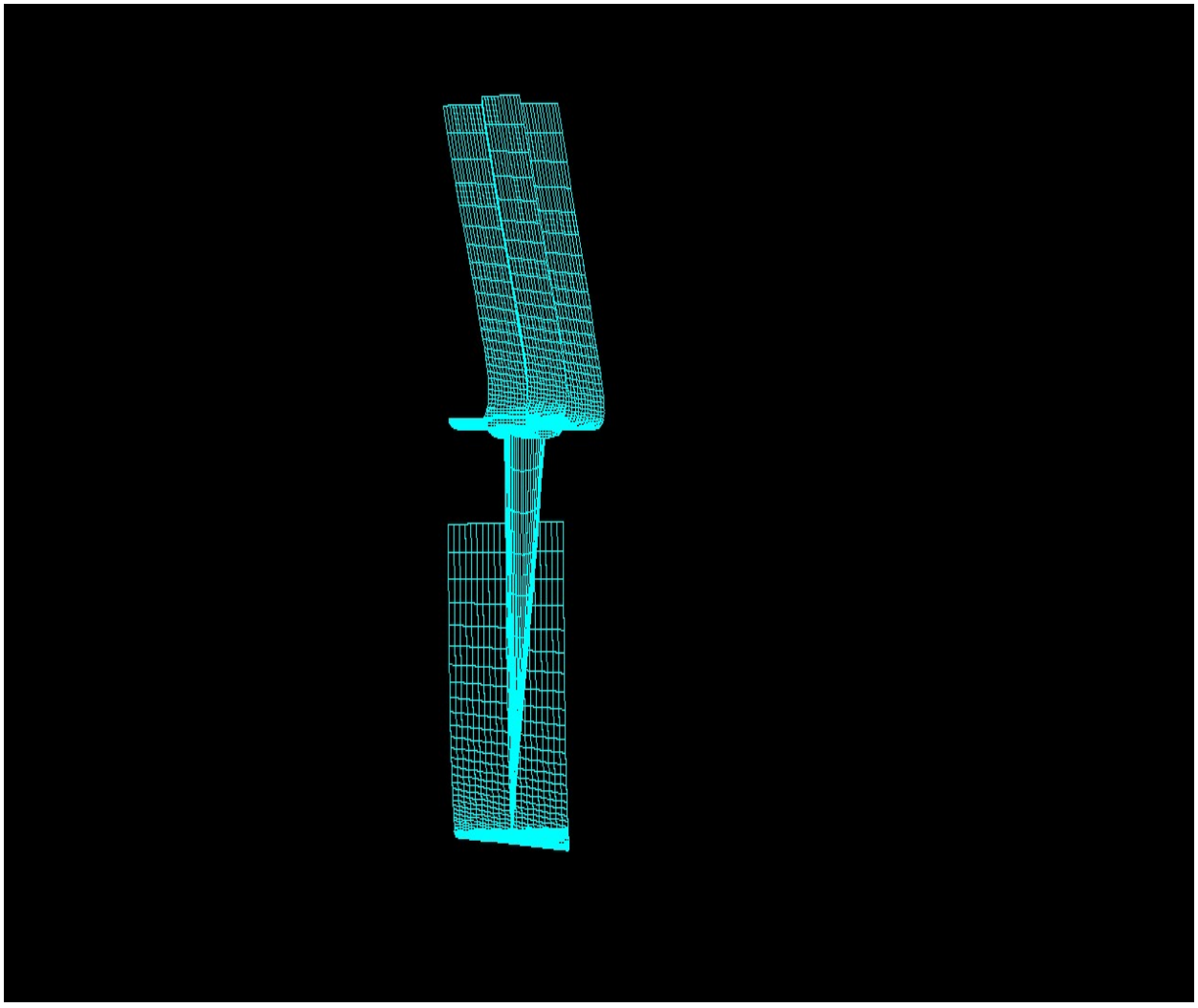

Figure A.20 Beam 14

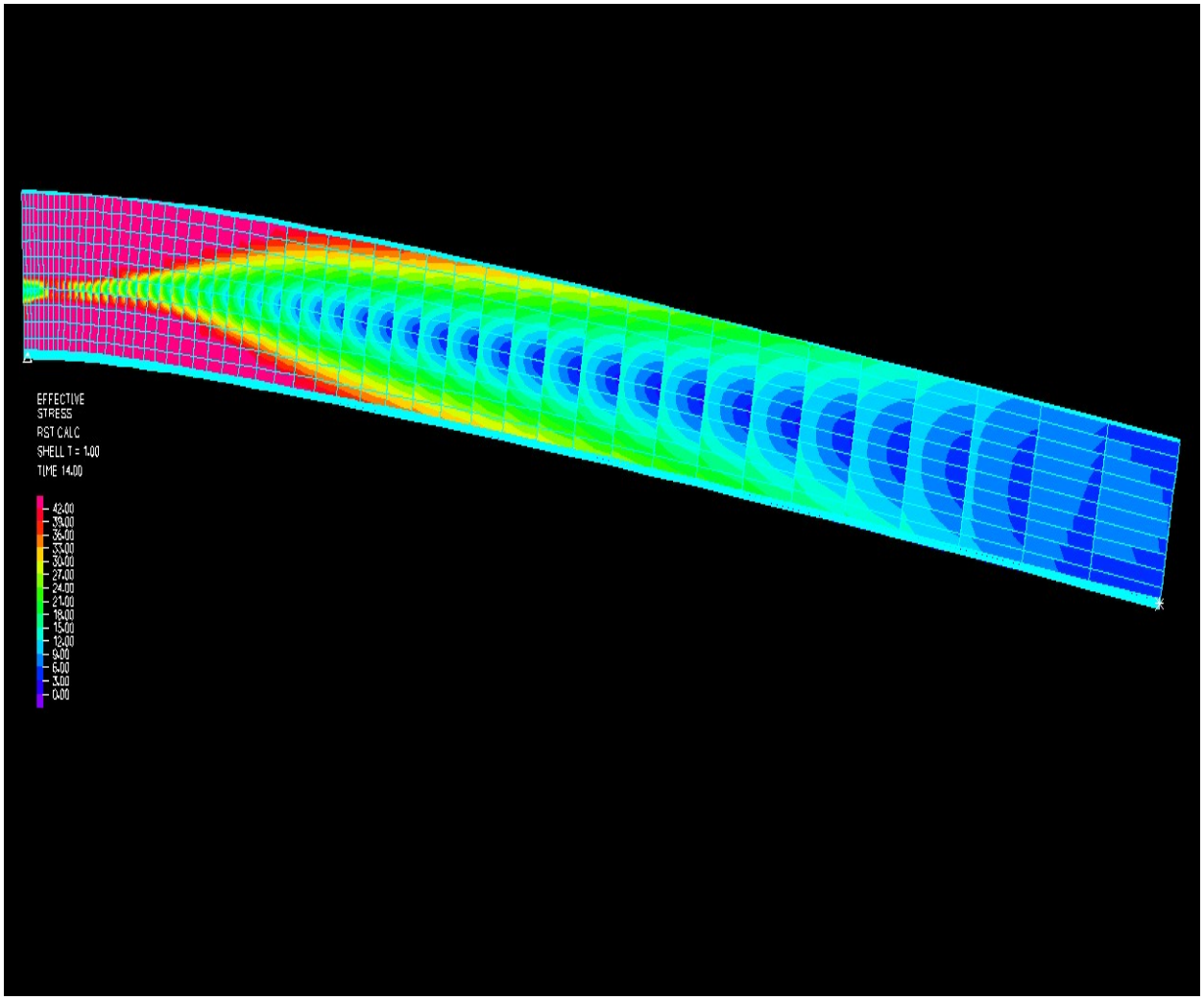

Figure A.21 Beam 14

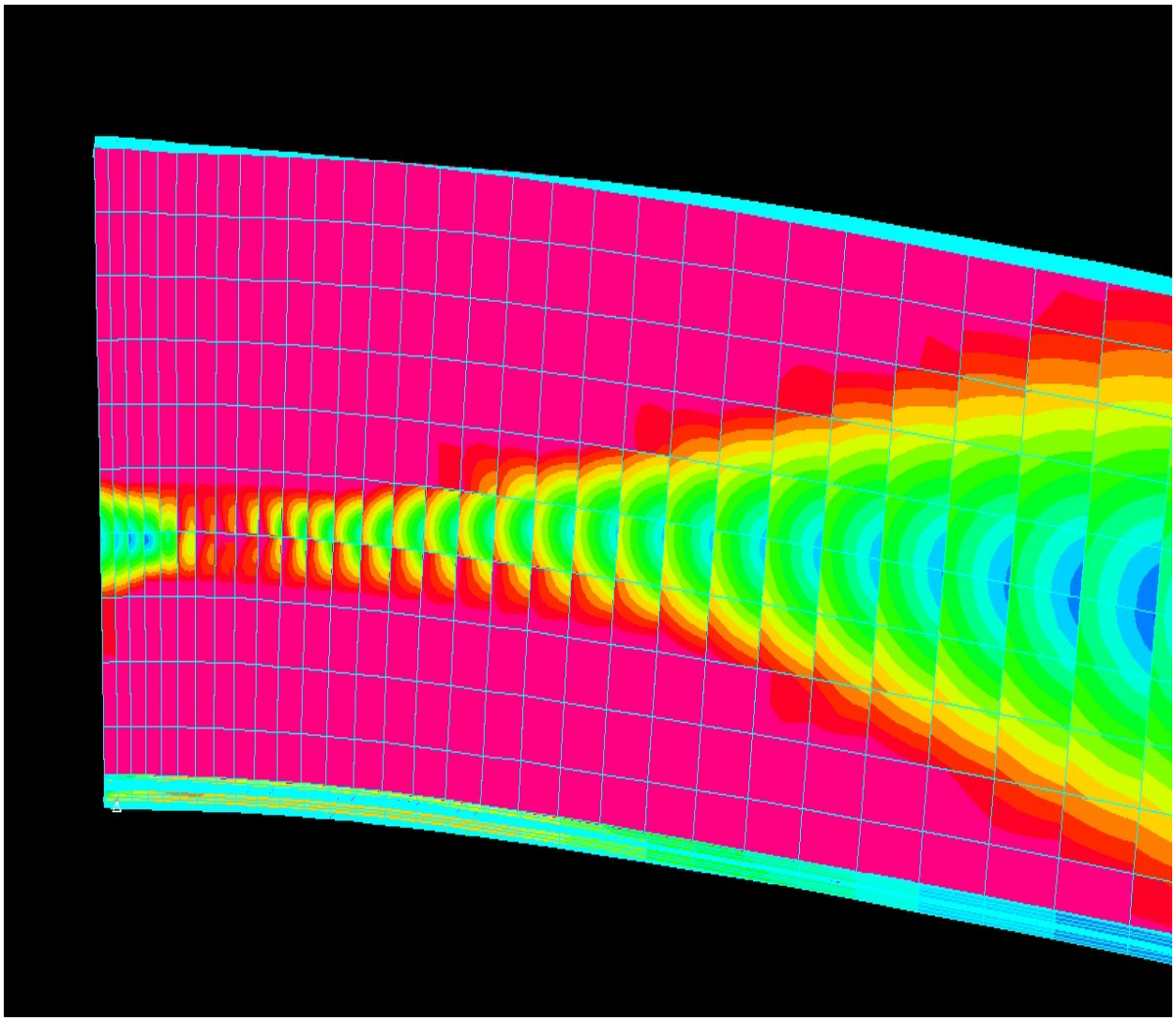

Figure A.22 Beam 14

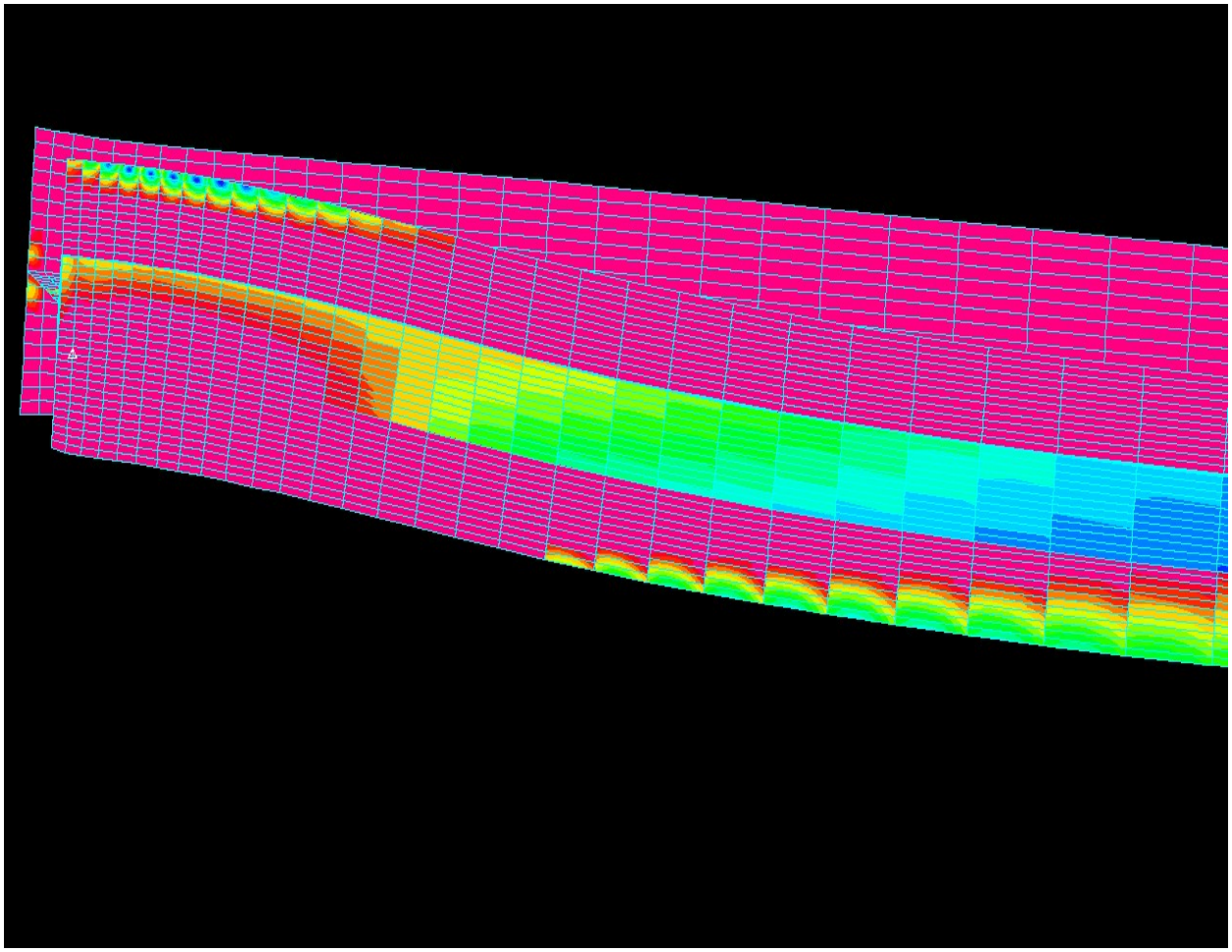

Figure A.23 Beam 14

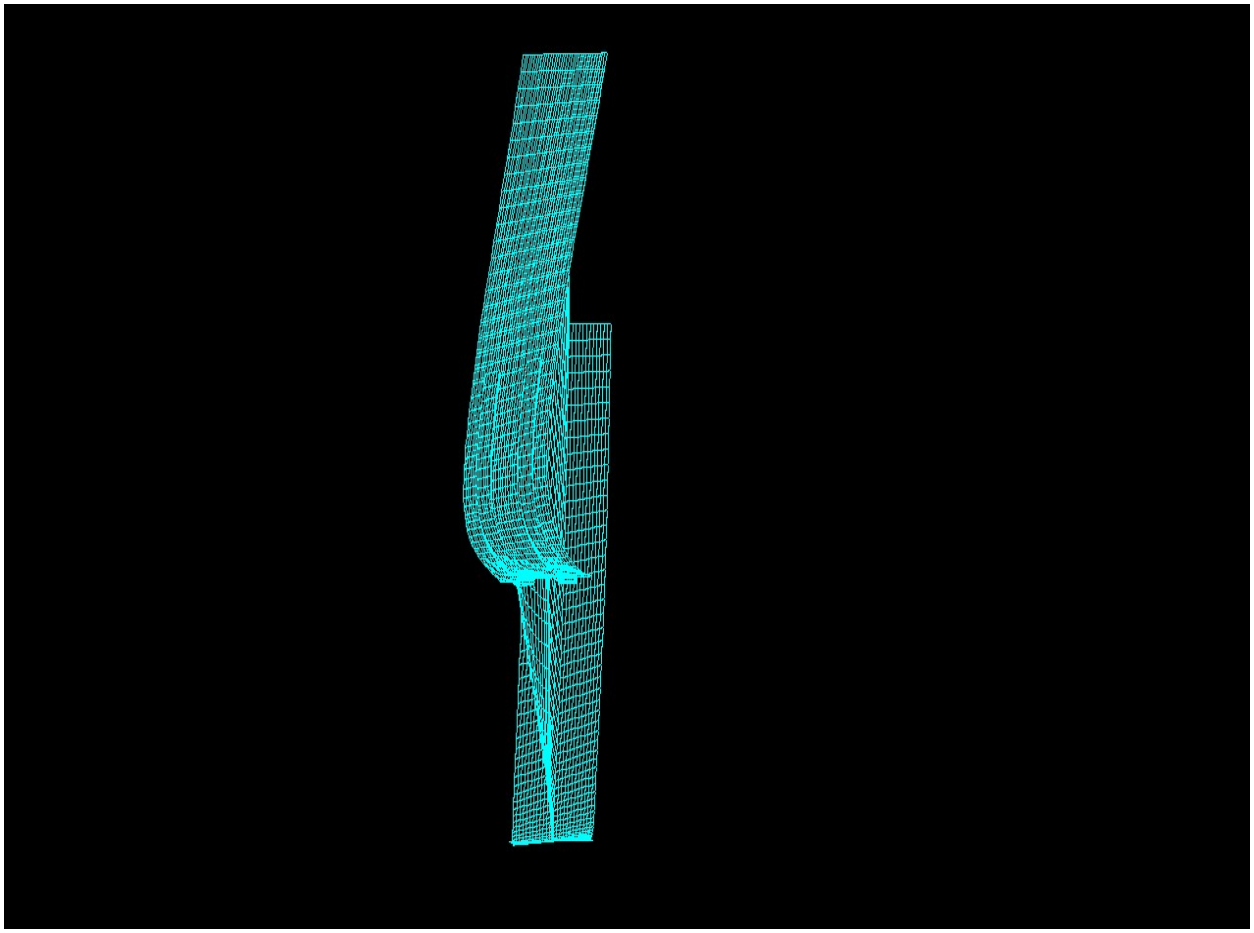

Figure A.24 Beam 15

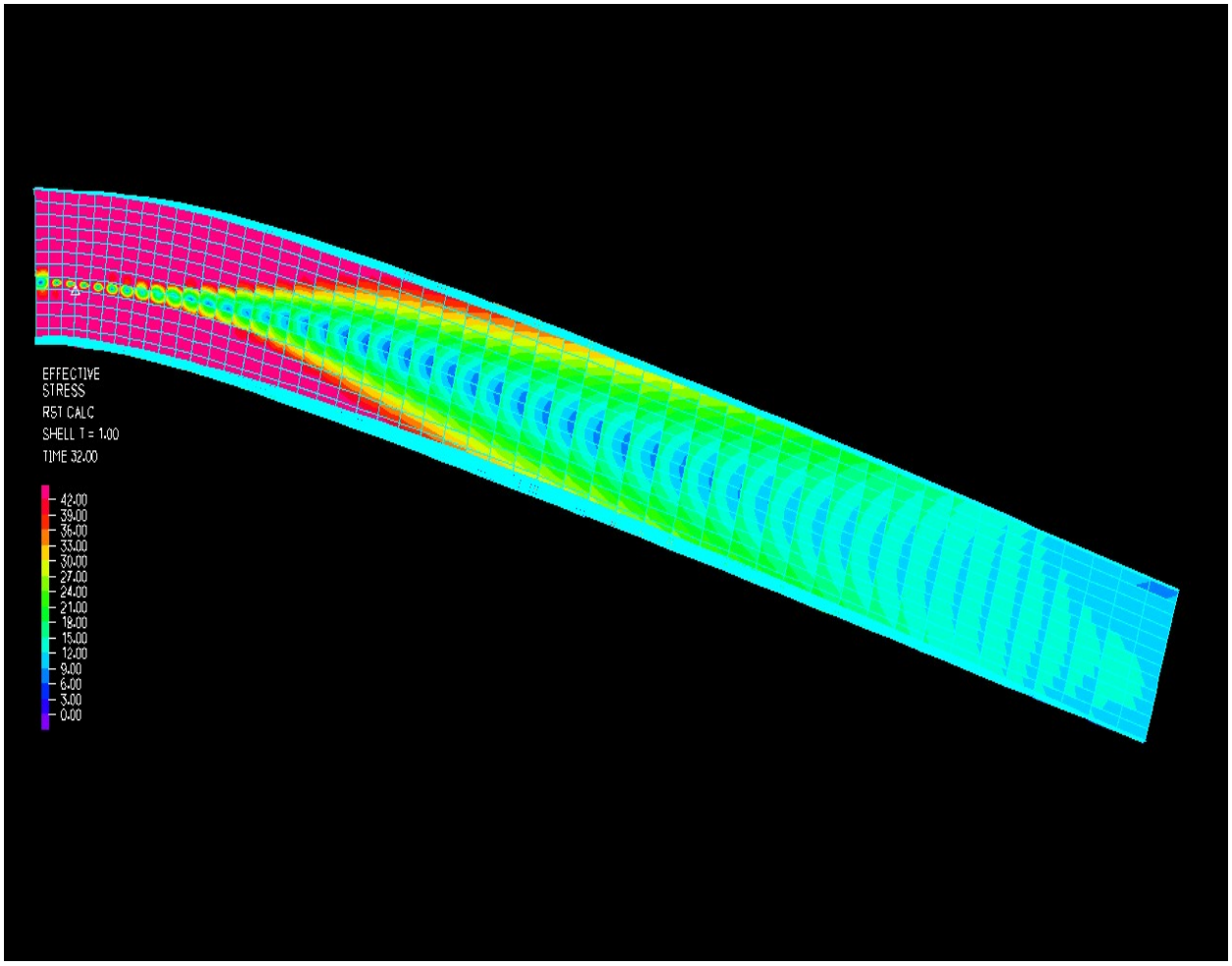

Figure A.25 Beam 15

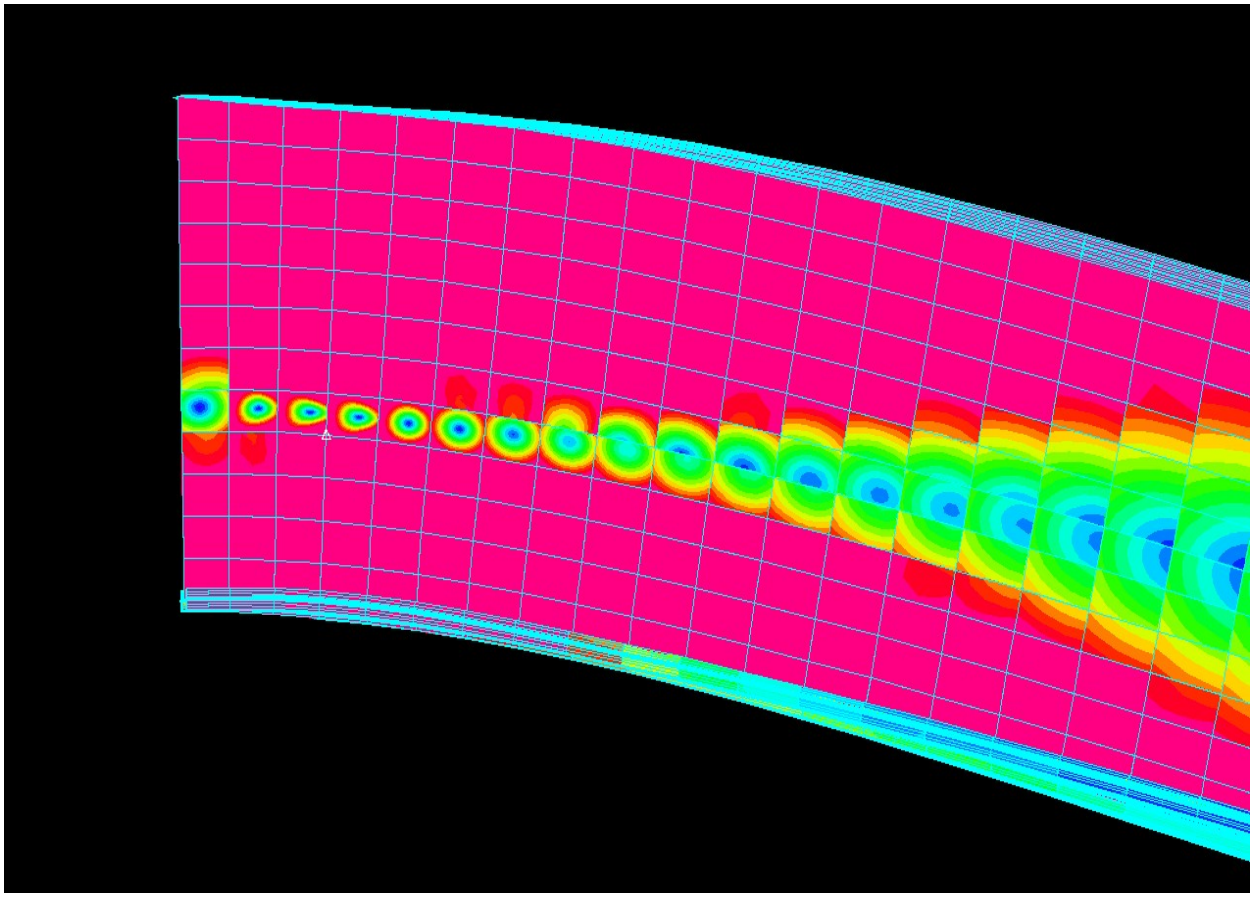

Figure A.26 Beam 15

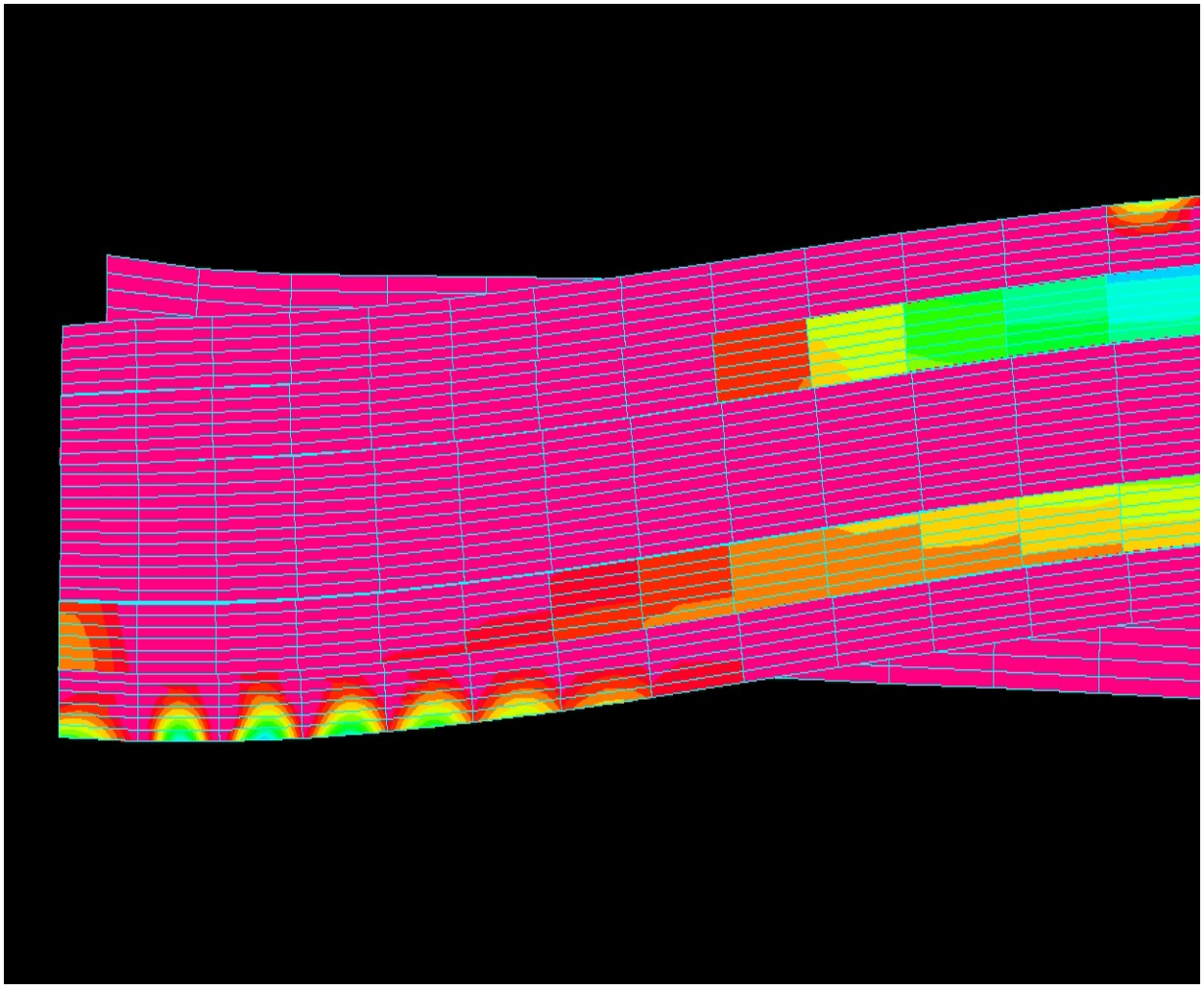

Figure A.27 Beam 15

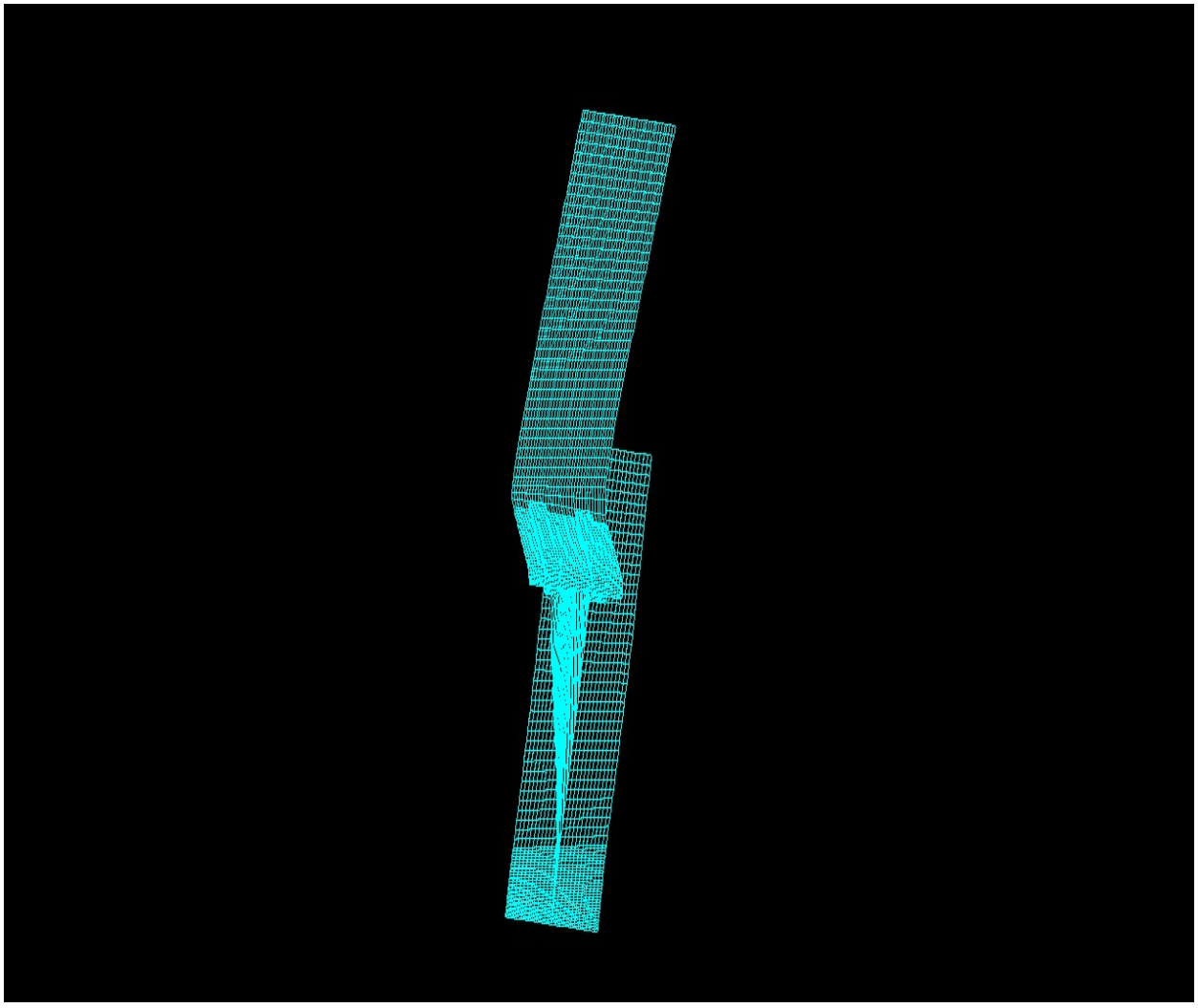

Figure A.28 Beam 16

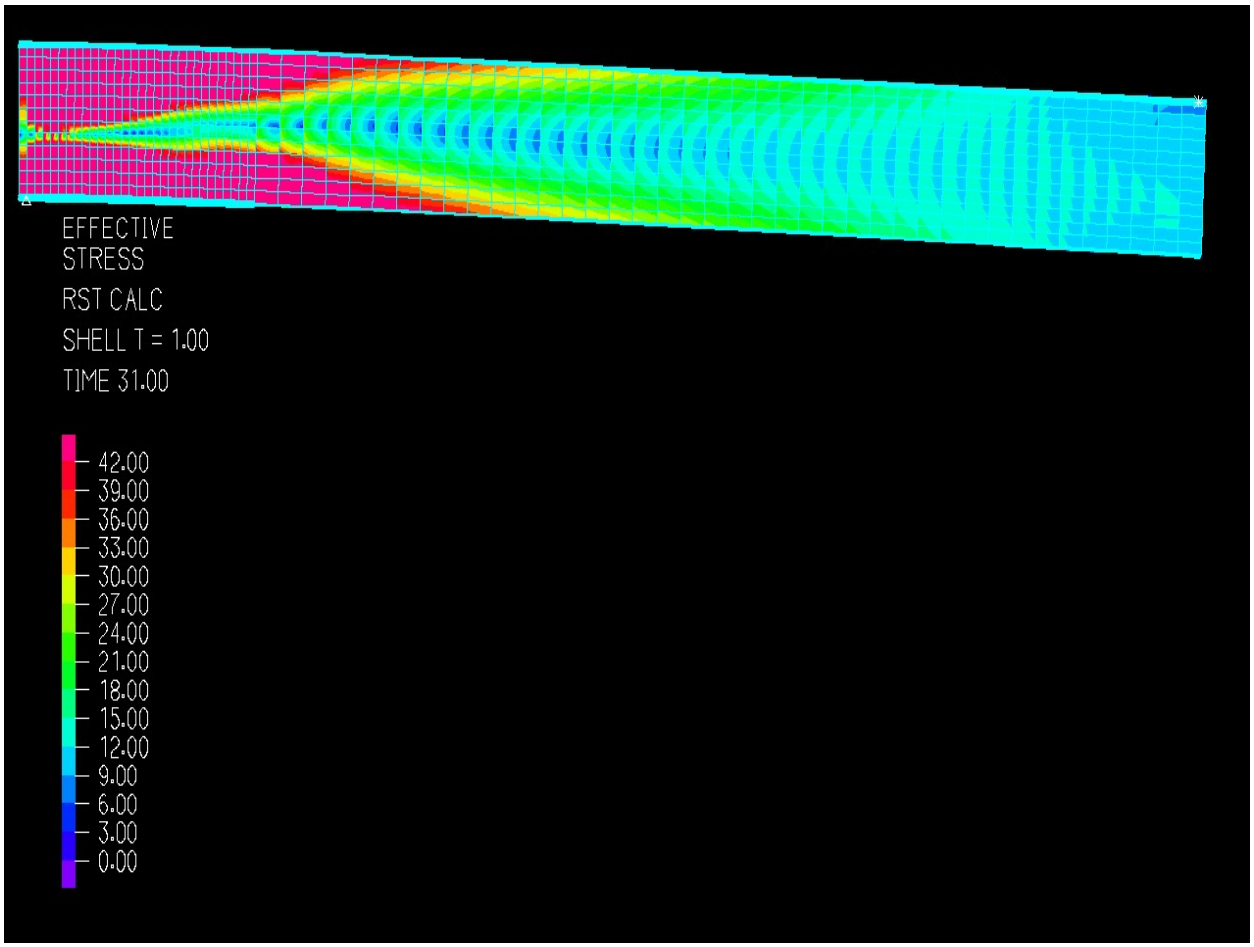

Figure A.29 Beam 16

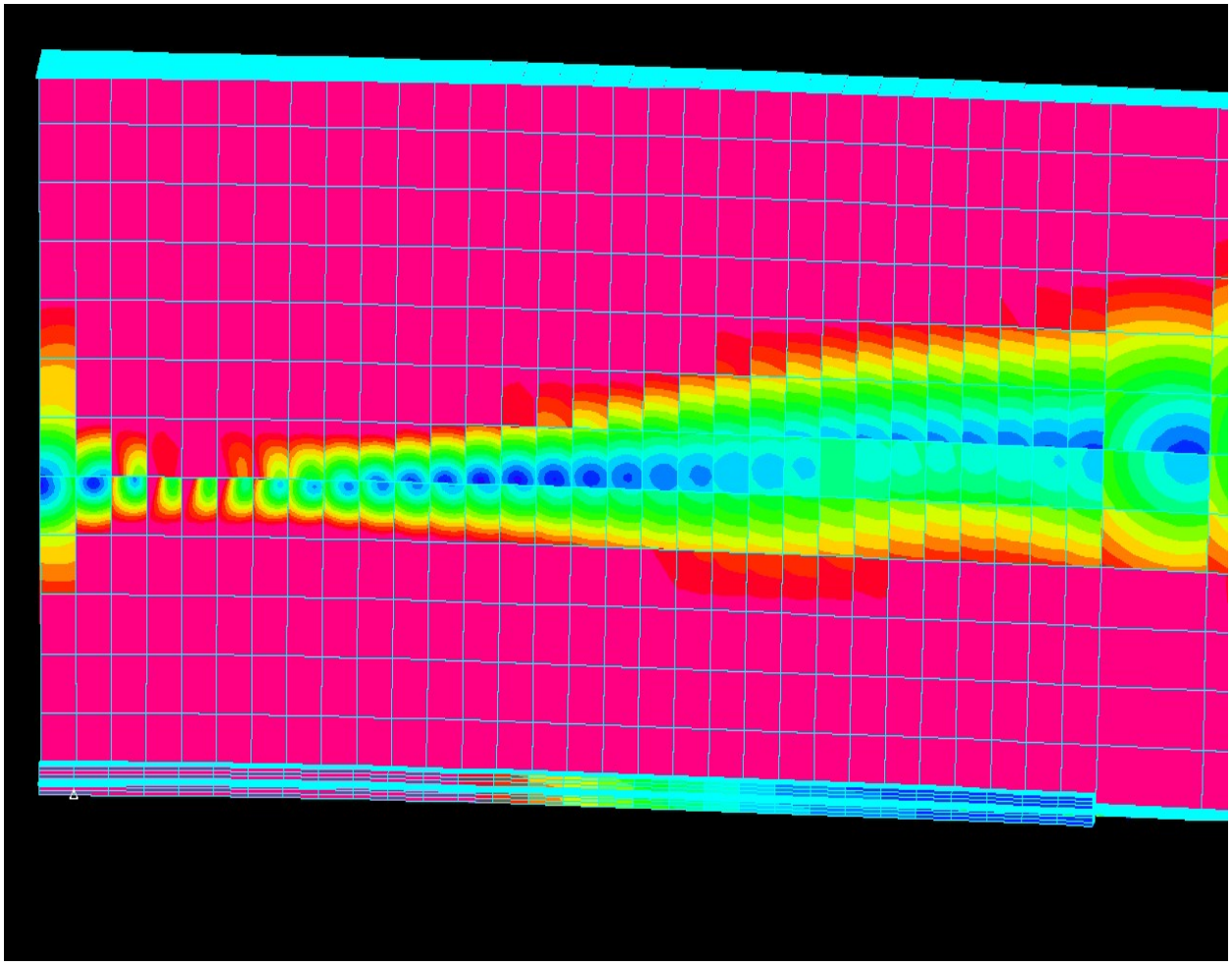

Figure A.30 Beam 16

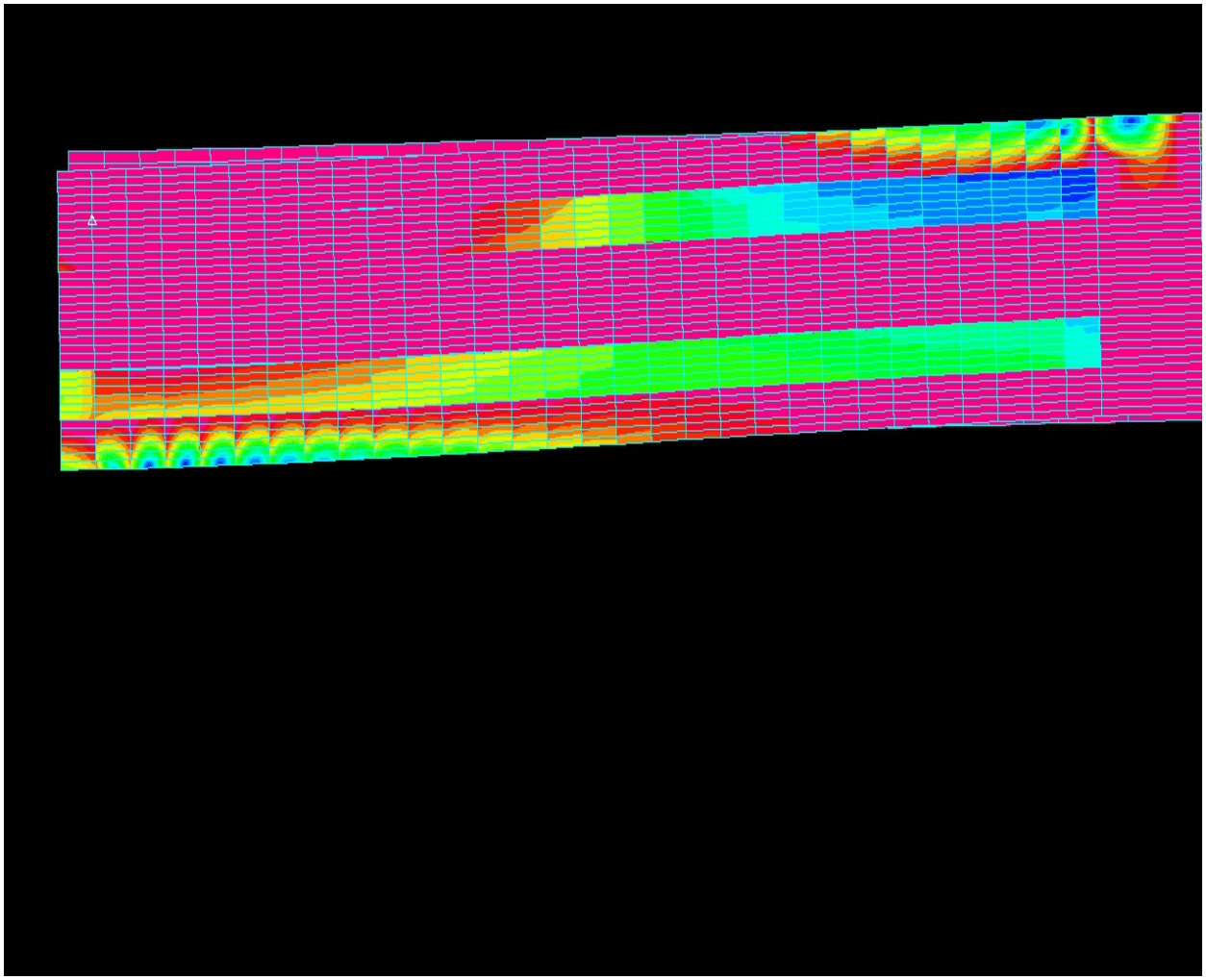

Figure A.31 Beam 16

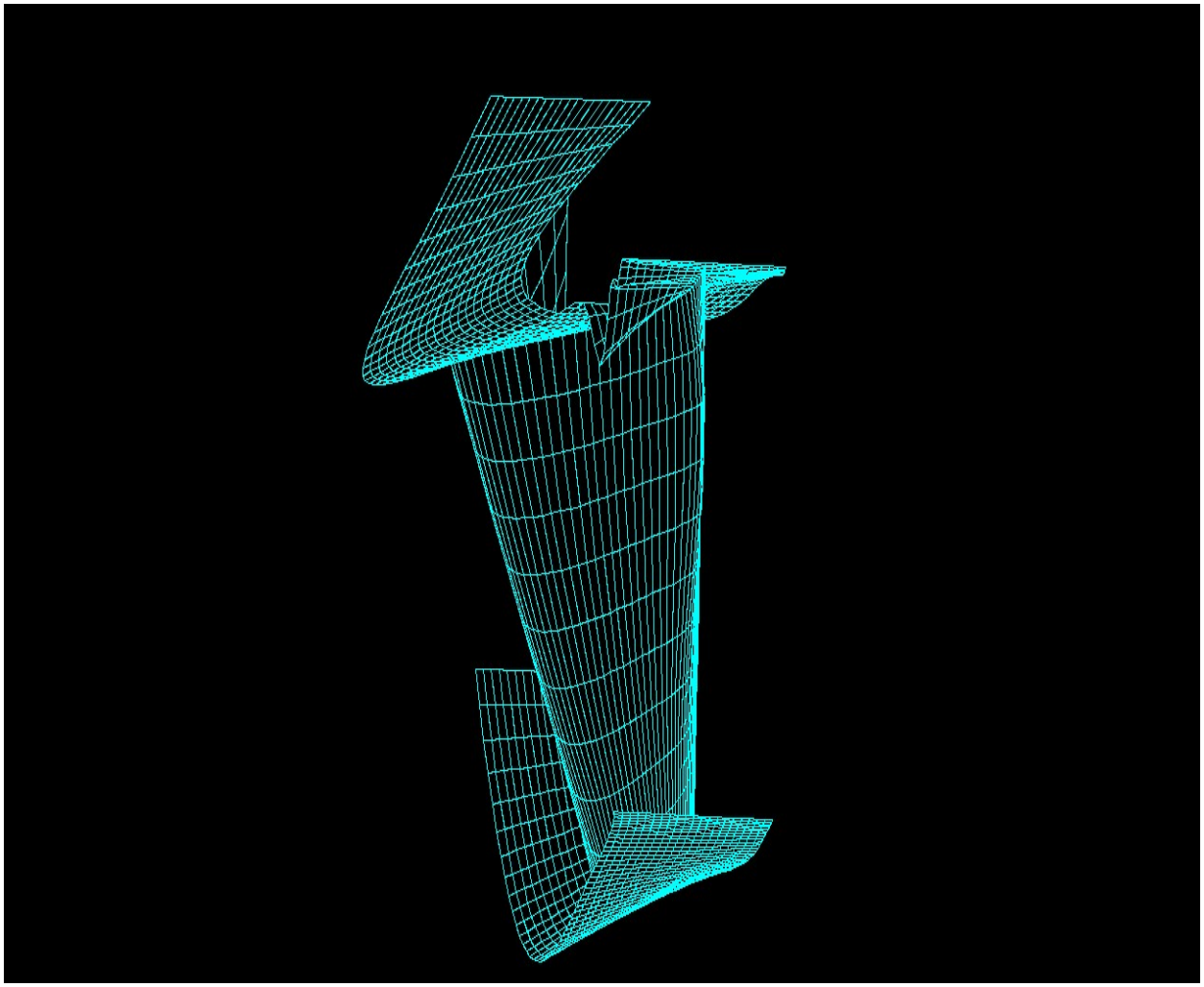

Figure A.32 Bare Steel 2

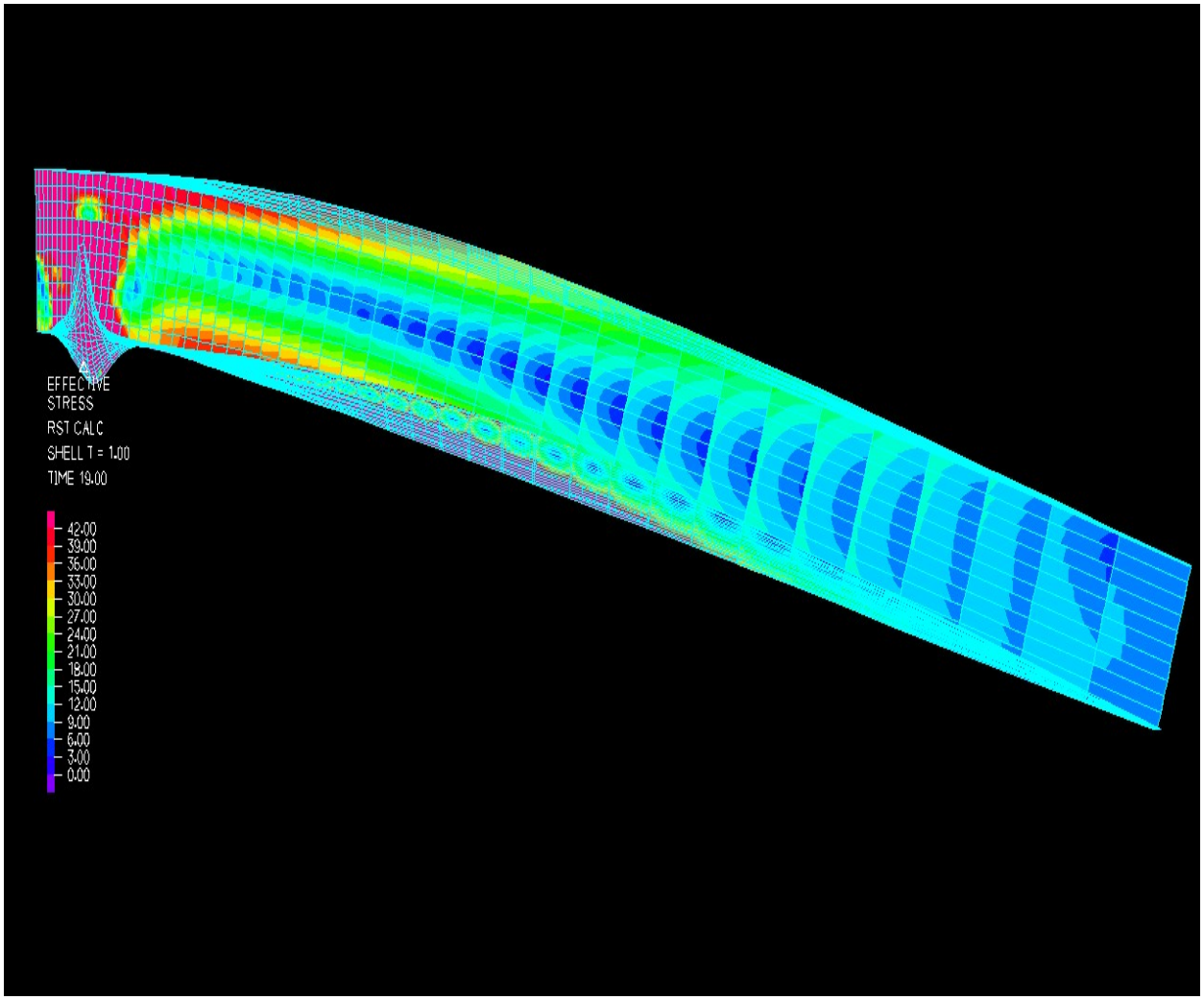

Figure A.33 Bare Steel 2

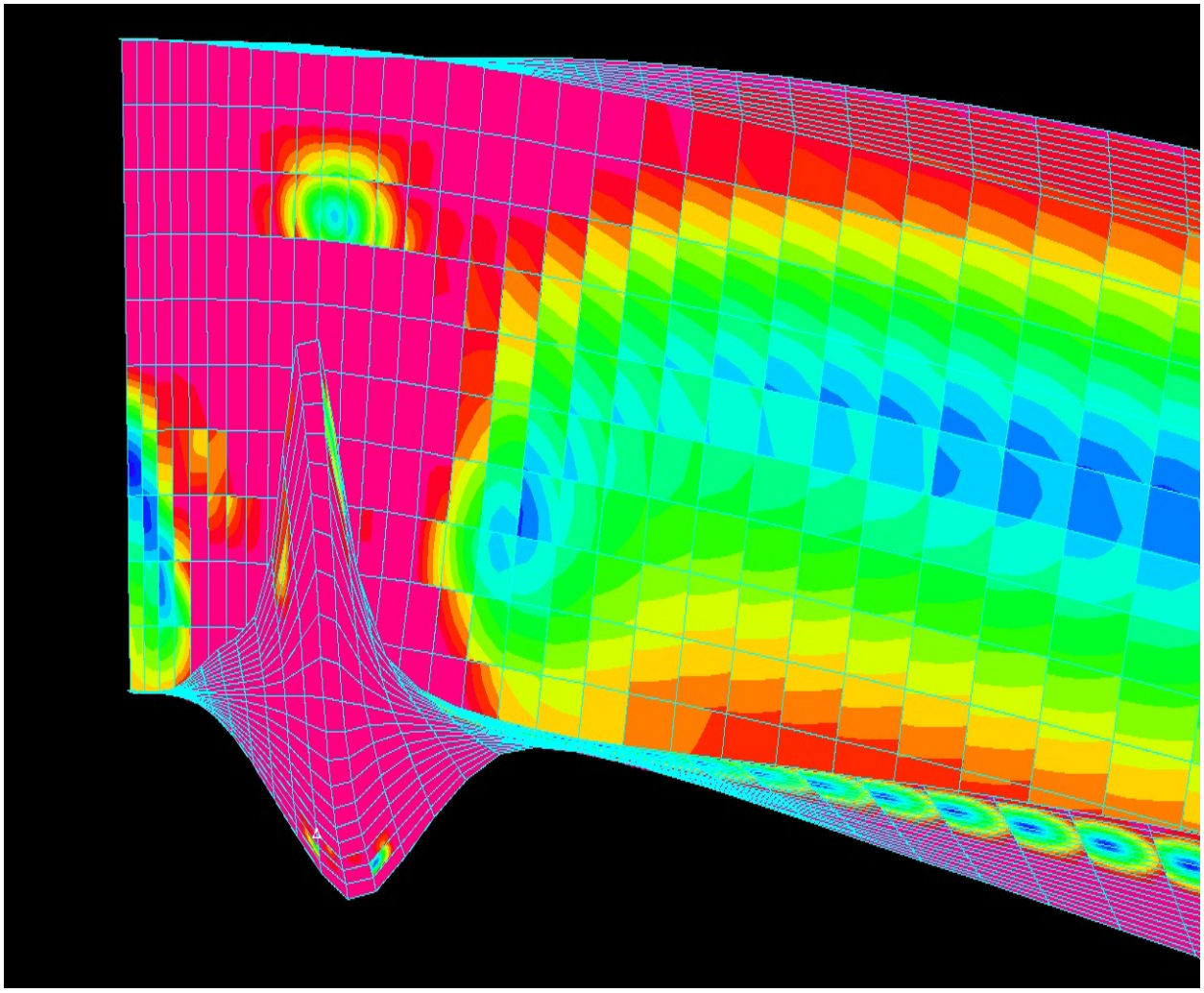

Figure A.34 Bare Steel 2

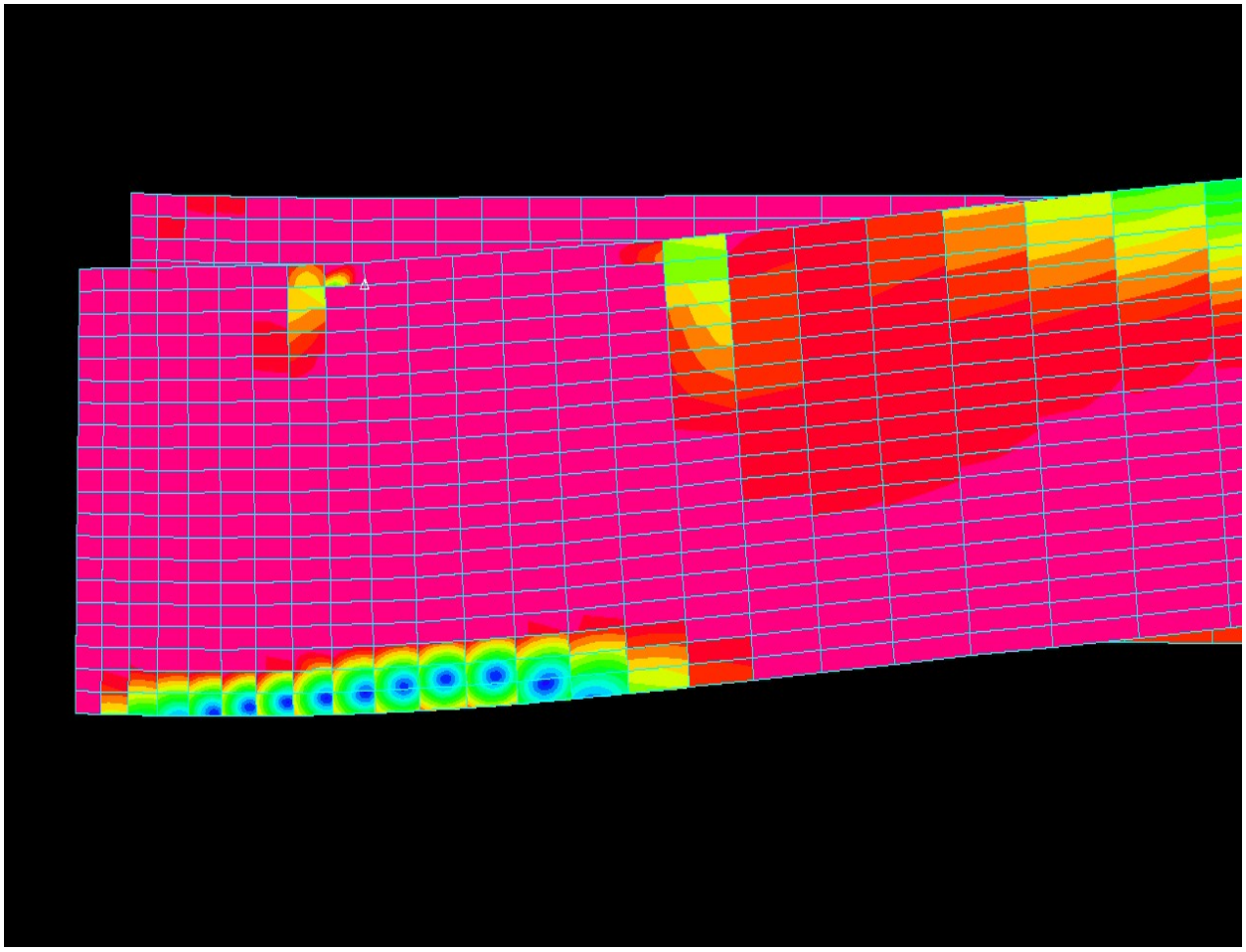

Figure A.35 Bare Steel 2

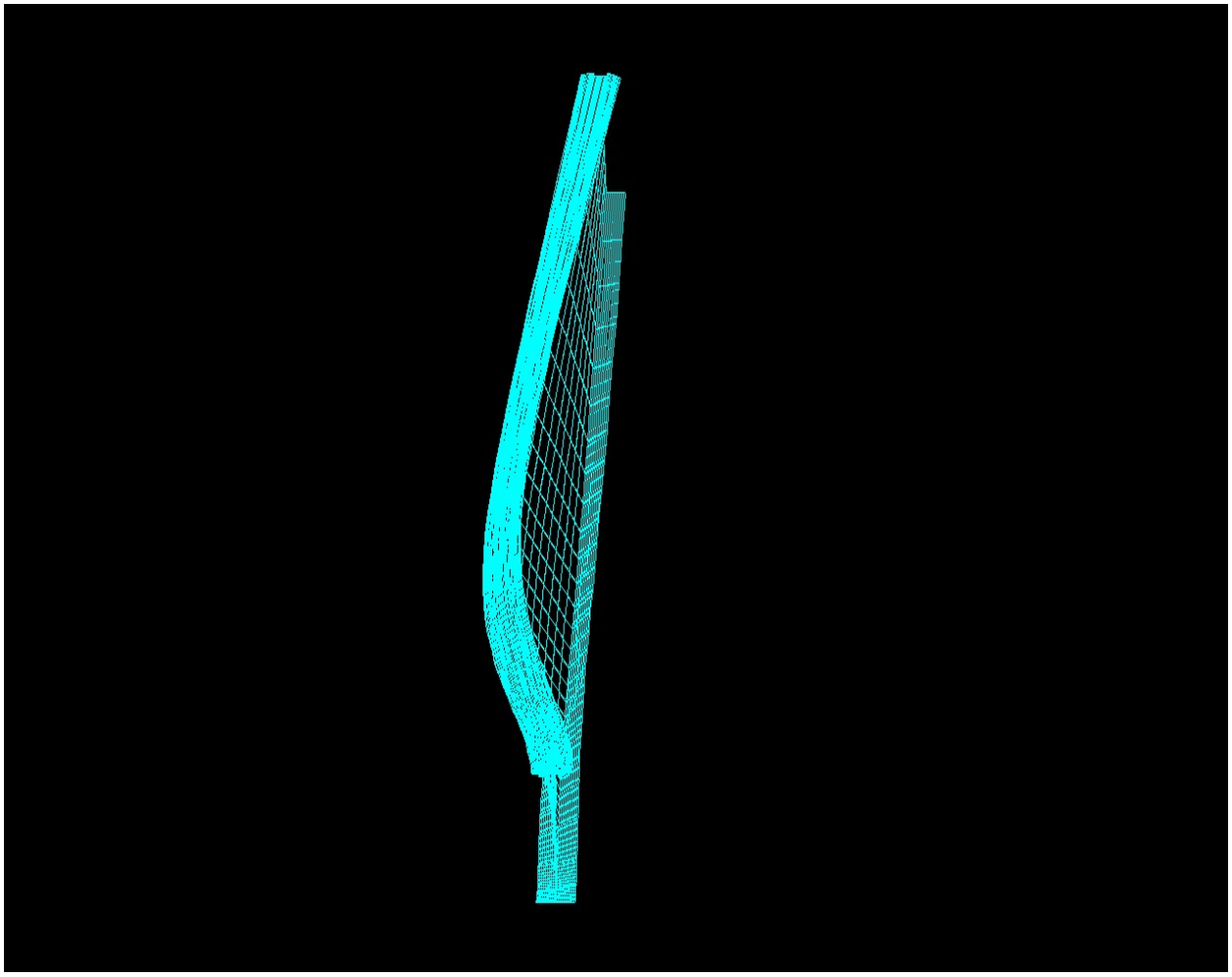

Figure A.36 Beam 10

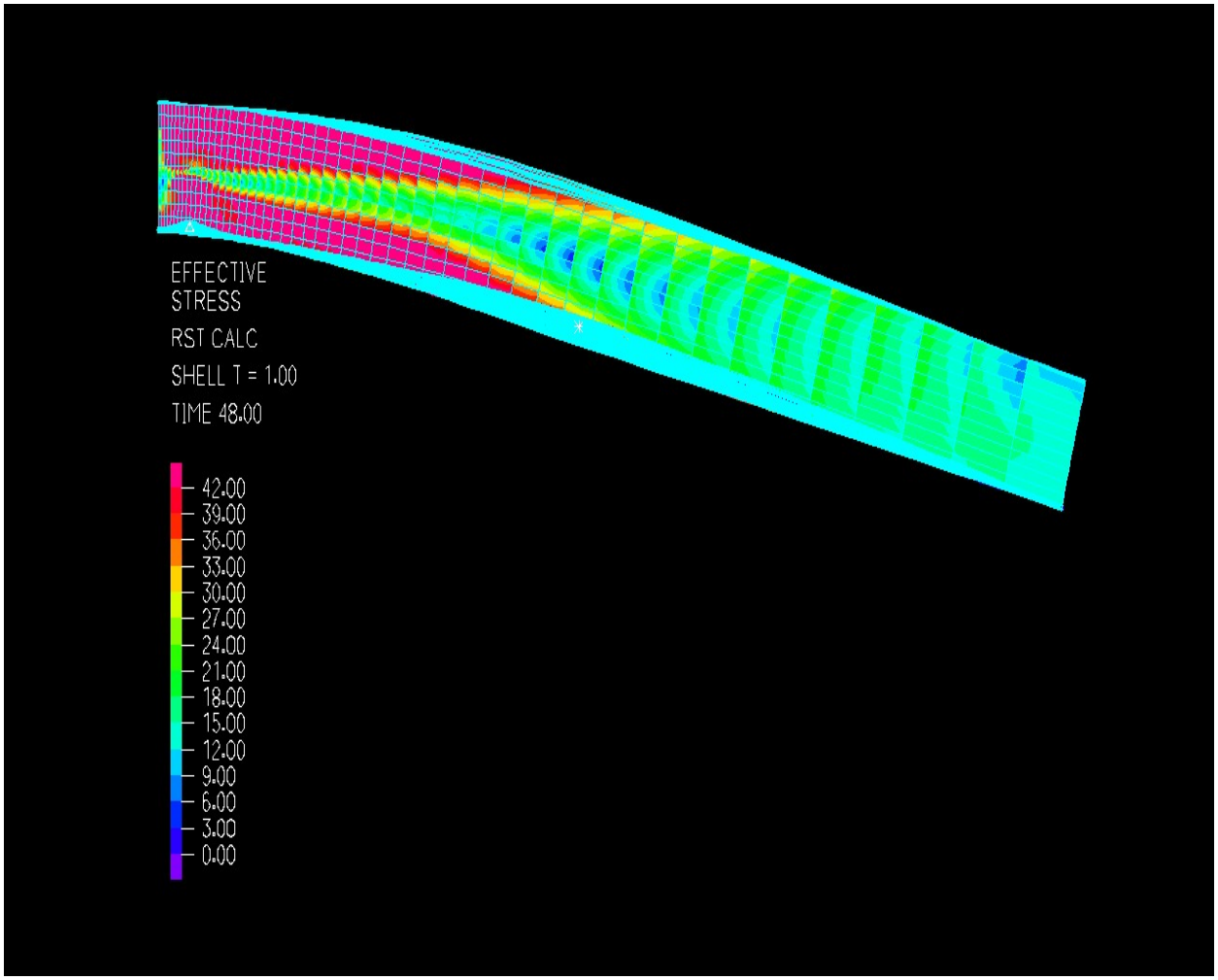

Figure A.37 Beam 10

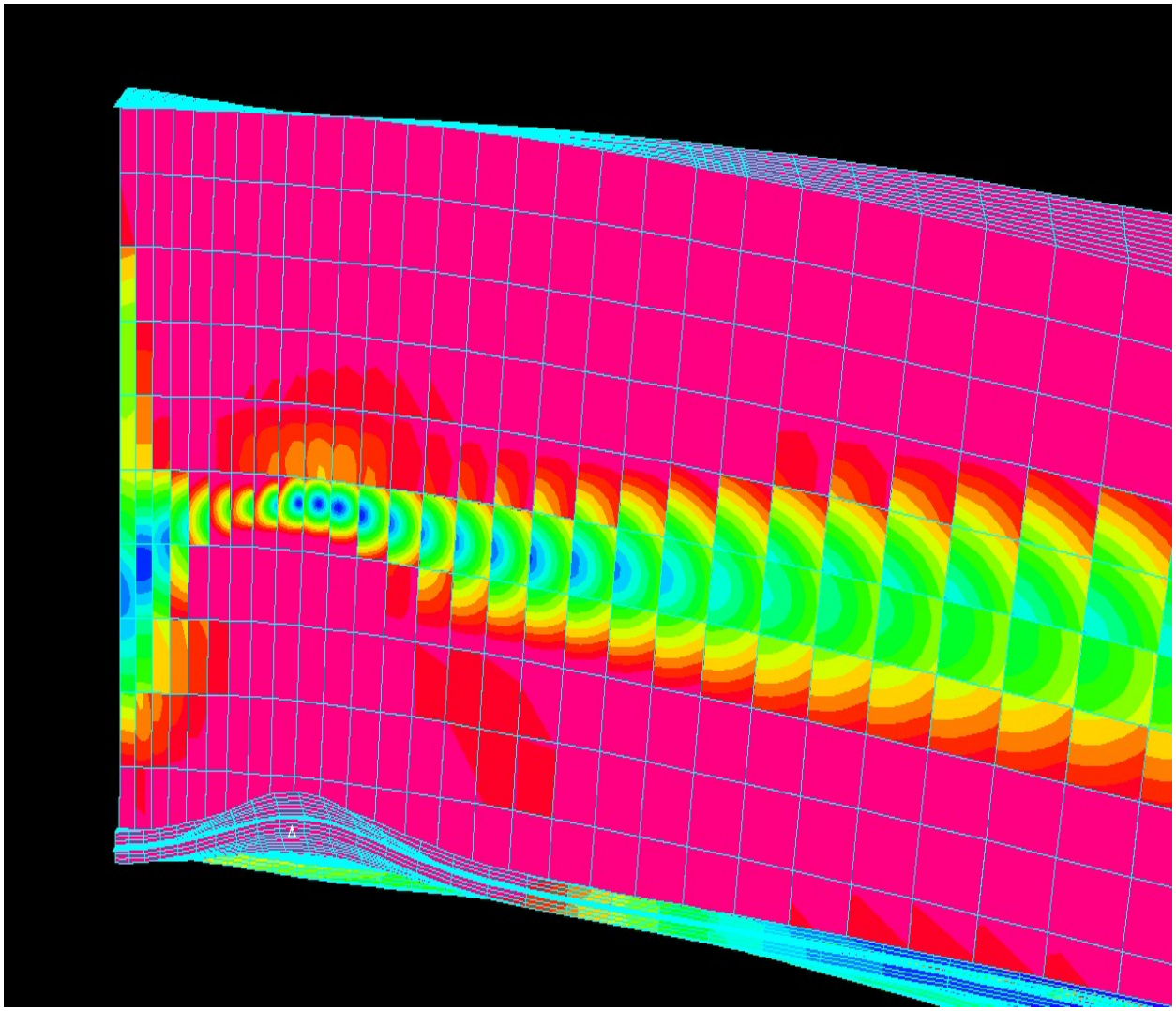

Figure A.38 Beam 10

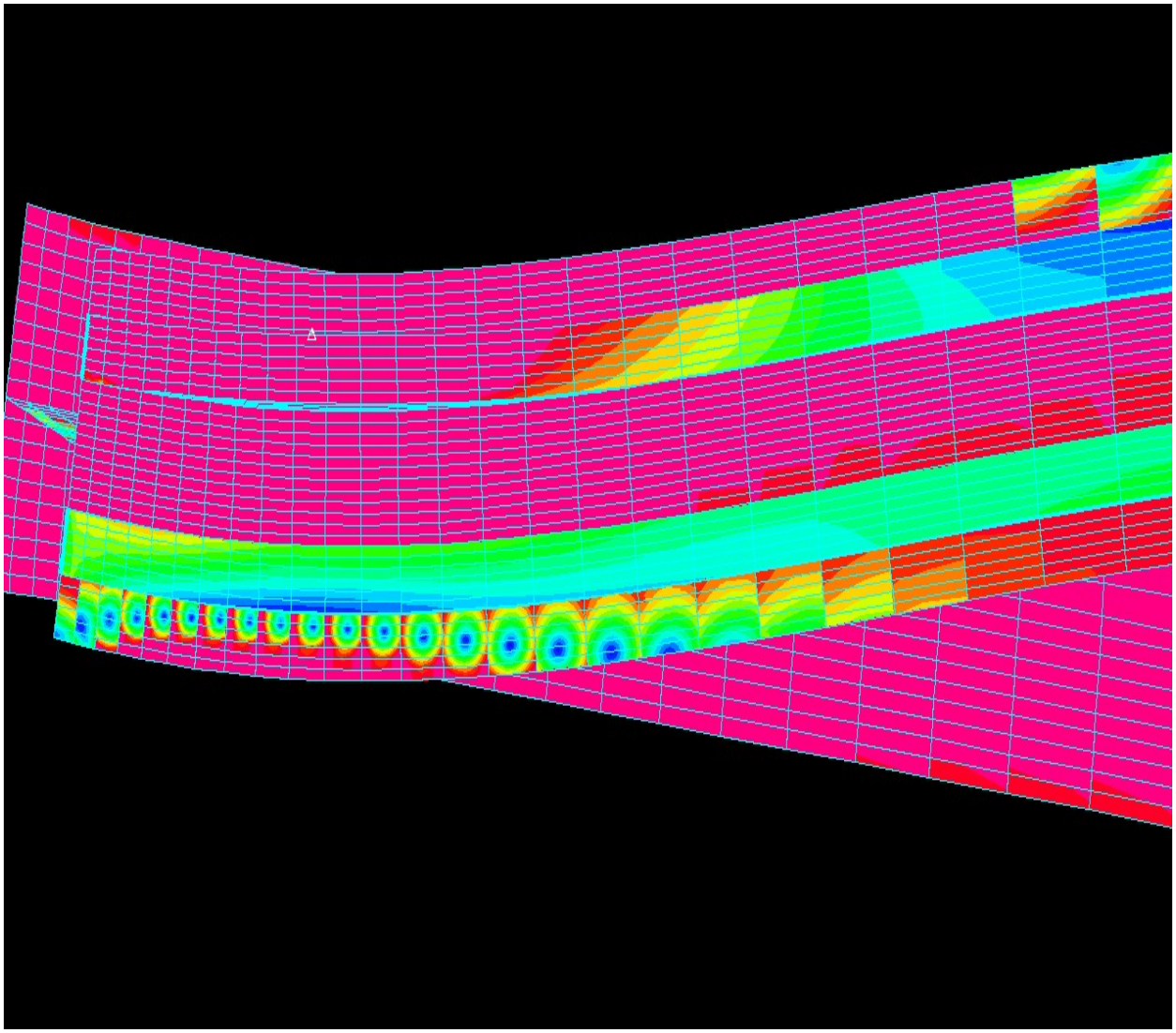

Figure A.39 Beam 10

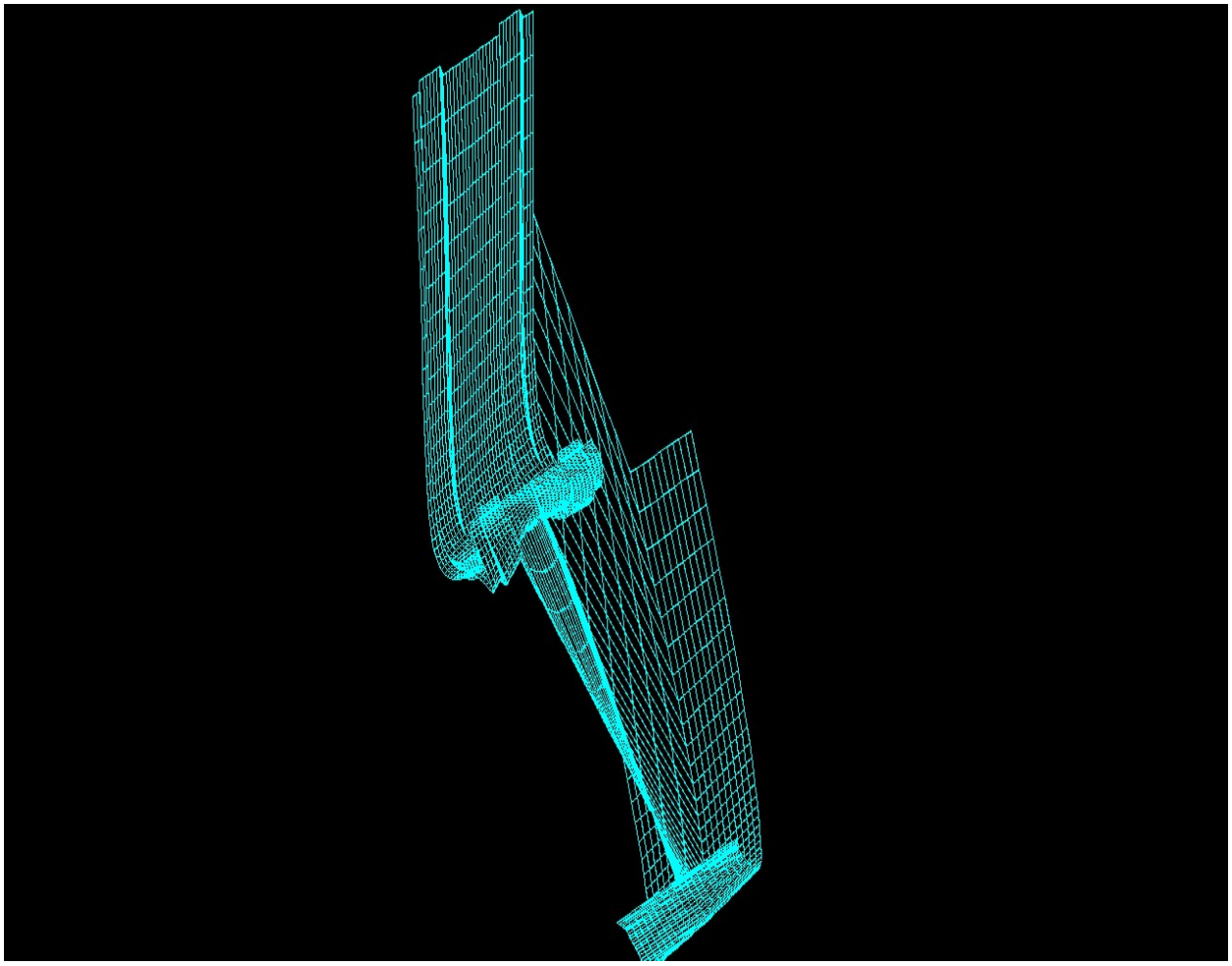

Figure A.40 Beam 17

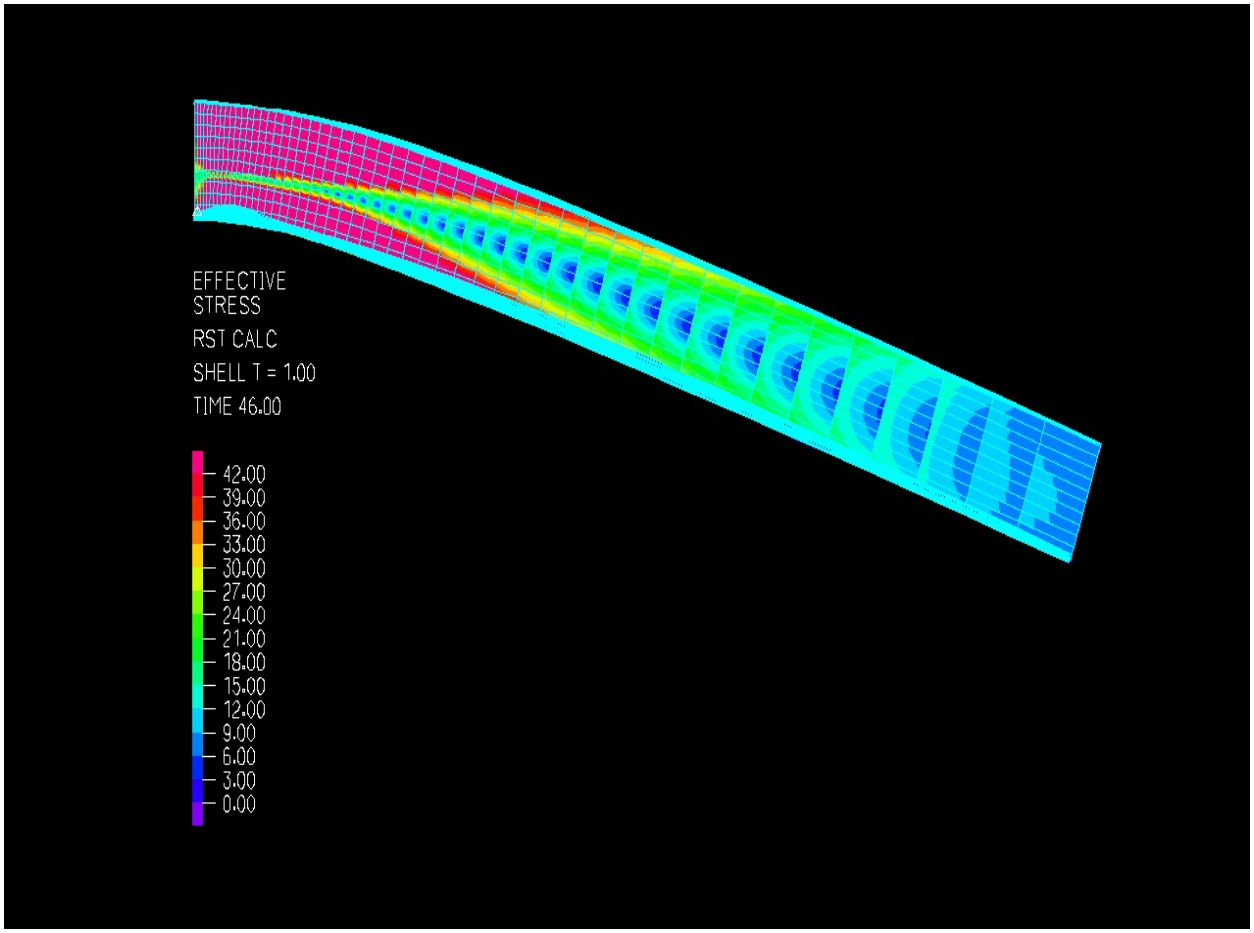

Figure A.41 Beam 17

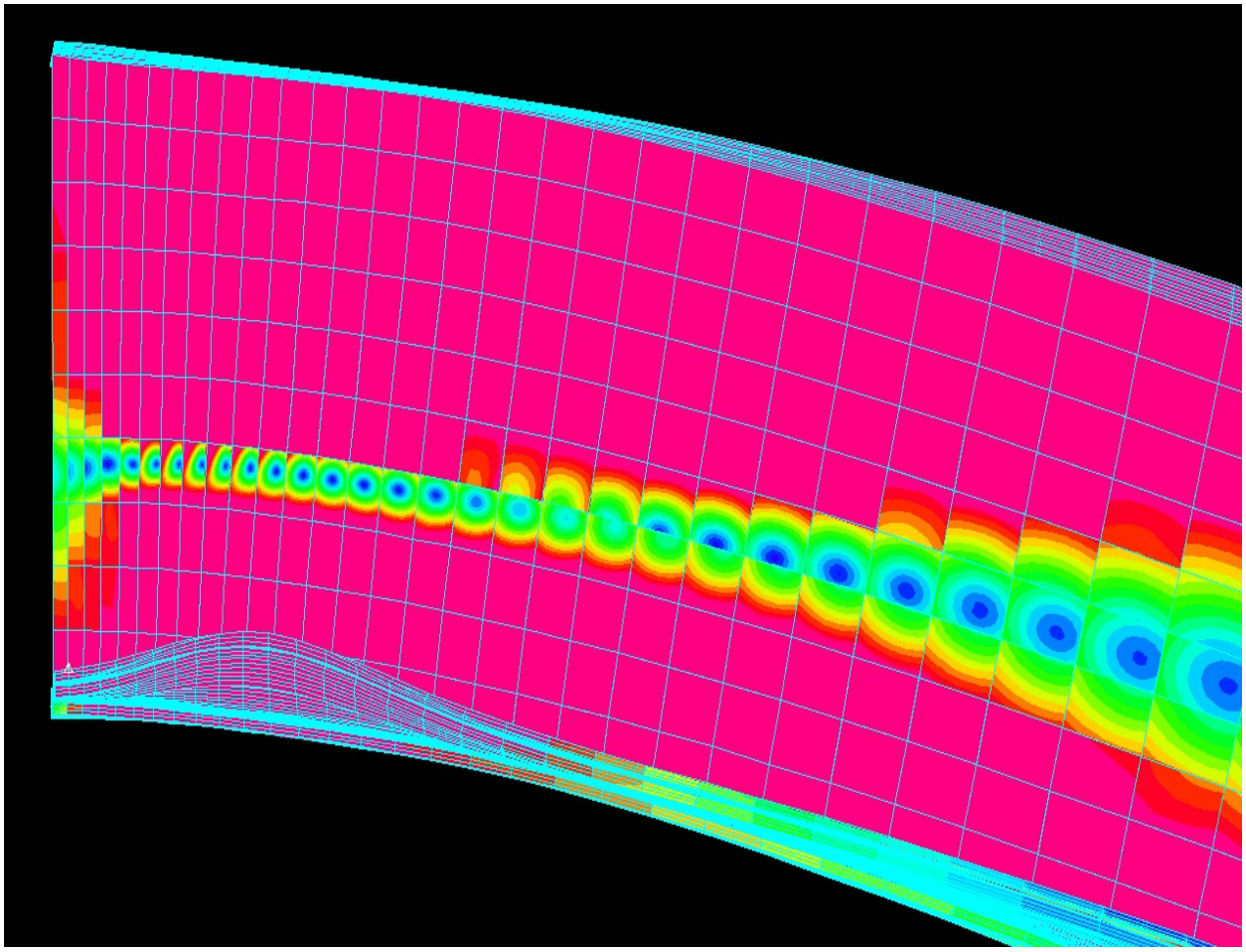

Figure A.42 Beam 17

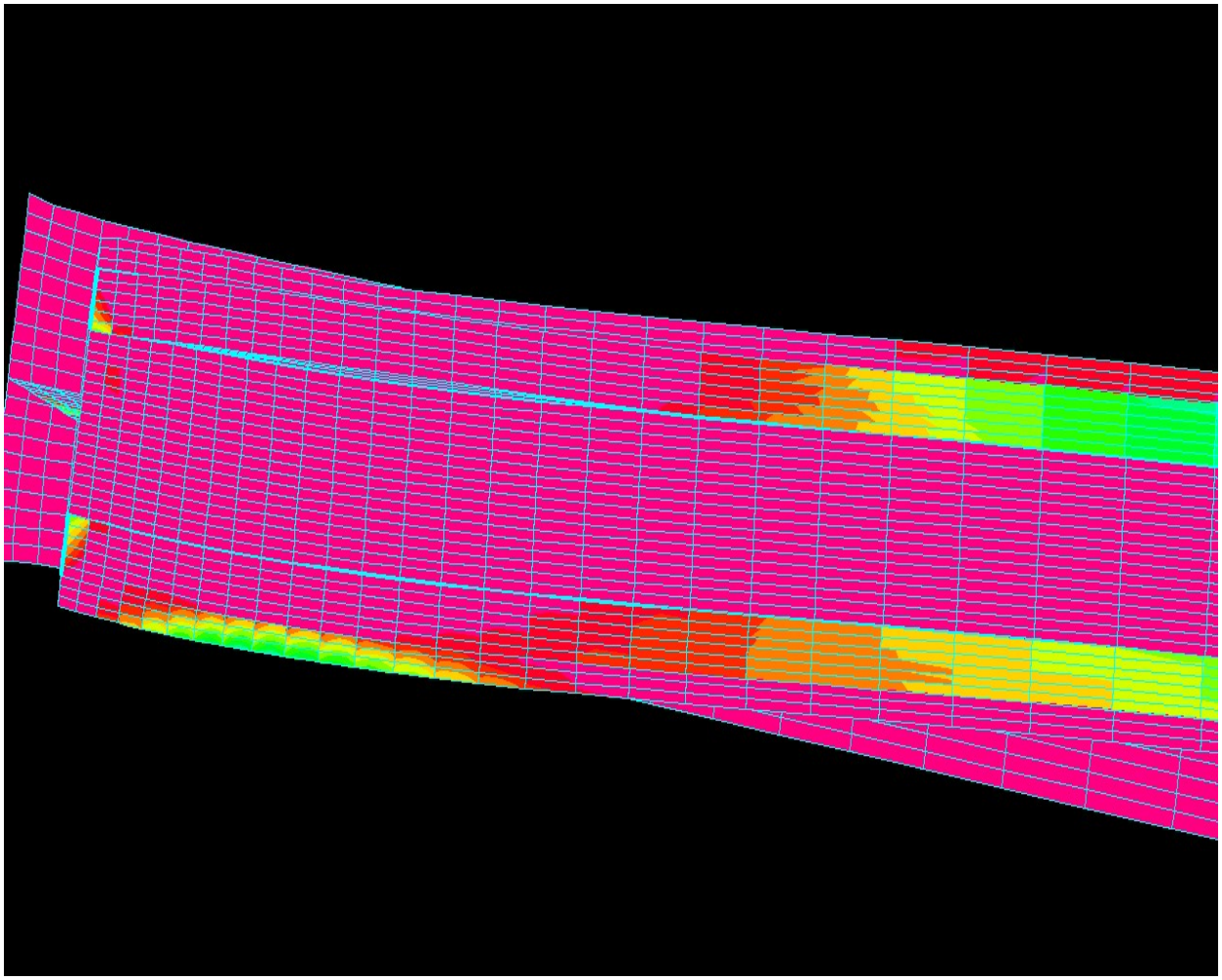

Figure A.43 Beam 17

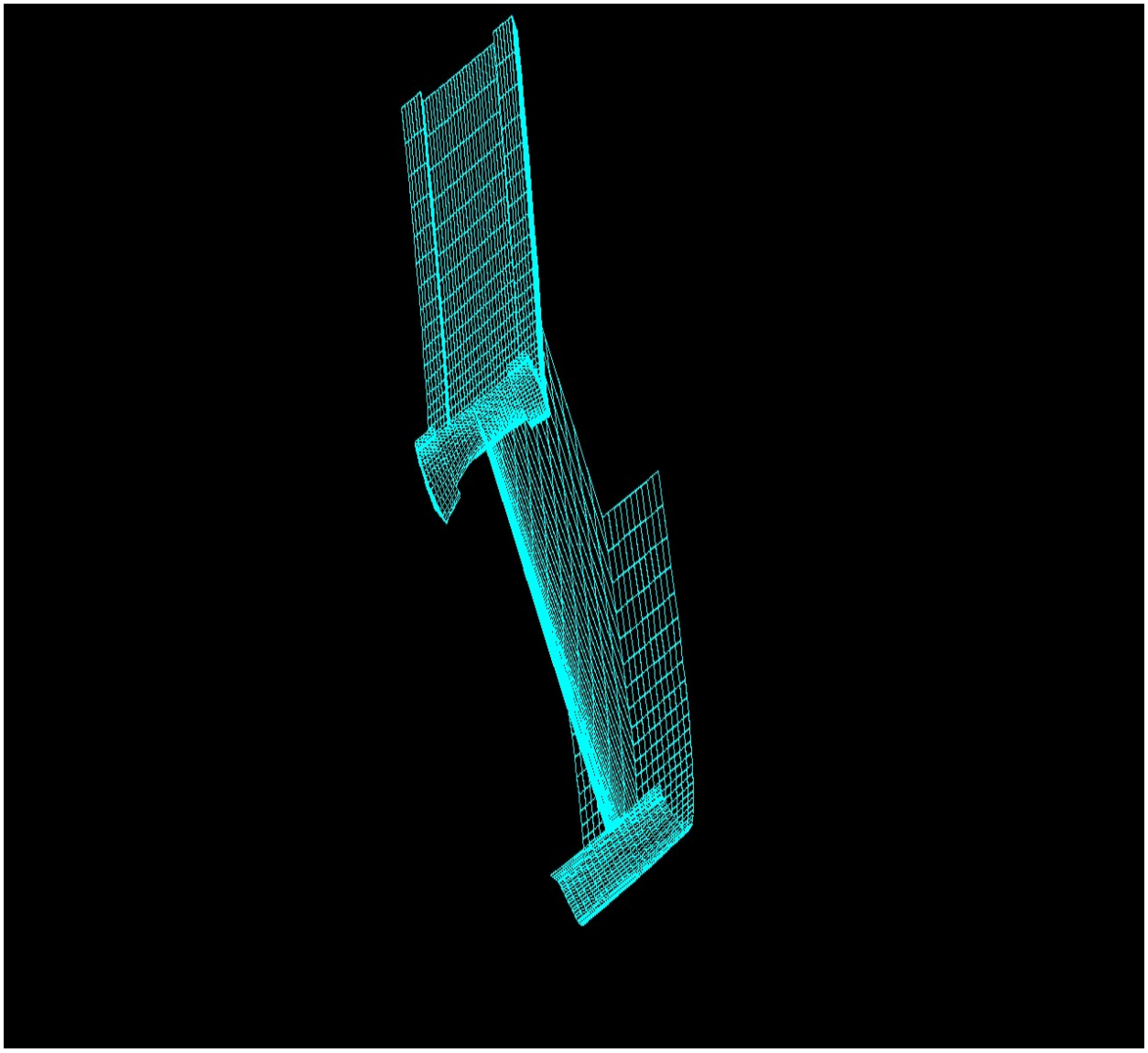

Figure A.44 Beam 18

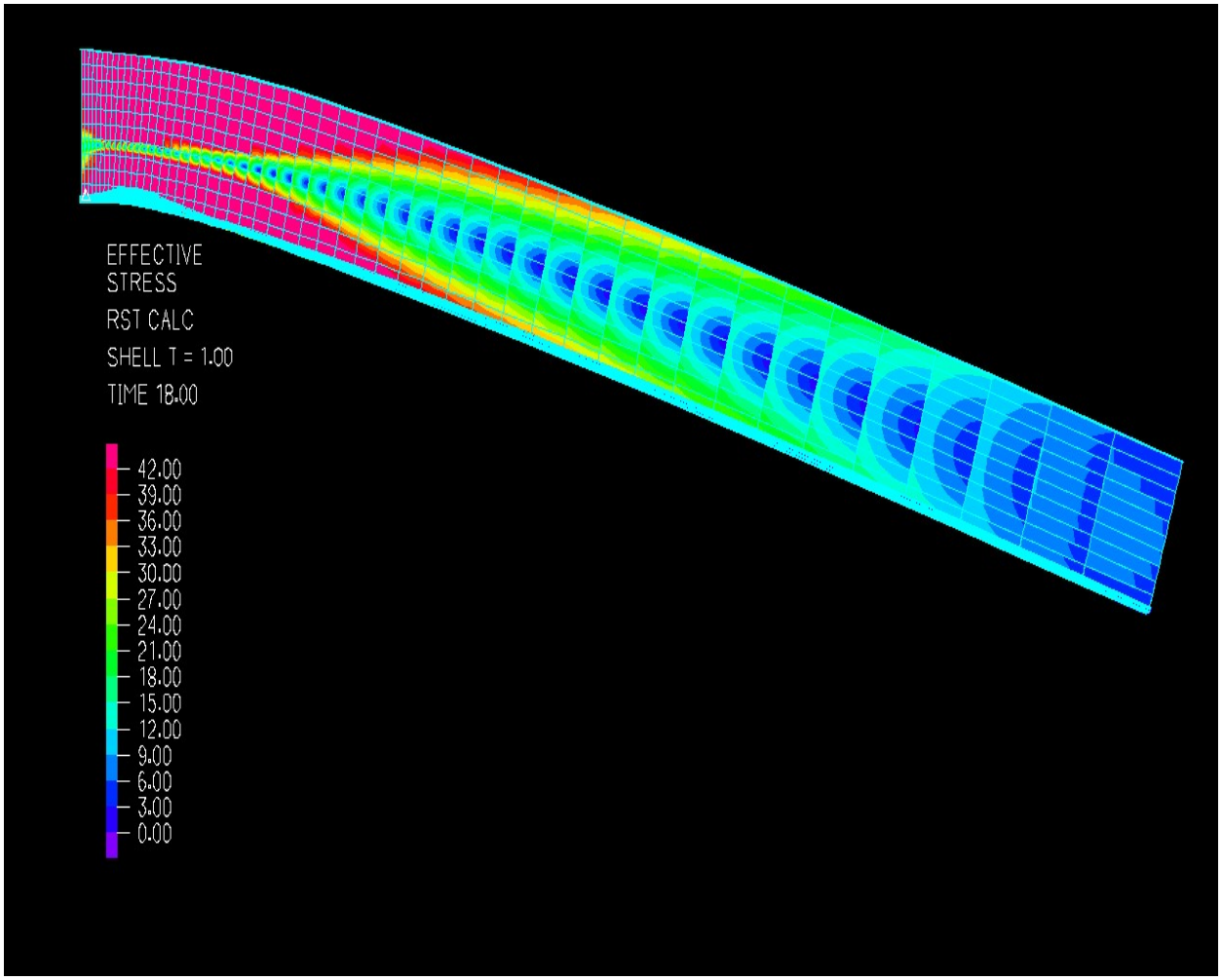

Figure A.45 Beam 18

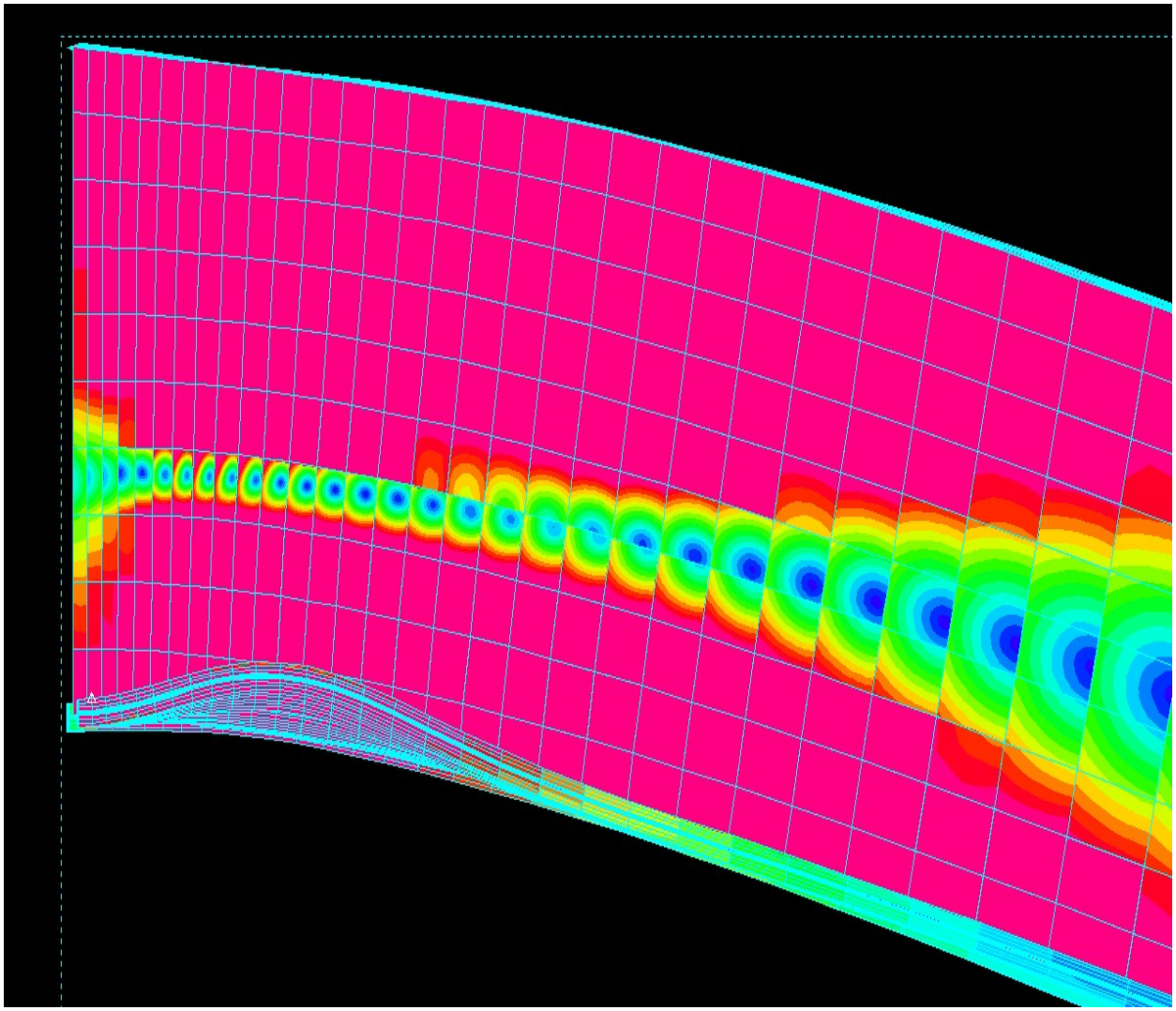

Figure A.46 Beam 18

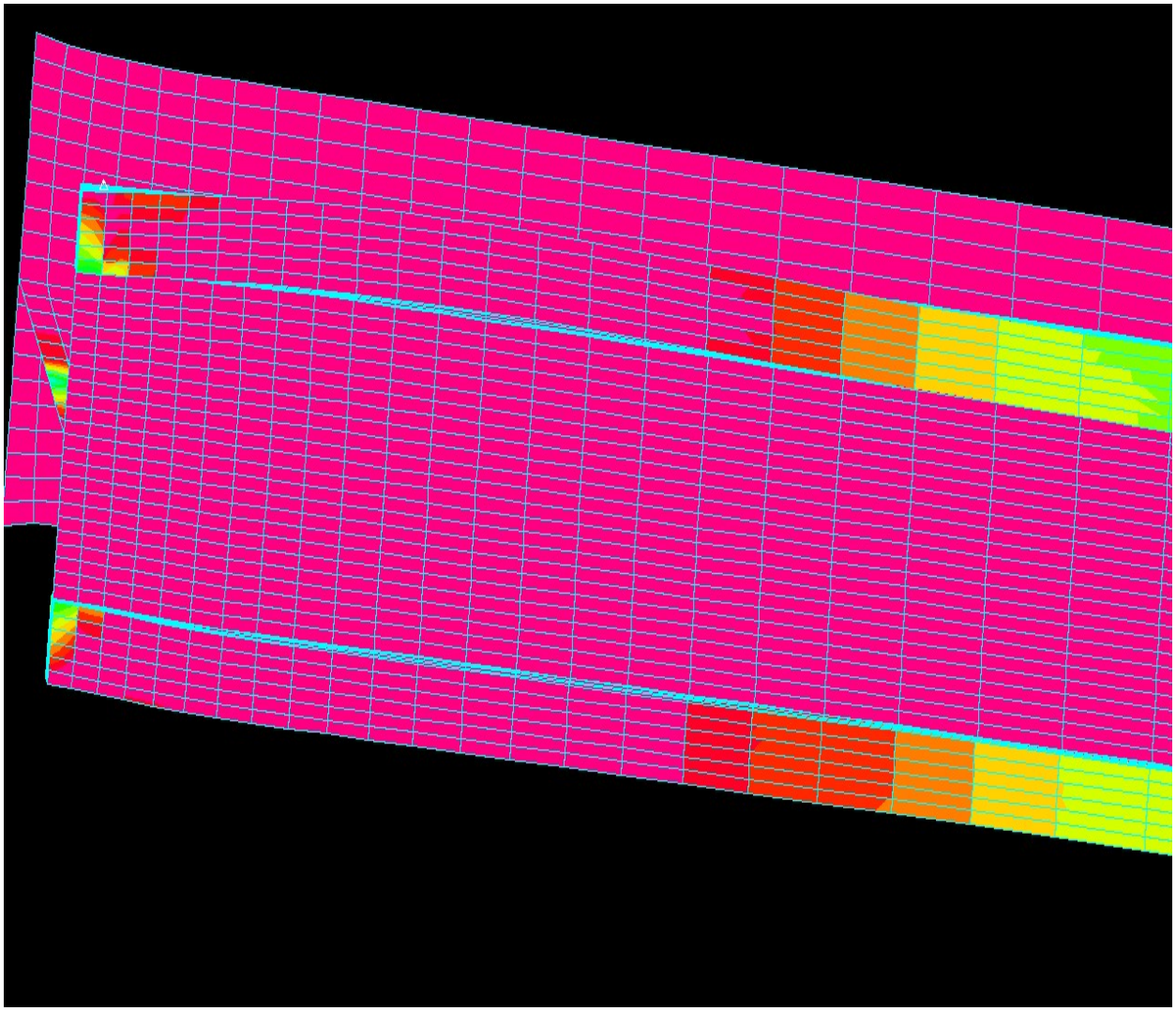

Figure A.47 Beam 18

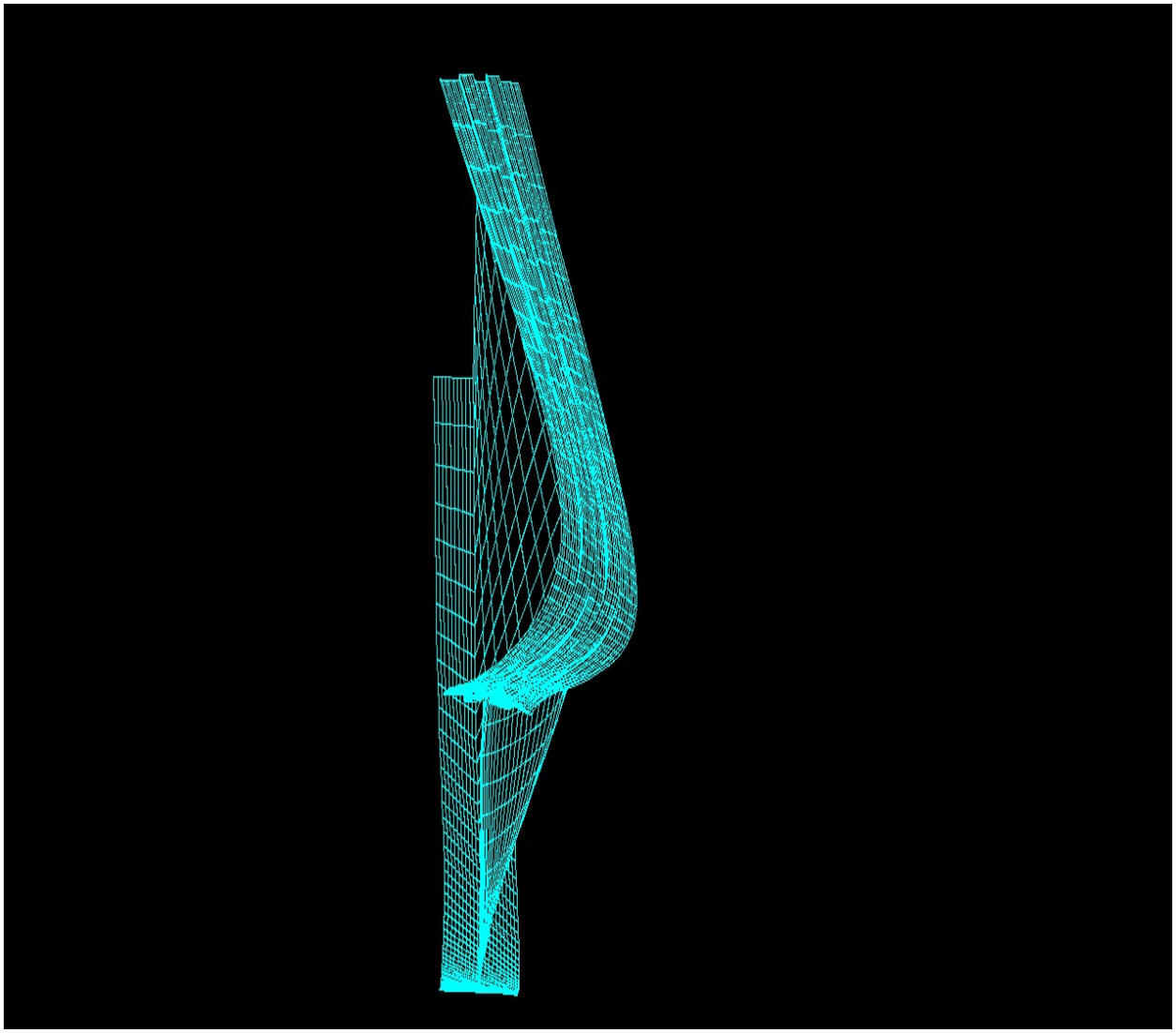

Figure A.48 Beam 19

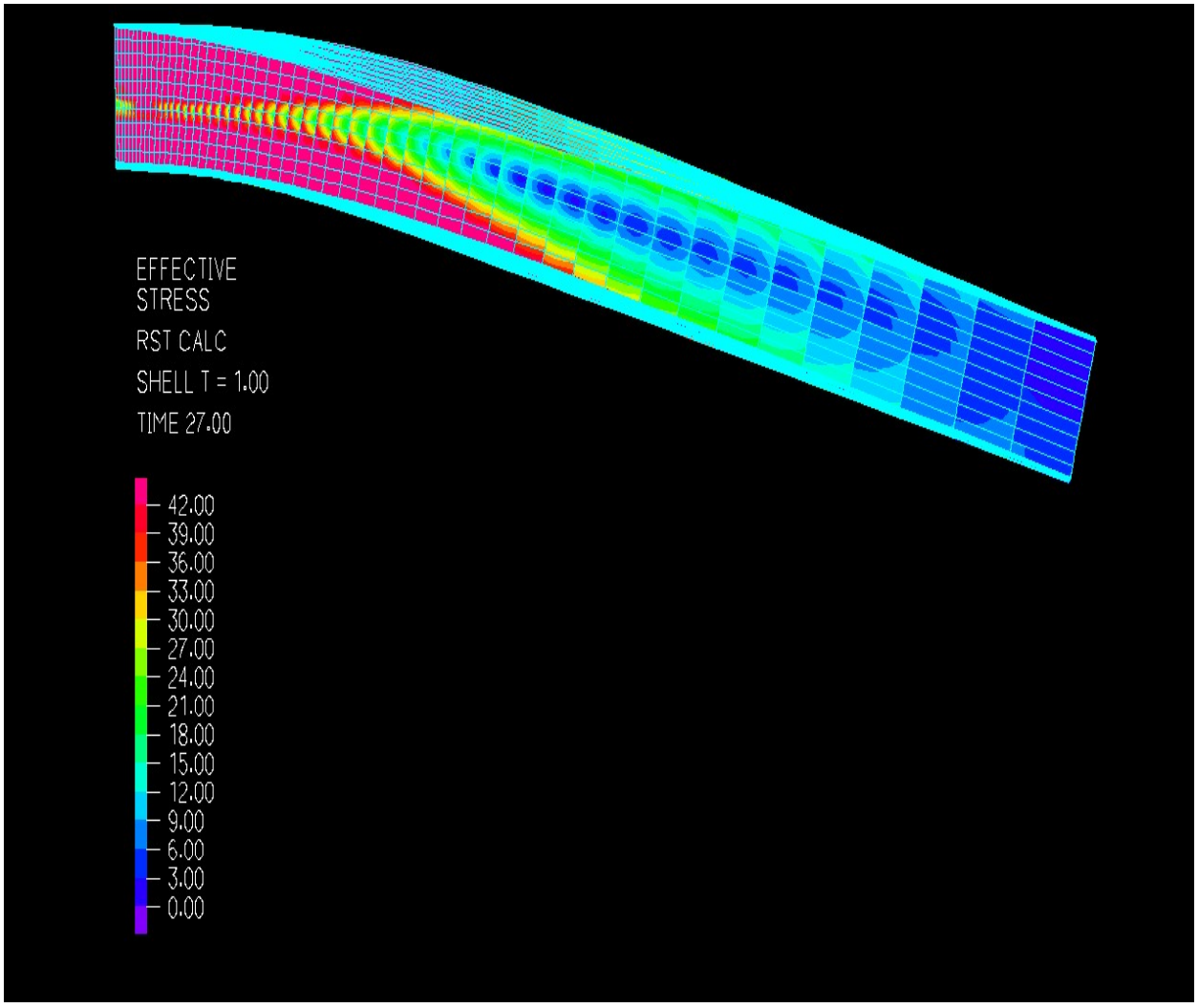

Figure A.49 Beam 19

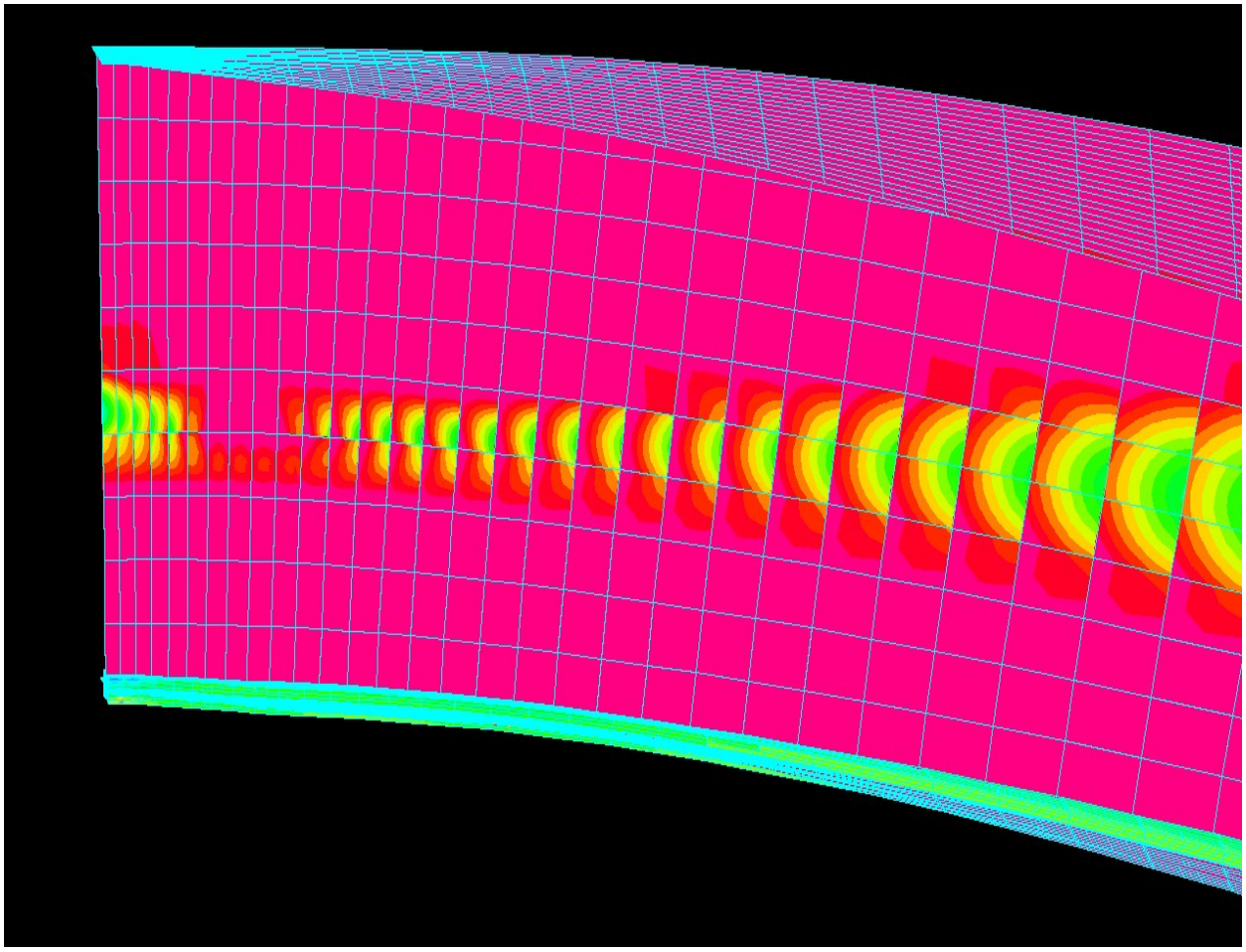

Figure A.50 Beam 19

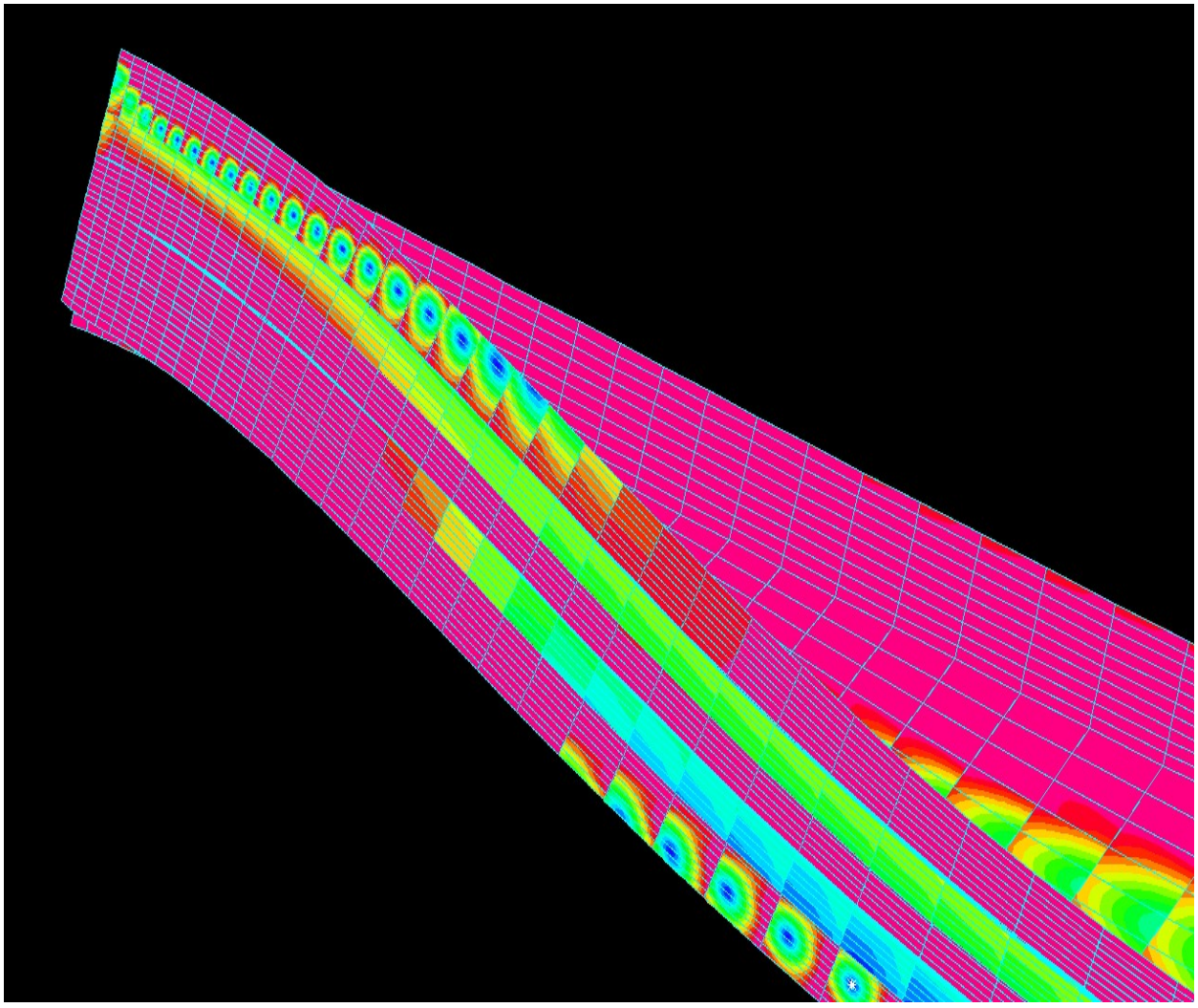

Figure A.51 Beam 19

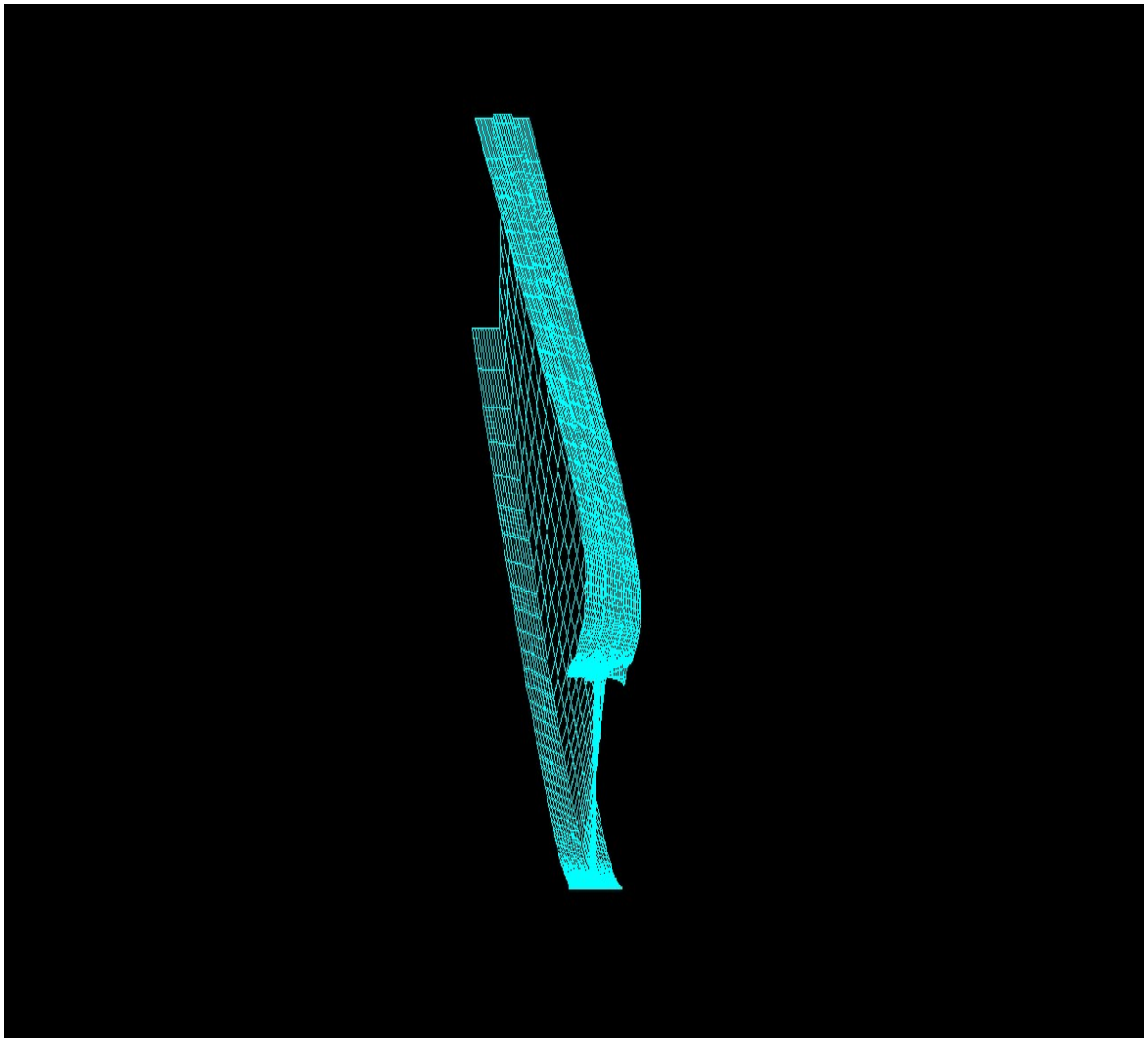

Figure A.52 Beam 20

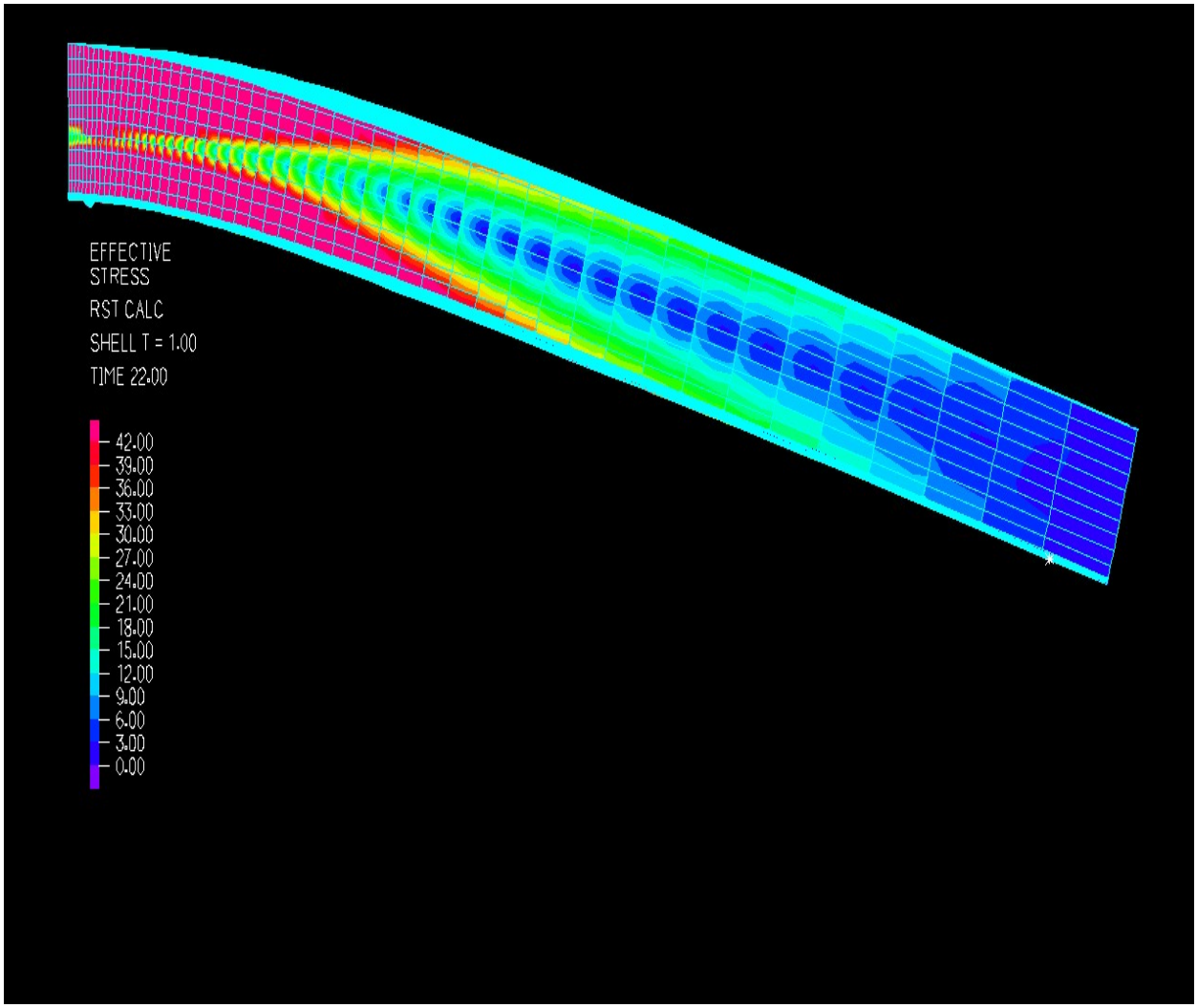

Figure A.53 Beam 20

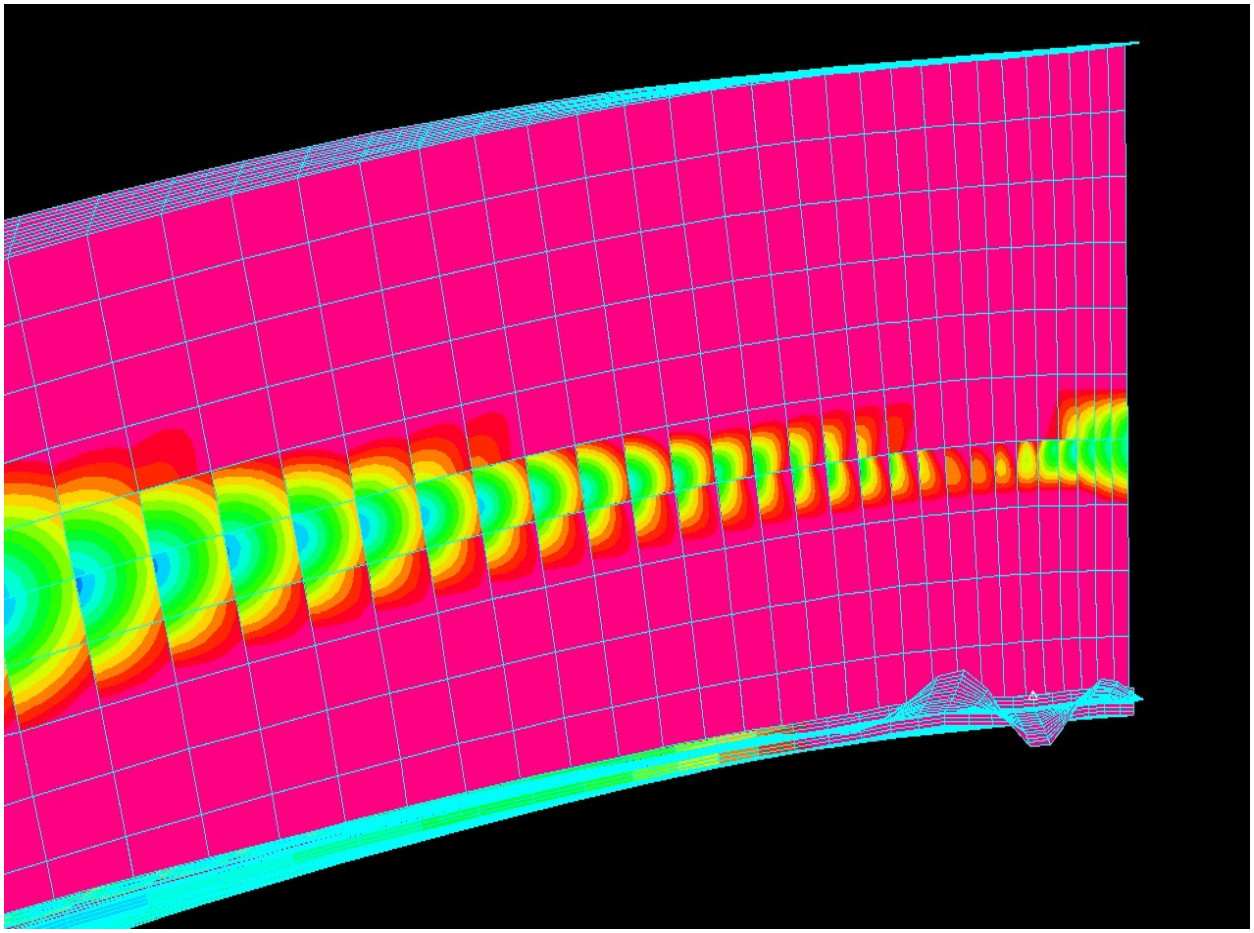

Figure A.54 Beam 20

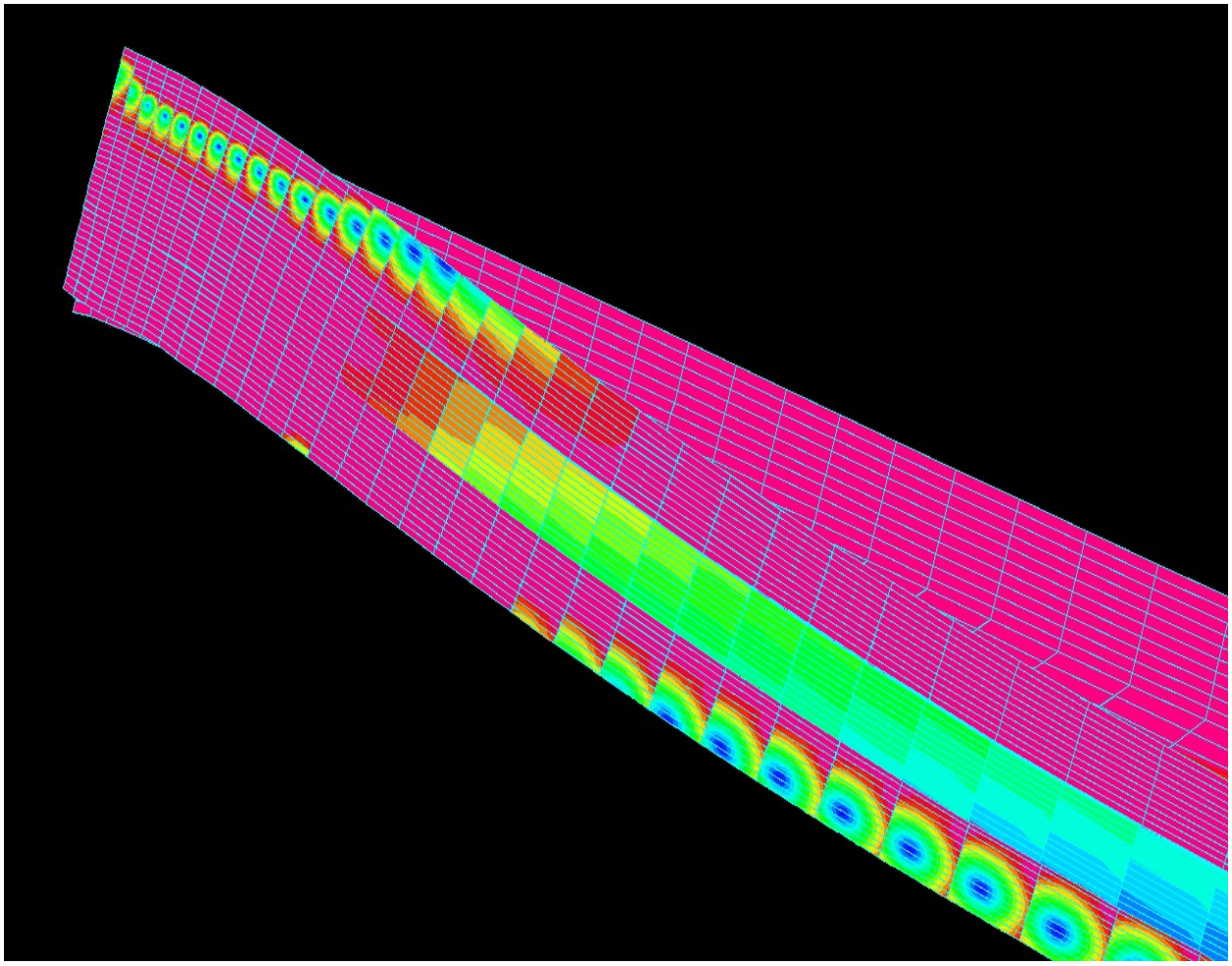

Figure A.55 Beam 20

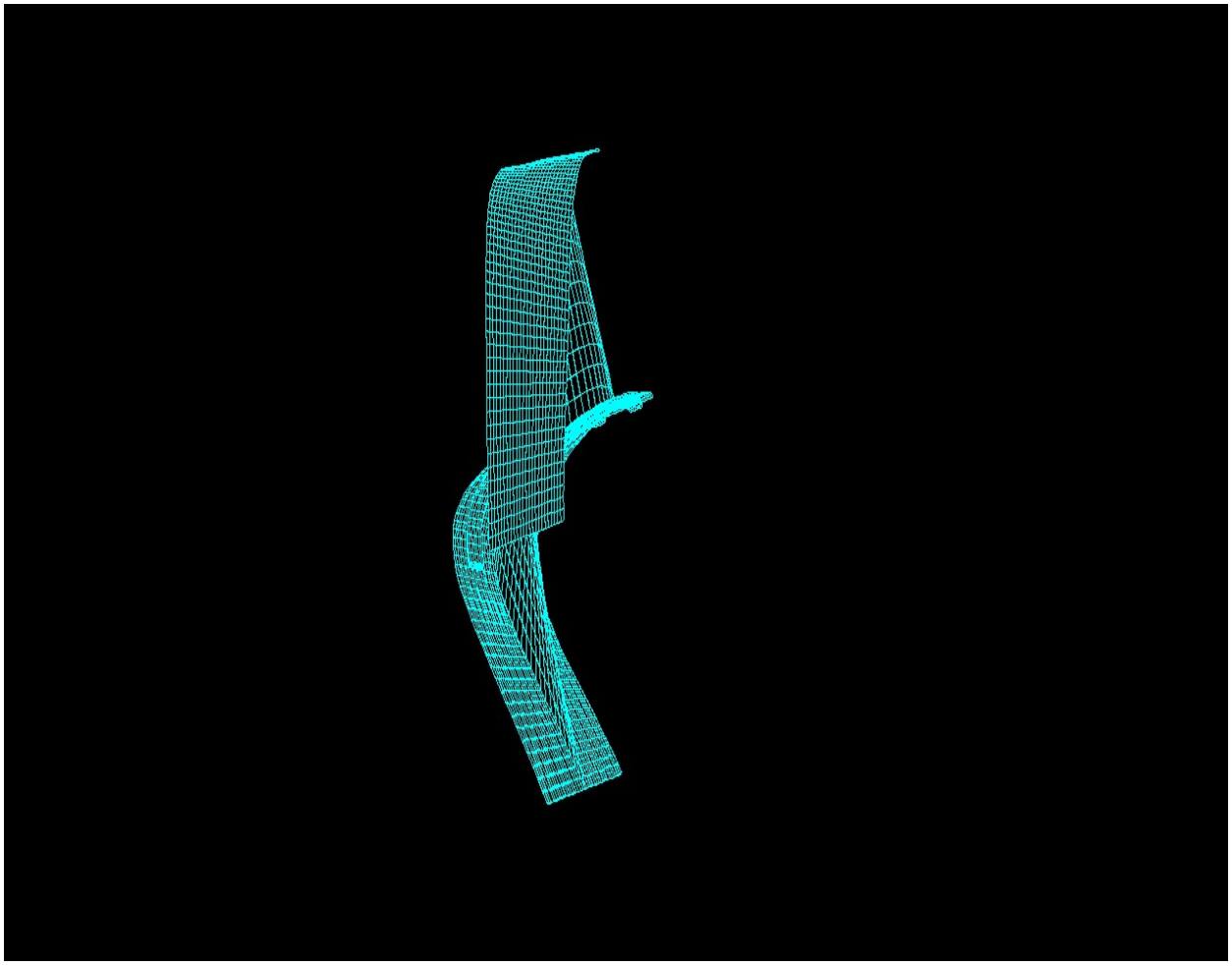

Figure A.56 Beam 21

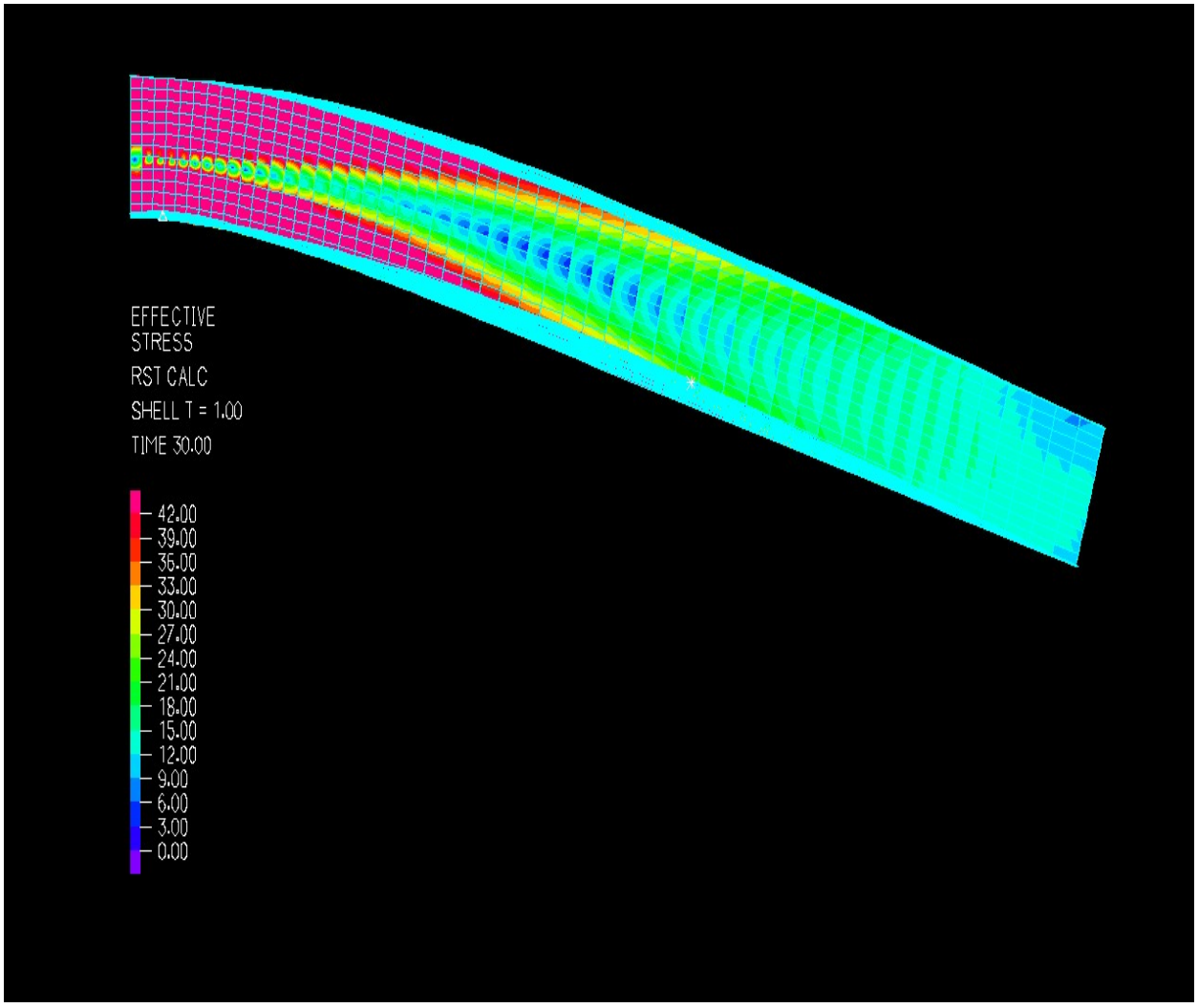

Figure A.57 Beam 21

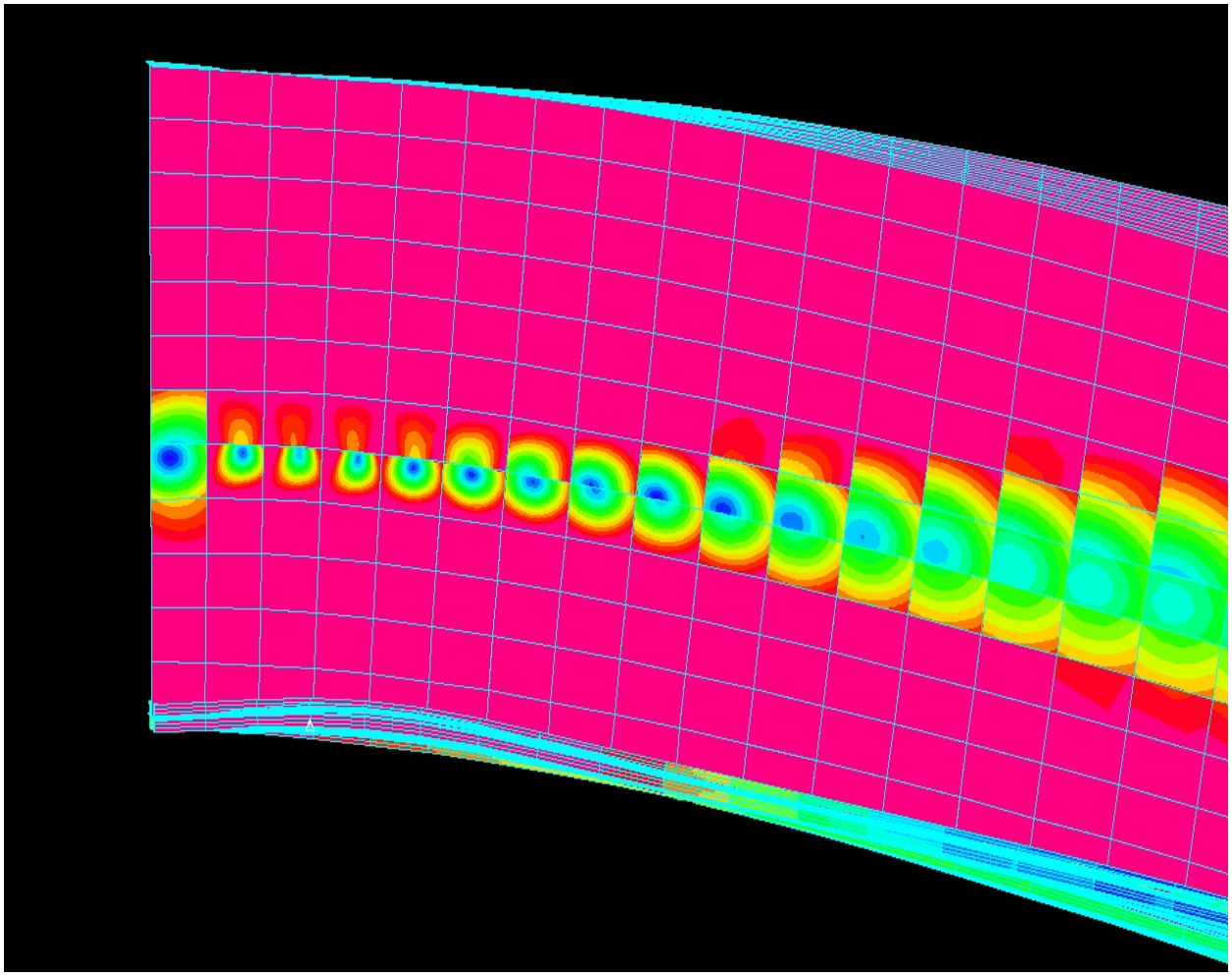

Figure A.58 Beam 21

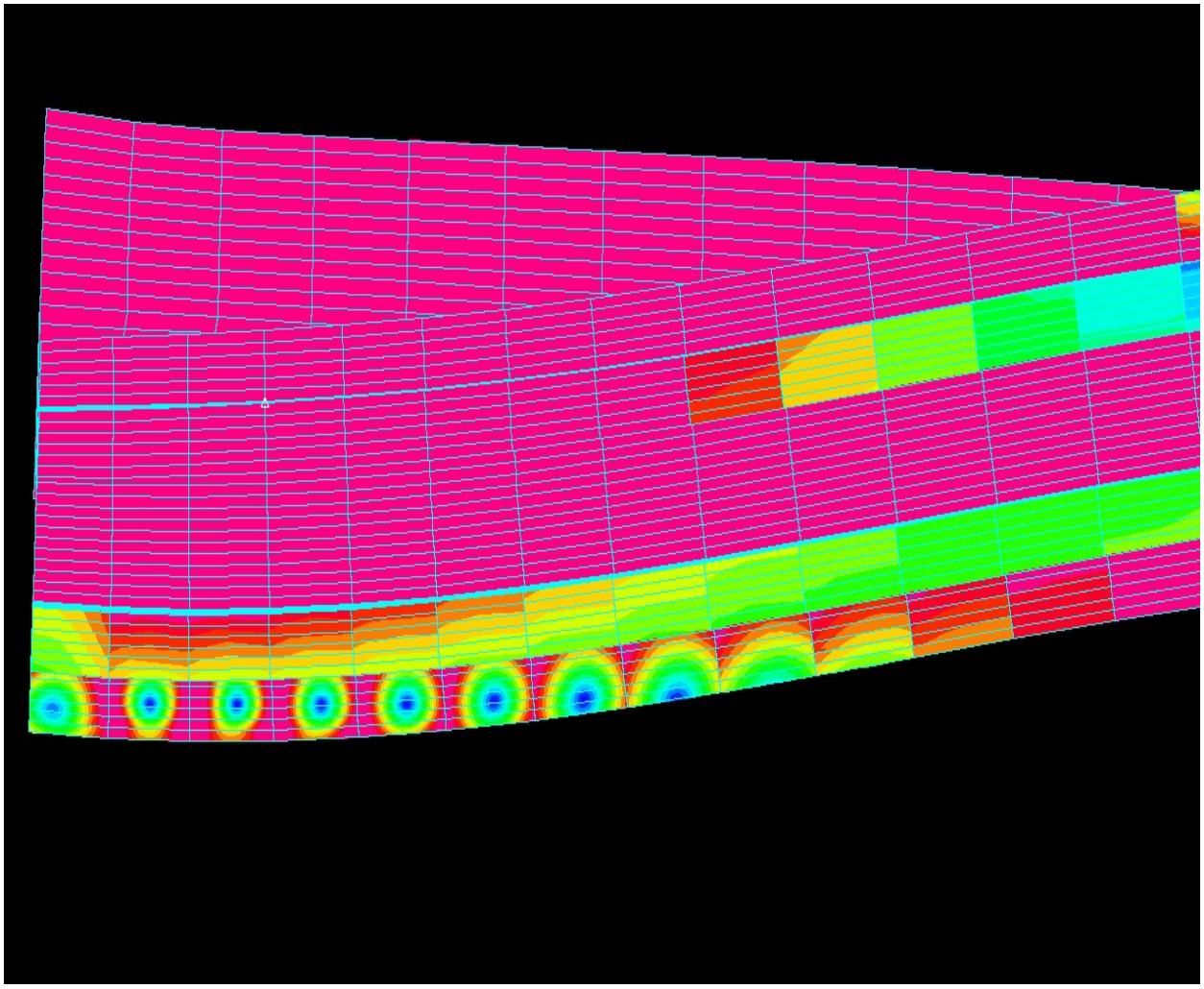

Figure A.59 Beam 21

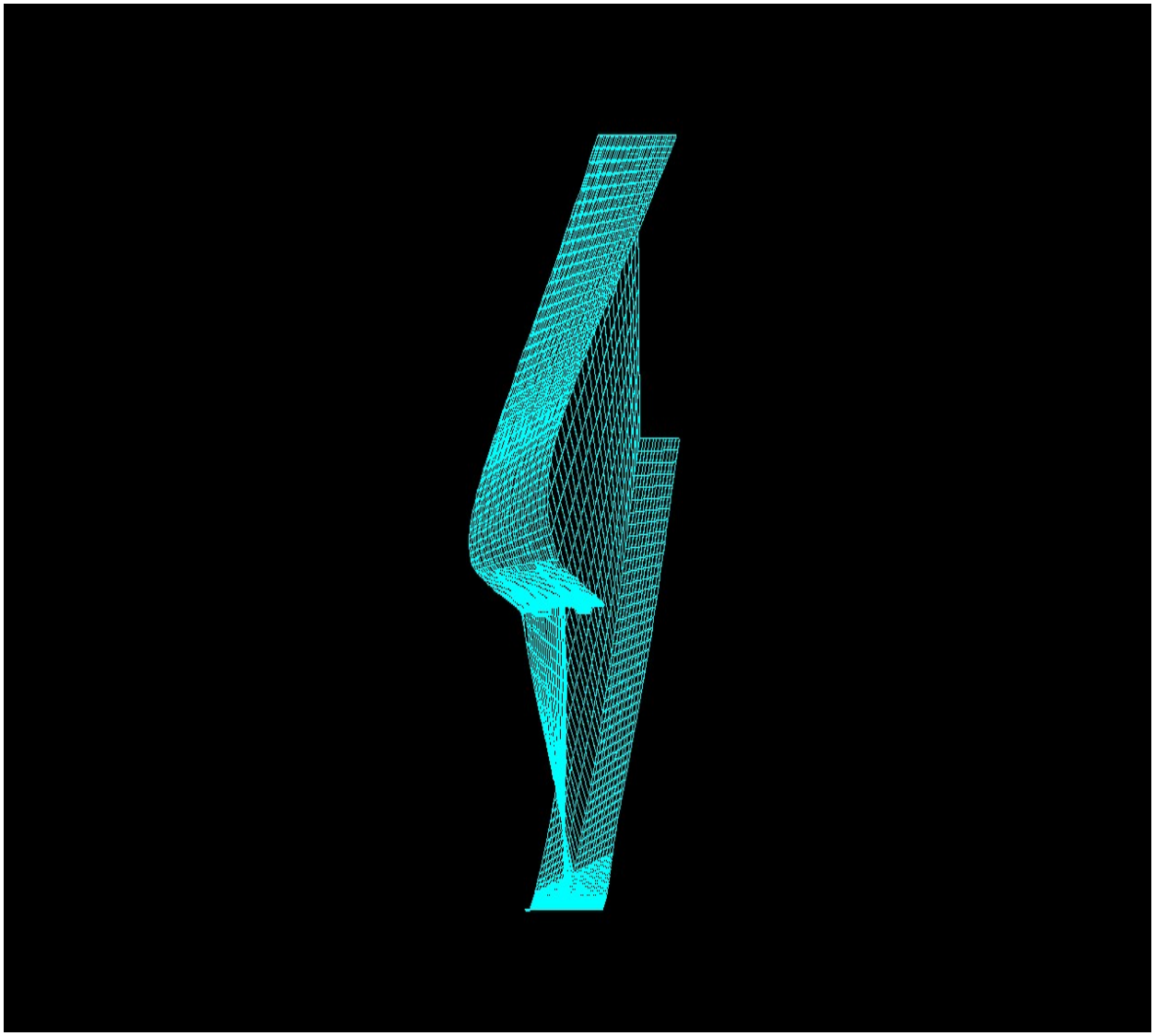

Figure A.60 Beam 22

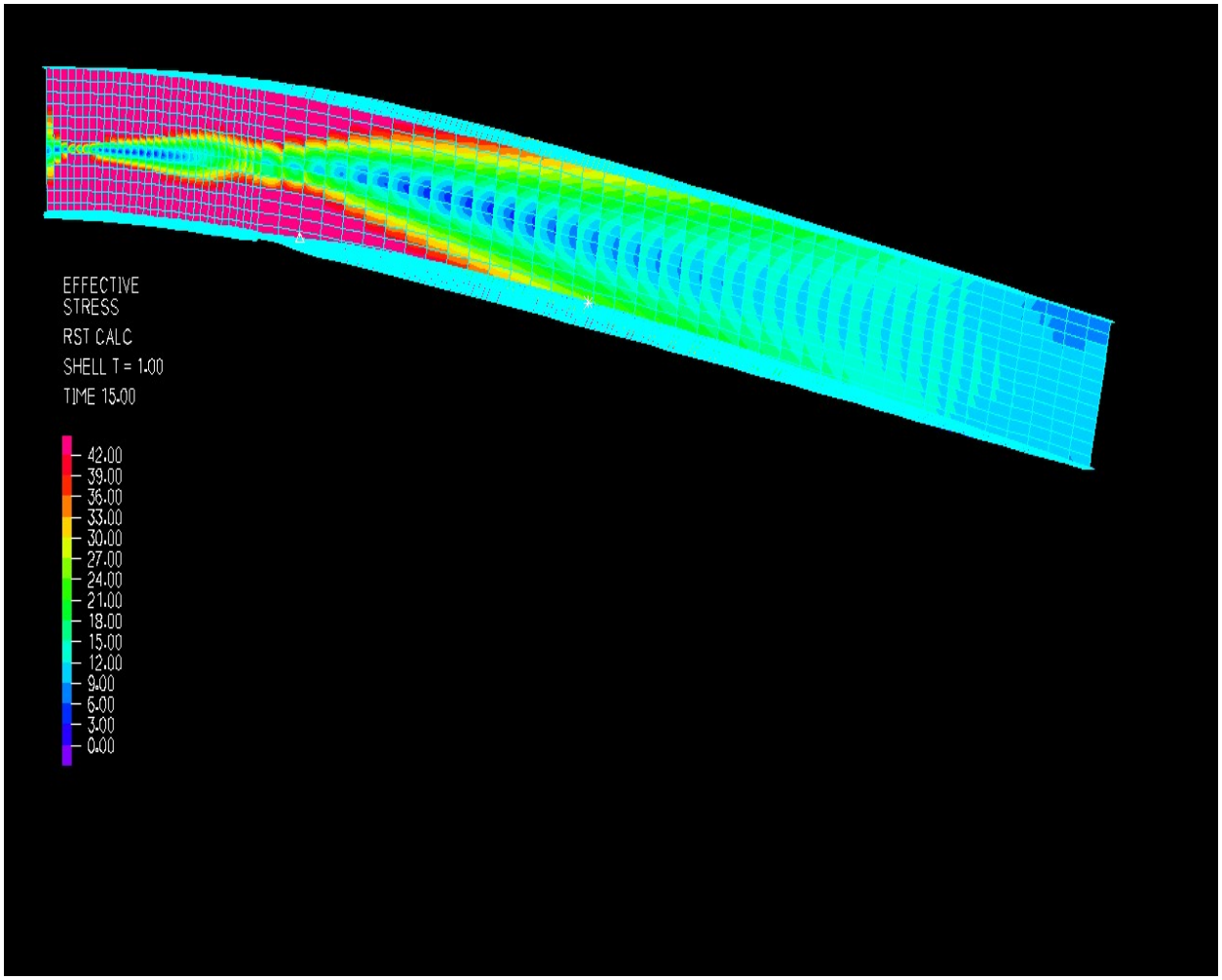

Figure A.61 Beam 22

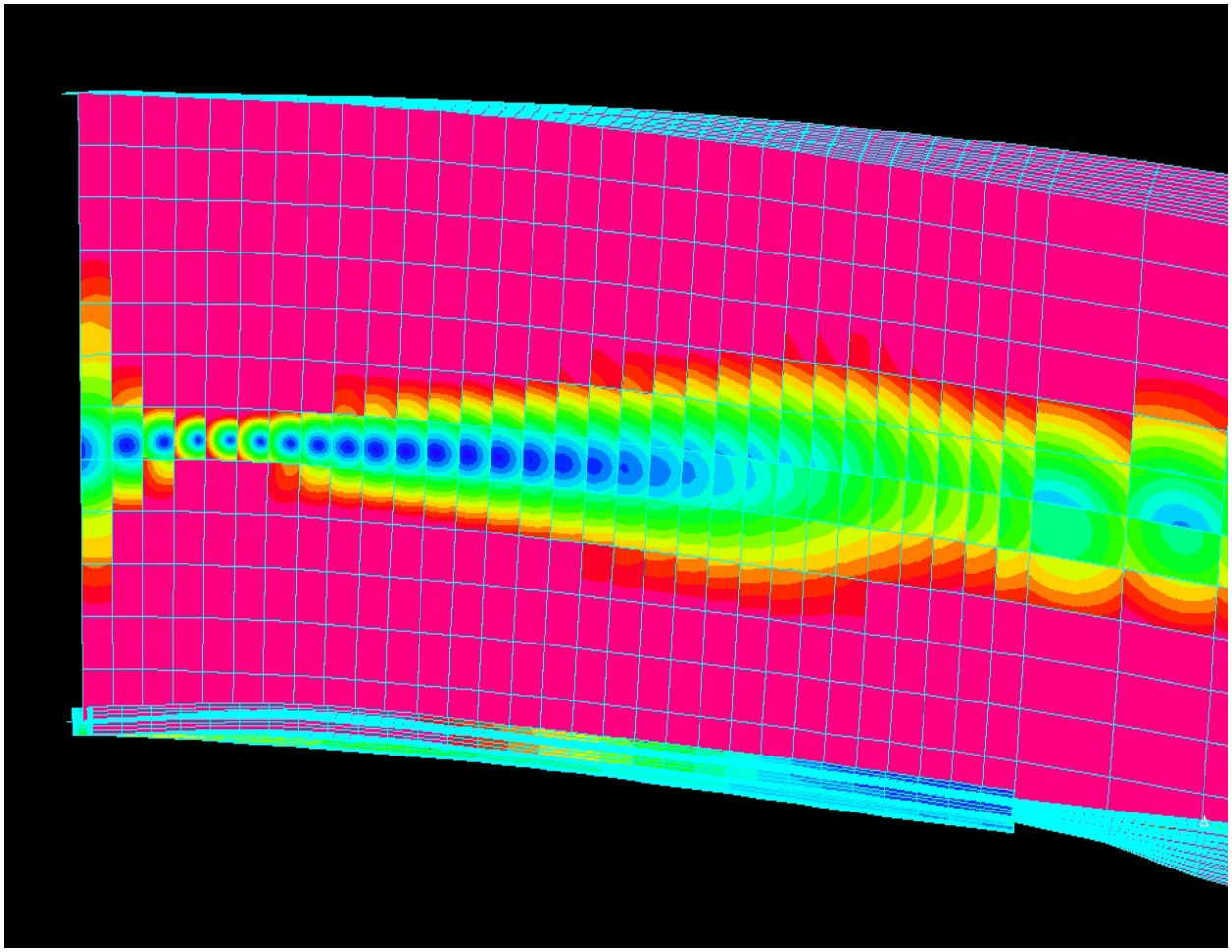

Figure A.62 Beam 22

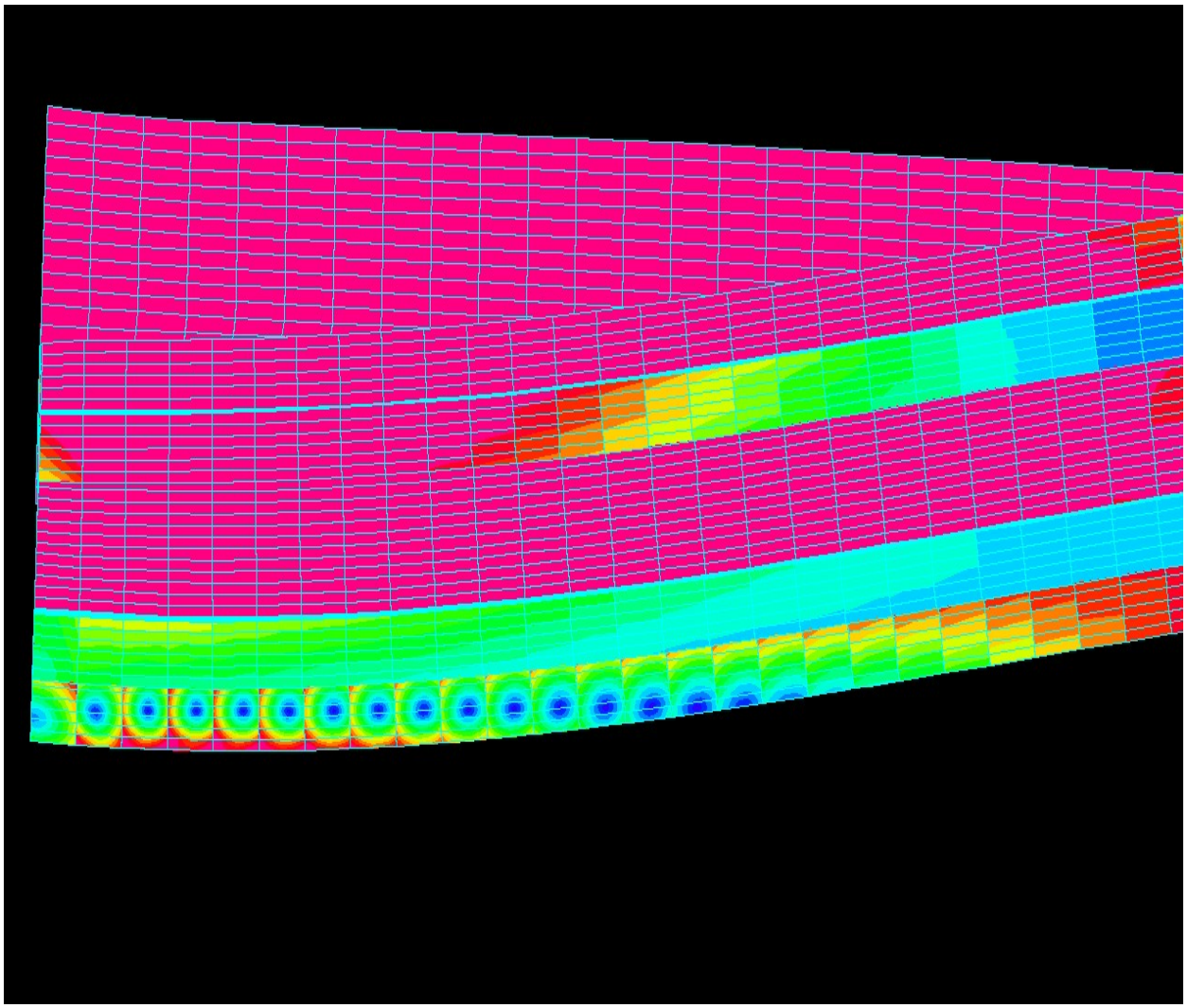

Figure A.63 Beam 22

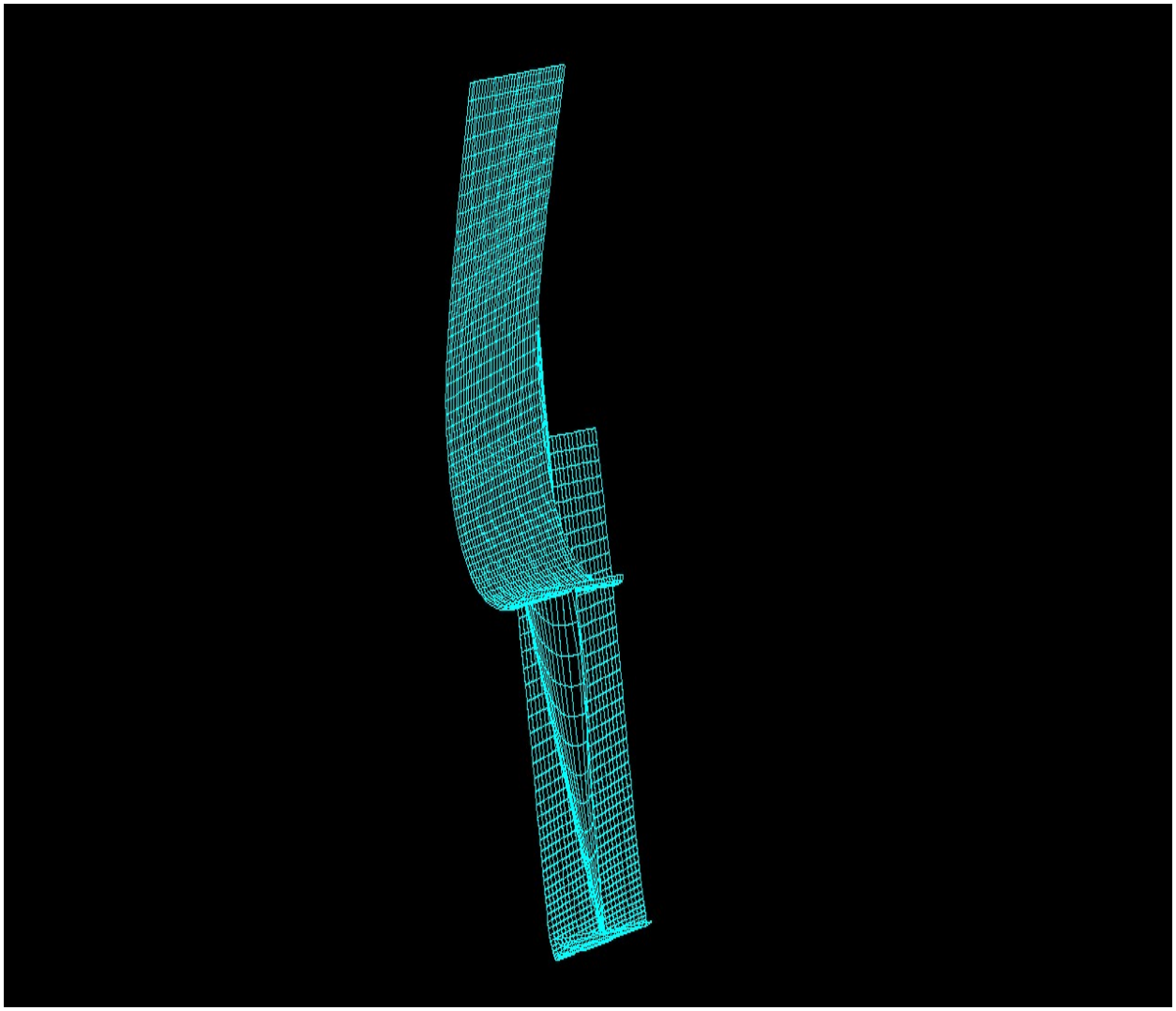

Figure A.64 Beam 30

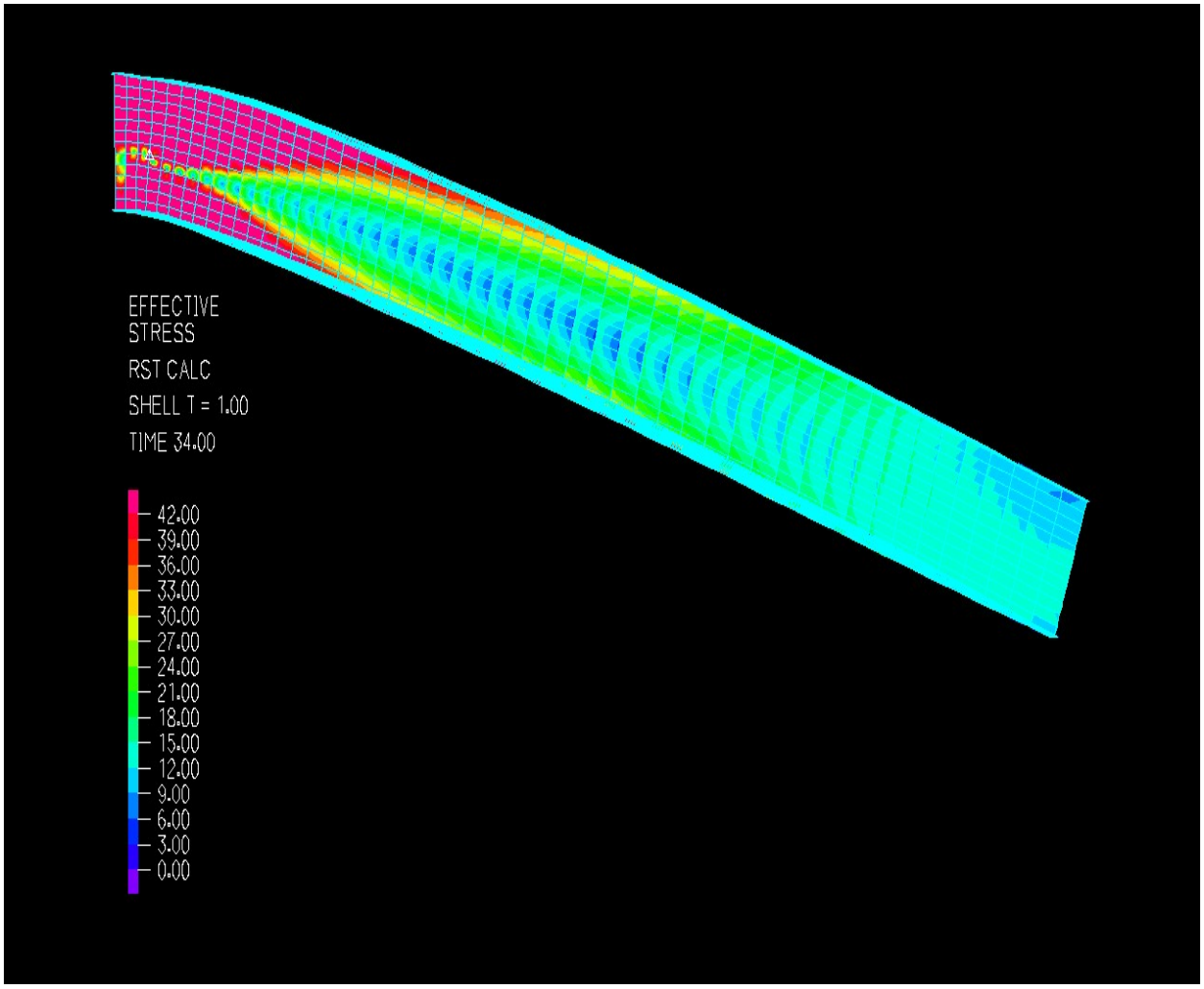

Figure A.65 Beam 30

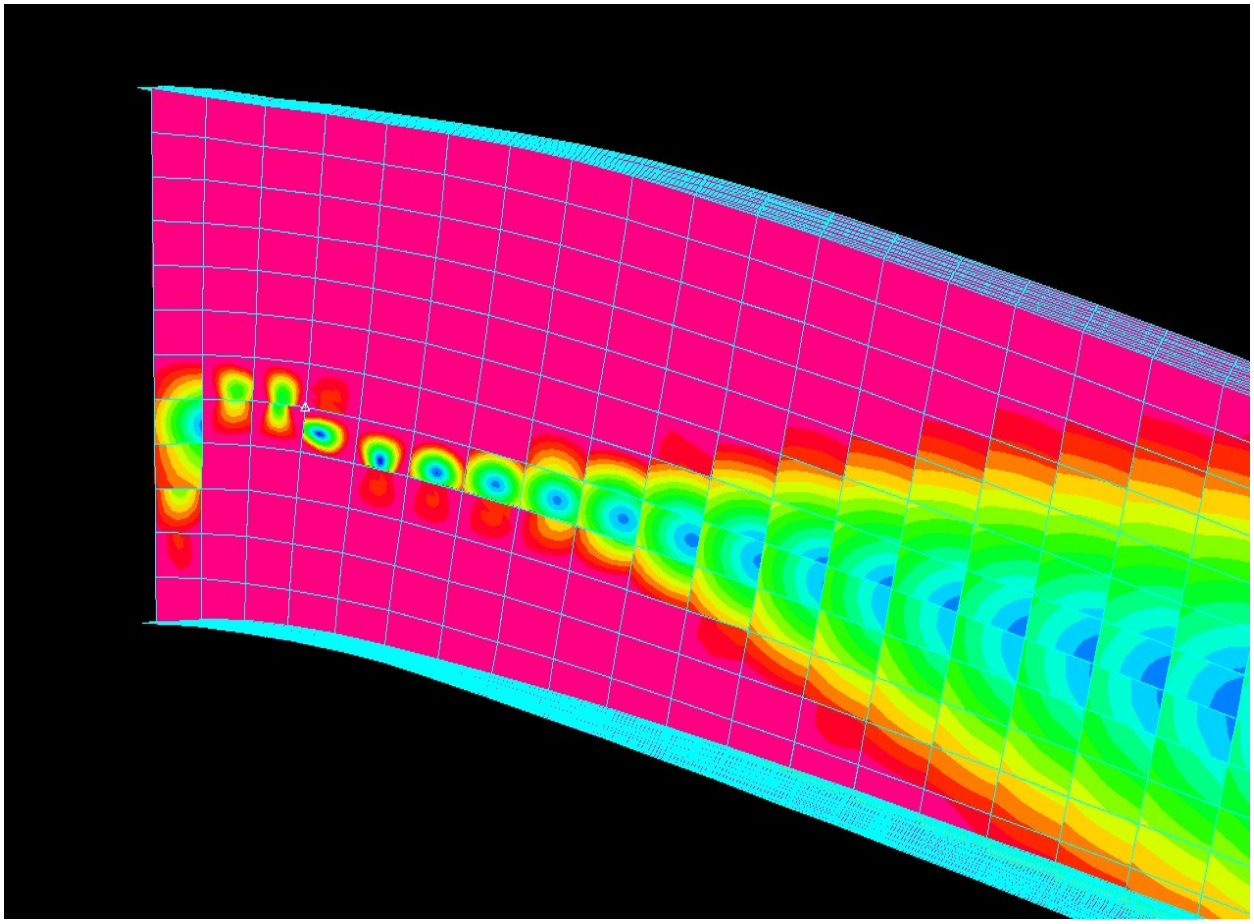

Figure A.66 Beam 30

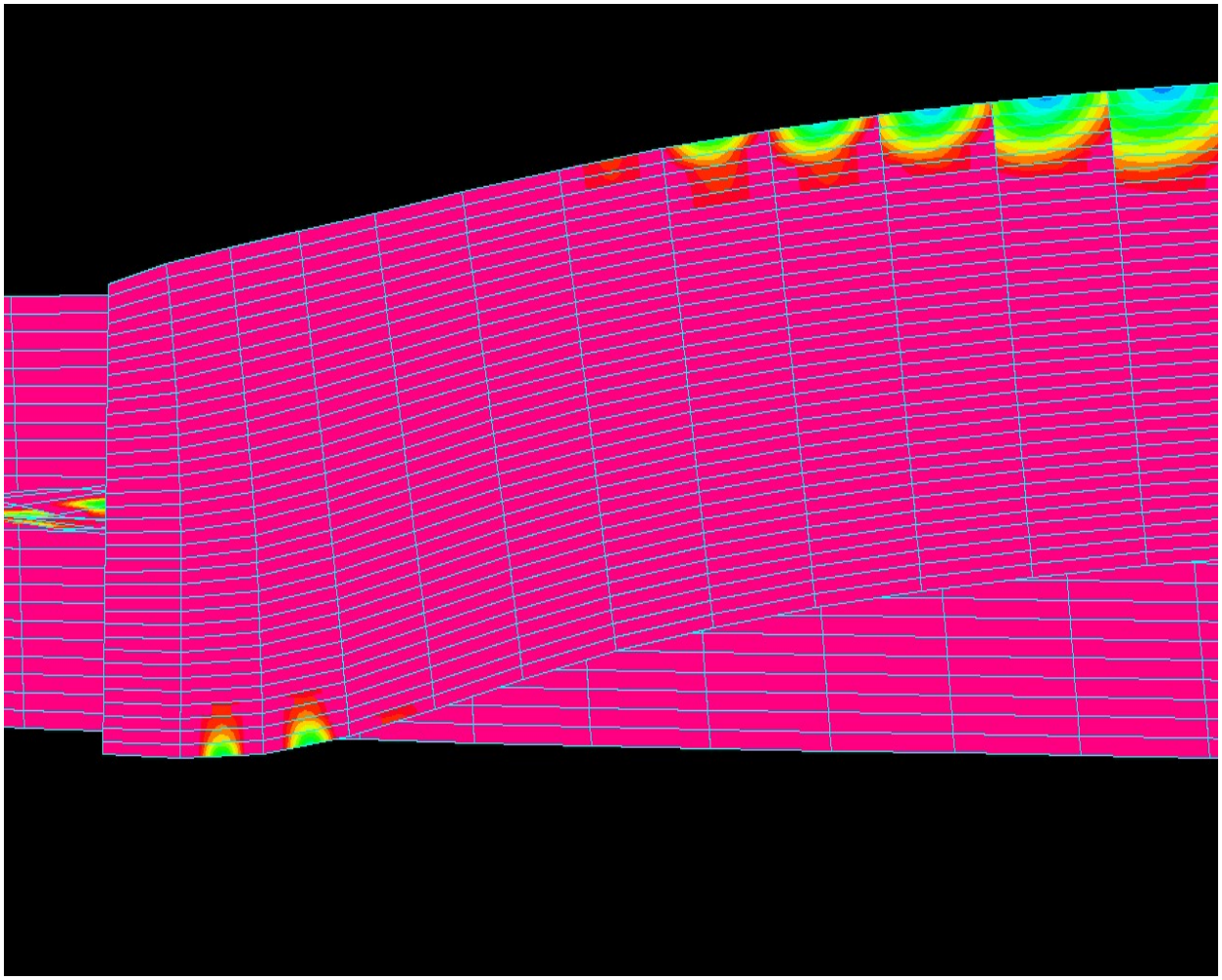

Figure A.67 Beam 30

BIBLIOGRAPHY

Buyukozturk, O., Gunes, O., Karaca, E., (2003) Progress on understanding debonding problems in reinforced concrete and steel members strengthened using FRP composites, *Construction and Building Materials*, Vol. 18, pp 9-19.

Cadei, J.M.C., Stratford, T.J., Hollaway, L.C., Duckett, W.G., (2004) Strengthening metallic structures using externally bonded fiber-reinforced polymers. *CIRIA Publication No. C595*. CIRIA, London, 233 pp.

Chacon, A., Chajes, M., Swinehart, M., Richardson, D. and Wenczel, G. (2004) Applications of Advanced Composites to Steel Bridges: A Case Study on the Ashland Bridge. *Proceedings of the 4th Advanced Composites for Bridges and Structures Conference*, Calgary, Canada.

Cosenza, E., Manfredi, G., Realfonzo, R., (1997) Behavior and Modeling of Bond of FRP Rebars To Concrete, *ASCE Journal of Composites for Construction*, Vol. 1, No. 2, pp 40-51.

Duthinh, D., Starnes, M., (2004) Strength and Ductility of Concrete Beams Reinforced with Carbon Fiber-Reinforced Polymer Plates and Steel, *ASCE Journal of Composites for Construction,* Vol. 8, No. 1, pp 59-69.

Ekiz, E., El-Tawil, S. Parra-Montesinos, G. and Goel, S. (2004) Enhancing Plastic Hinge Behavior in Steel Flexural Members Using CFRP Wraps, *Proceedings of the 13the World Conference on Earthquake Engineering*, Vancouver, August 2004.

El Damatty, A.A., Abushagur, M., (2003) Testing and modeling of shear and peel behavior for bonded steel/FRP connections, *Thin Walled Structures*, Vol. 41, pp 987-1003.

Karbhari, V.M. and Shulley, S.B. (1995) Use of Composites for Rehabilitation of Steel Structures – Determination of Bond Durability, *ASCE Journal of Materials in Civil Engineering*, Vol 7, No. 4. pp 239-245.

Mertz, D.R., Gillespie, J.W., Chajes, M.J. and Sabol, S.A. (2002) The Rehabilitation of Steel Bridge Girders Using Advanced Composite Materials, *Final Report to the Transportation Research Board for NCHRP-IDEA Project 51*, 25 pp.

Mertz, D.R. and Gillespie, J.W. (1996) Rehabilitation of Steel Bridge Girders Through the Application of Advanced Composite Materials, *Final Report to the Transportation Research Board for NCHRP-IDEA Project 11*, 30 pp.

Miller, T.C., Chajes, M.J., Mertz, D.R. and Hastings, J.N. (2002) Strengthening of a Steel Bridge Girder Using CFRP Plates. *ASCE Journal of Bridge Engineering*, Vol 6, No. 6, pp 514-522.

Moran, D.A., Pantelides, C.P., (2002) Stress-Strain Model for Fiber-Reinforced Polymer-Confined Concrete, *ASCE Journal of Composites for Construction*, Vol. 6, No. 4, pp 233-240.

Momber, A.W., Koller, S., Dittmers, H.J., (2004) Effects of Surface Preparation Methods on Adhesion of Organic Coatings to Steel Substrates, *JPLC,* pp. 44-50.

Patnaik, A.K. and Bauer, C.L. (2004) Strengthening of Steel Beams with Carbon FRP Laminates. *Proceedings of the 4th Advanced Composites for Bridges and Structures Conference*, Calgary, Canada.

Sayed-Ahmed, E.Y. (2004) Strengthening of Thin-walled Steel I-Section Beams Using CFRP Strips. *Proceedings of the 4th Advanced Composites for Bridges and Structures Conference*, Calgary, Canada.

Sen, R. Liby, L. and Mullins, G. (2001) Strengthening Steel Bridge Sections Using CFRP Laminates, *Composite: Part B*, Vol. 32, pp 309-322.

Sonobe, Y., Hiroshi, F., Okamoto, T., Kani, N., Kimura, K., Kobayashi, K., Masuda Y., Matsuzaki, Y., Mochizuki, S., Nagasaka, T., Lhimizu, A., Tanano, H., Tanigaki, M., Teshigawara, M., (1997) Design Guidelines of FRP Reinforced Concrete Building Structures, *ASCE Journal of Composites for Construction*, Vol. 1, No. 3, pp 90-115.

Tavakkolizadeh, M and Saadatmanesh, H (2003) Strengthening of Steel-Concrete Composite Girders using Carbon Fiber Reinforced Polymers Sheets, *ASCE Journal of Structural Engineering*, Vol. 129, No. 1, pp 30-40.

Wu, Z., Yuan, H., Niu, H., (2002) Stress Transfer and Fracture Propagation in Different Kinds of Adhesive Joints, *ASCE Journal of Engineering Mechanics*, Vol. 128, No. 5, pp 562-573.

Yost, J.R., Goodspeed, C.H., Schmeckpeper, E.R., (2001) Flexural Performance of Concrete Beams Reinforced with FRP Grids, *ASCE Journal of Composites for Construction,* Vol. 5, No. 1, pp 18-25.

Yost, J.R., Schmeckpeper, E.R., (2001) Strength and Serviceability of FRP Grid Reinforced Bridge Decks, ASCE Journal of Bridge Engineering, Vol. 6, No. 6, pp 605-612.

Yulismana, J. (2005) Expeirmental Study Of The Behavior Of Fiber Reinforced Polymer Deck System, PhD Dissertation, *University of Pittsburgh*.